The Chromatin Remodelling Contributions of Snf2l in Cerebellar Granule Neuron Differentiation

Laura Rose Goodwin

Thesis submitted to the
Faculty of Graduate and Postdoctoral Studies
In partial fulfillment of the requirements for the degree of
Master of Science

Department of Biochemistry, Microbiology and Immunology

Faculty of Medicine
University of Ottawa

© Laura Rose Goodwin, Ottawa, Canada, 2018

Abstract

Recent studies have uncovered *de novo* mutations of the gene encoding the chromatin remodelling protein Snf2l in patients with schizophrenia, Rett-like syndrome and intellectual disability. Snf2l and its closely related protein, Snf2h, play a critical role in embryonic and post-natal brain development. Murine models lacking functional Snf2h or Snf2l point to complementary activities of these remodelers; Snf2h cKO mice present with a significantly reduced cerebellum, while Snf2l Ex6DEL (exon 6 deleted) cerebella are larger than their wild-type counterparts. Granule neuron progenitors (GNPs) isolated from Ex6DEL cerebella display delayed cell cycle exit and hindered terminal differentiation compared to wild-type controls. Moreover, loss of Snf2l activity results in widespread transcriptome shifts which underlie the Ex6DEL GNP differentiation phenotype. In particular, key transcription factors are differentially expressed without Snf2l remodelling activity. We confirm that ERK pathway activation is misregulated in Ex6DEL GNPs, possibly in response to elevated fibroblast growth factor 8 (Fgf8) expression in these cultures. We find that Snf2l activity maintains the chromatin landscape throughout GNP differentiation, as Ex6DEL cultures have a global increase in chromatin accessibility. We suggest that Snf2l-mediated chromatin condensation is responsible for proper regulation of gene expression programs in GNP differentiation.

Acknowledgements

I must firstly thank my supervisor, Dr. David Picketts. I am grateful for the trust he has placed in me several times over the course of my degree. His guidance (and much appreciated patience) have allowed me to grow into this role, and I'm grateful for the opportunities he has made available to me.

Second, I must thank the second most crucial component to this thesis; the mice I worked with. Without them, none of this work would have been possible. I wish to thank all the adorable pups and determined breeders who made my research possible.

Next, I turn my attention to the Picketts lab. Most important to this work, I am deeply thankful to Keqin Yan, who has provided me with priceless tips, advice and demonstrations. I next wish to thank Jacob Marenger, a third year student at the time of his work with me in the lab. His help and enthusiasm were welcomed over the course of a summer, and he assisted me in generating preliminary data and optimizing experiments. David Cook, a PhD candidate in the Vanderhyden lab at the time of writing, has provided me with exceptional training and advice on my sequencing endeavours, and made the process significantly less daunting. Many thanks are owed to the remainder of the Picketts lab I had the chance to work with during my degree, and to the close friends I made at the OHRI in the past two years.

Finally, I want to thank my at-home support system, without whom none of this would be possible. My family has always encouraged me in the pursuit of my goals, even when it meant sacrificing weekends, family time and holidays in order to go in to the lab. My amazing fiancé Ryan suffered the brunt of the challenges of my degree with me. I'm so grateful for his help, patience and encouragement and I look forward to doing the same for him as he completes his PhD.

Table of Contents

Abstract ii

Acknowledgements iii

List of Abbreviations vi

List of Figures viii

List of Tables ix

1. Introduction 1

1.1 The importance of chromatin and its dynamic landscape 1

1.1.1 The nucleosome 1

1.1.2 Beads on a string: the role of packaging 1

1.1.3 Distorting and displacing the histone octamer 4

1.2 ISWI nucleosome remodelling proteins form part of the SWI2/SNF2 superfamily of chromatin remodellers 4

1.2.1 ISWI domains and structural features 5

1.2.2 Snf2h and Snf2l – collaborating to build a mind 6

1.3 Neurodevelopment 9

1.3.1 Early embryonic development 9

1.3.2 The emerging cerebellum 10

1.4 ISWI mouse models 12

1.4.1 Snf2h cKO mouse model 12

1.4.2 Ex6DEL Snf2l mouse model 12

1.5 ISWI proteins are the molecular motors for chromatin remodelling complexes 13

1.5.1 The importance of non-catalytic subunits 13

1.5.2 Complex-specific activity during development 15

1.6 Intellectual disability (ID), neurodevelopmental disease (NDD) and autism spectrum disorder (ASD) 19

1.7 Emerging evidence for involvement of ISWI remodelling complexes in NDDs 20

1.7.1 Recent leads on a new suspect: Snf2l and ID 20

1.7.2 ISWI and the cerebellum in ASD 21

1.7.3 WICH complex and Williams-Beuren syndrome 23

1.7.4 CECR2 and Cat eye syndrome 24

1.7.5 Wnt deregulation and schizophrenia 24

1.8 Aims and rationale 25

2. Materials and Methods 26

2.1 Mouse Work 26

2.1.1 Animal Care 26

2.1.2 Mouse lines 26

2.1.3 Genotyping 27

2.1.4 Nucleic acid visualization 28

2.2 GNP 28

2.2.1 Isolation and *In vitro* Culture 28

2.2.2 BrdU Pulse Labelling 29

2.2.3 Immunostaining and Counting 29

2.2.4 Cell Viability 31

2.3 Protein Analysis 31

2.3.1 Cerebellar Protein Isolation ... 31
2.3.2 GNP Protein Isolation ... 31
2.3.3 Immunoblotting ... 32
2.3.4 Protein Quantification by Densitometry ... 33
2.3.5 Co-Immunoprecipitation (coIP) ... 33
2.4 Sequencing ... 34
2.4.1 RNA Isolation ... 34
2.4.2 RNA-seq Preparation ... 34
2.4.3 RNA-seq ... 35
2.4.4 RNA-seq Processing and Analysis ... 35
2.4.5 ATAC-seq Sample and Library Preparation ... 36
2.4.6 ATAC-seq Processing and Analysis ... 38
2.5 Quantitative PCR (qPCR) ... 39
2.5.1 Reverse Transcription ... 39
2.5.2 qPCR ... 40

3. Results ... 41
3.1 Snf2l is required for timely differentiation of granule neurons *in vitro* ... 41
3.1.1 Wild-type cerebellar GNPs differentiate within 3 days ... 41
3.1.2 Loss of Snf2l activity hinders GNP terminal differentiation ... 43
3.1.3 Snf2l exon 6 is not required to mediate complex binding but complex hierarchy may be skewed ... 50
3.2 Widespread disruption of GNP transcriptome upon inactivation of Snf2l ... 53
3.2.1 Ex6DEL GNP differentiation is associated with altered transcription ... 53
3.2.2 WT and Ex6DEL DEGs undertake transcriptionally unique differentiation pathways 56
3.2.3 Ex6DEL GNP and GN are transcriptionally distinct from their WT counterparts ... 59
3.2.4 Differential expression of key genes mediating cerebellar development and cell cycle control ... 62
3.2.5 Key transcription factors are associated to gene expression shifts in Ex6DEL cells ... 63
3.2.6 Up-regulation of ERK activation does not result in TF activity ... 63
3.3 Loss of Snf2l activity results in increased chromatin accessibility ... 67
3.3.1 Accessibility at genomic features is not modified by Snf2l ... 67
3.3.2 Genome wide chromatin accessibility is increased at TSS ... 69
3.3.3 Ex6DEL chromatin landscape remains open in differentiated cells ... 71
3.3.4 DARs from Ex6DEL GNPs resemble earlier progenitor cell populations ... 74

4. Discussion ... 77
4.1 Snf2l activity is required for timely differentiation of GNPs ... 77
4.2 Terminal differentiation without Snf2l remodelling occurs according to a distinct mechanism compared to WT GNPs ... 78
4.3 A role for Snf2l in mediating chromatin compaction underlying cell differentiation ... 81
4.4 Compensation by chromatin remodelling complexes ... 84
4.5 Future Directions ... 87

References ... 90

Appendix ... 101

Curriculum Vitae ... 114

List of Abbreviations

ACF = ATP-utilizing chromatin assembly and remodelling factor
ASD = autism spectrum disorder
AT = A/T rich
ATAC-seq = Assay for Transposase-Accessible Chromatin sequencing
Atoh1 = mouse atonal homolog 1
ATP = adenosine triphosphate
ATRX = α-thalassemia mental retardation X-linked
BAF = brahma-associated factor
BPTF = Bromodomain PHD Finger Transcription Factor
BrdU = Bromodeoxyuridine
BRG1 = Brahma-related factor 1
BRM = Brahma
cDNA = complementary DNA
CECR2 = Cat Eye Syndrome Chromosome Region, Candidate 2
CERF = CECR2-containing remodelling factor
CHD = chromodomain
ChIP = chromatin immunoprecipitation
CHRAC = chromatin accessibility complex
cKO = conditional knock-out
coIP = co-immunoprecipitation
Ct = threshold cycle
CTCF = CCCTC binding factor
DAR = differentially accessible region
DDT = DNA-binding homeobox/Different Transcription and chromatin remodelling factors
DEG = differentially expressed gene
DIV = days *in vitro*
DNA= deoxyribonucleic acid
E = embryonic
EGL = external germinal layer
En = engrailed
ERK = extracellular signal-regulated kinase
FC = fold change
FGF = fibroblast growth factor
Foxg1 = forkhead box G1
gDNA = genomic DNA
GFAP = Glial fibrillary acidic protein
GN = granule neuron
GNP = granule neuron progenitor
GO = Gene Ontology
GTP = Guanosine-5'-triphosphate
H = histone
HDAC = histone deacetylase
ID = intellectual disability

IGL = internal germinal layer
IP = immunoprecipitation
ISWI = imitation switch
K = lysine
KO = knock-out
MAPK = mitogen-activated protein kinase
Me = methyl
MECP2 = Methyl-CpG-binding protein 2
mESC = mouse embryonic stem cell
mRNA= messenger RNA
Ms = mouse
NFR = nucleosome free region
NND = neurodevelopmental disorder
NoRC = nucleosome remodelling factor
NTP = nucleotide triphosphate
NURF = nucleosome remodelling factor
P = post-natal
PCL = Purkinje cell layer
PCR = polymerase chain reaction
PTM = post-translational modification
QC = quality control
Rb = rabbit
Rn = normalized reporter signal
RNA = ribonucleic acid
RNA–seq = RNA sequencing
rRNA = ribosomal RNA
RSF = remodelling and spacing factor
SANT = Swi3, Ada2, N-Cor, and TFIIIB
Shh = sonic hedgehog
SLIDE = SANT-like ISWI domain
SMARCA1/5 = SWI/SNF-related, matrix-associated, actin-dependent regulator of chromatin, subfamily A, member 1/5
SNF2H = snf2-homolog
SNF2L = snf2-like
SWI2/SNF2 = sucrose non-fermentation/mating type switching 2
TES = transcription end site
TF = transcription factor
TFBS = transcription factor binding site
Tip5 = Transcription termination factor I-interacting protein 5
TSS = transcription start site
qRT-PCR = quantitative real-time polymerase chain reaction
VZ = ventricular zone
WICH = WSTF-imitation switch
WNT = wingless-type MMTV integration site family
WSTF = Williams syndrome transcription factor
WT = wild-type

List of Figures

Figure 1. Post-translational modifications (PTMs) affecting chromatin condensation.....**3**
Figure 2. Conserved functional motifs of mammalian ISWI.....**7**
Figure 3. Granule neuron progenitor (GNP) maturation in post-natal cerebellar development.....**11**
Figure 4. Loss of Snf2l activity results in increased cerebellar size.....**14**
Figure 5. ISWI chromatin remodelling complexes.....**16**
Figure 6. Schematic of reported disease-associated mutations in *SMARCA1*.....**22**
Figure 7. 72h GNP differentiation timecourse *in vitro*.....**42**
Figure 8. Cerebellar GNP cultures have limited glial contamination.....**44**
Figure 9. GNPs isolated from Ex6DEL mice express Snf2l isoform lacking ATP binding exon 6.....**45**
Figure 10. Terminal differentiation of Snf2l Ex6DEL GNPs is delayed *in vitro*.....**47**
Figure 11. Ex6DEL cultures prolong expression of proliferation markers and delay expression of differentiation markers.....**48**
Figure 12. Ex6DEL GNPs remain in a prolonged S-phase during *in vitro* differentiation.....**49**
Figure 13. ISWI interacting partner protein abundance is dynamic during GNP differentiation.....**51**
Figure 14. The Ex6DEL protein retains the ability to interact with CECR2 .....**52**
Figure 15. Loss of active Snf2l leads to widespread transcriptome disruptions during GNP differentiation.....**55**
Figure 16. WT GNP differentiation requires substantial transcriptomic shifts to mediate cell cycle exit and neuron development.....**57**
Figure 17. DEGs regulating Ex6DEL GNP differentiation indicate disruption of developmental pathways and reduced ability to differentiate.....**58**
Figure 18. WT and Ex6DEL granule neuron progenitor cells are transcriptionally distinct.....**60**
Figure 19. WT and Ex6DEL *in vitro* differentiation does not generate identical granule neuron populations.....**61**
Figure 20. Gene expression programs in Ex6DEL GNPs are temporally regulated and governed by unique TFs.....**64**
Figure 21. The ERK pathway is disrupted in Ex6DEL GNPs but it does not modify Elk1 TF activity.....**66**
Figure 22. Chromatin accessibility distribution across genomic features is unchanged upon loss of active Snf2l.....**68**
Figure 23. Snf2l mediates chromatin accessibility at the transcription start site (TSS).....**70**
Figure 24. Snf2l Ex6DEL differentiation is associated with greater chromatin accessibility.....**72**
Figure 25. Loss of active Snf2l results in aberrantly open chromatin regions in both progenitors and differentiated cells.....**73**
Figure 26. Ex6DEL GNP differentiation requires increased number of DARs compared to WT process.....**75**
Figure 27. Ex6DEL accessibility at TSS is similar to earlier lineage mouse embryonic stem cells (mESC) **76**

List of Tables

Table 1. Genotyping primers.....**28**
Table 2. Antibodies used for immunofluorescence and immunoblotting.....**30**
Table 3. ATAC-seq primers.....**37**
Table 4. qPCR primers.....**40**

1. Introduction

1.1 The importance of chromatin and its dynamic landscape

1.1.1 The nucleosome

Fundamentally, the nucleosome is comprised of eight core histone proteins (or their variants) around which approximately 147 bp of DNA can coil itself. This multimer is generally composed of two histone H2A-H2B (H2A-H2B) dimers, as well as a histone H3-H4 tetramer. Together, the bulk of the histone proteins associate via their hydrophobic surfaces to form the dense core of the nucleosome. Histones also possess basic histone tails, stretches of single amino acids which reside externally to the packaged histone octamer. These tails are found protruding from the bulk of the nucleosome. While the histone octamer is responsible for the physical twining of DNA along its surface, the histone tails can harbour a multitude of post-translational covalent modifications which can be exploited to modify nucleosome positioning, DNA accessibility and gene expression[1]. In this manner, the role of the nucleosome is two-fold; it allows for compact packaging of DNA within the nucleus and it provides a platform to regulate gene expression by influencing genome accessibility.

1.1.2 Beads on a string: the role of packaging

Chromatin is a broad term to describe DNA and its associated proteins. While this description is vague, a constant and important component of chromatin is the nucleosome. The abundance of nucleosomes at any given loci can dictate greater

chromatin structure, and DNA accessibility in the three-dimensional space. The 'beads on a string' concept in biology simplifies the role of nucleosomes in the genomic space regarding chromatin; the nucleosomes ('beads') are typically regularly spaced across DNA ('string') in order to form ordered nucleosome arrays. Loci of high nucleosome compaction are known as 'heterochromatin' in which DNA accessibility is physically reduced. Indeed, telomeres and centromeres are maintained in a heterochromatic state[2]. These regions permanently remain heterochromatic and thus are described as constitutive heterochromatin. In addition, facultative heterochromatin encompasses genomic regions that have the potential to form heterochromatin, which is the case in the inactivation of the second X chromosome in females[3]. While early lineage cells have very little facultative heterochromatin (and are therefore in a pluripotent state), differentiation into particular lineages is accompanied by increases in heterochromatin which allow the cell to refine transcriptional output towards the needs of the differentiated cell (and therefore lose their pluripotency)[4]. Finally, the euchromatic portion of the genome represents more accessible regions which can be modified to influence gene expression.

While the physical presence of nucleosomes on a gene can directly affect transcriptional output, nucleosomes and DNA can themselves be modified to alter gene expression. Indeed, histone tail and DNA modifications can serve as effective methods of altering transcription at a genome-wide level, and the variety of possible post-translational modifications allows for fine-tuning of this output. Key post-translational modifications (PTMs) altering the chromatin landscape are DNA methylation and histone tail modifications (Fig 1). DNA methylation promotes reduced DNA accessibility and

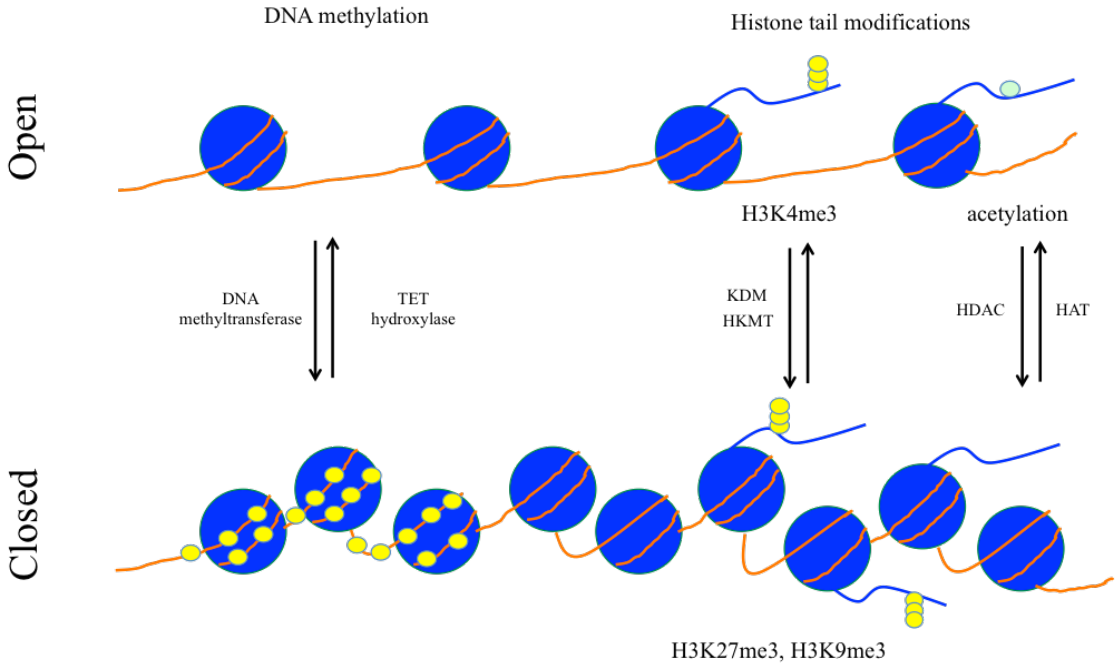


Figure 1. Post-translational modifications (PTMs) affecting chromatin condensation. Open (top) and closed (bottom) chromatin is represented with histone octamers (blue circles) along DNA (orange). Presence of DNA methylation leads to chromatin condensation; methyl groups are added to DNA by DNA methyltransferases, and removed by TET hydroxylases. Protruding N-terminal histone tails (blue) can also be modified, most commonly by methylation (yellow) and acetylation (light blue). Lysine methylation can be added or removed to histone tails by histone lysine methyltransferases (HKMT) and lysine demethylases (KDM), respectively. Acetylation status is regulated by histone acetylases (HAT) and histone deacetylases (HDAC). H3K4me3 and acetylation are typically found in regions of accessible chromatin, while H3K27me3 and H3K9me3 are found at repressed loci.

repress transcription, while histone tail PTMs are more heterogeneous. The H3K9me3 and H3K27me3 marks are associated with heterochromatin, H3K4me3 and acetylation are generally found at active loci[5,6]. Precise addition and removal of these marks is carried out by chromatin-modifying enzymes, referred to as histone 'writers' and 'erasers', respectively. The changes in chromatin condensation catalyzed by the targeted PTMs added or removed by these enzymes greatly influence DNA accessibility and thus transcriptional output[1,7] (summarized in Fig 1).

1.1.3 Distorting and displacing the histone octamer

The presence of nucleosomes represents a physical barrier to transcription, and therefore represents a powerful tool in the regulation of gene expression. However, in order to support the dynamic requirements of the transcriptome of a cell, nucleosomes must often be displaced to alter greater chromatin compaction. Nucleosome remodelling proteins rely on ATP hydrolysis in order to catalyze the displacement of the histone octamer along a DNA template. Repositioning is carried out in small increments of a few base pairs at once, wherein DNA from the nucleosome is first pushed out of the core which creates enough strain in order to allow for DNA to be accepted into the other side of the nucleosome[8,9]. The strain then allows for DNA to travel through the nucleosome in order to generate displacement along the DNA template[10].

1.2 ISWI nucleosome remodelling proteins form part of the SWI2/SNF2 superfamily of chromatin remodellers

The archetypal chromatin remodelling enzyme is the yeast SWI2/SNF2 ATP-dependent nucleosome remodeller, and its closely related mammalian homologues are the BRG1 and BRM proteins[11,12]. Characterization of the yeast remodelling protein was carried out through mating type switching (SWI) and growth on sucrose (SNF) variants[11,13], which ultimately were both found to result from the same gene[14]. High sequence homology amongst the ATPase domains of chromatin remodelling proteins has allowed for the distinction of 4 major mammalian remodelling families; SWI/SNF, Imitation Switch (ISWI), CHD and Ino80 as well as ATR-X[10]. They are distinguished by the inclusion of interaction domains and subtle differences in their remodelling activities. ISWI was first extracted from the nucleosome remodelling factor (NURF) complex in *Drosophila*[15,16]. Only one homolog of ISWI is found in *Drosophila* and is similar to human ISWI isoform Snf2h[17]. Two closely related homologues, Isw1 and Isw2, have been characterized in yeast[18]. Finally, there are two mammalian homologs of ISWI; Snf2h and Snf2l[19]. For this thesis, the discussion will be limited to the ISWI family of proteins.

1.2.1 ISWI domains and structural features

ISWI remodelling proteins contain an N-terminal catalytic ATPase domain which also mediates DNA interactions, while the C-terminus contains the characteristic HAND-SANT-SLIDE domain, which allows for binding to linker DNA in addition to providing interactions with the histone H4 tail[19–23]. Additionally, ISWI proteins contain two autoregulatory motifs, AutoN and NegC[10] (Fig 2). In order to efficiently restructure chromatin, ISWI is only capable of sliding nucleosomes on sufficient lengths of nucleosome arrays, as naked DNA template alone does not promote catalytic activity[15,24–

[29]. There is strong evidence to point towards an active, continuous sampling mechanism of ISWI along chromatin as measured by pixel-wise photobleaching profile evolution analysis. Average residency time was found to be between 1-2 ms but this time increases significantly in the event of ISWI being recruited for ATP-dependent remodelling[30]. ISWI remodelling often occurs at the transcription start site (TSS) of genes, as well as at the 3' end and has been found occupying both introns and exons[31]. In order to mediate loci-specific remodelling activities, ISWI interacts with TFs as well as other binding partners which carry conserved structural domains characteristic of ISWI interactions such as bromodomains, AT hooks and DDT[32] motifs which are critical to enhance their specificity and biological activity. ISWI proteins are generally well conserved across species[14,33]. They hold a central role in numerous cellular mechanisms relating to chromatin structure regulation, with reports of widespread roles as a gene regulator via remodelling of nucleosome arrays and nucleosome free regions (NFR)[34–37], establishment and replication of heterochromatin[38–40], DNA repair[41–45] and mediation of rRNA expression (reviewed in [46]).

1.2.2 Snf2h and Snf2l – collaborating to build a mind

Two mammalian ISWI isoforms have been identified, Snf2h (gene product of *Smarca5*) and Snf2l (*Smarca1*)[19]. *Smarca1* is an X-linked gene, while *Smarca5* is located on chromosome 8 in mice[47,48]. As Snf2h and Snf2l are structurally similar, expression of both of these would suggest contrasting mechanisms are being employed by both of these molecular motors in order to avoid functional redundancy. Indeed, these ISWI proteins

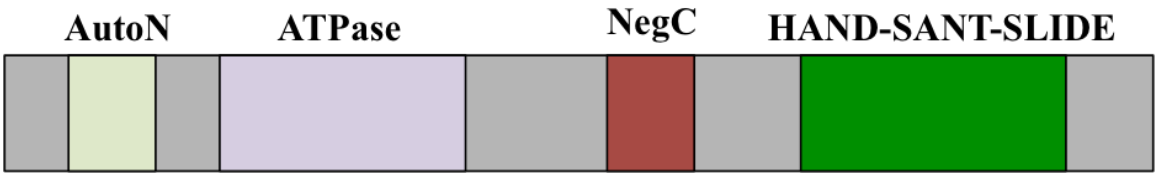


Figure 2. Conserved functional motifs of the mammalian ISWI proteins. Schematic representing the motif organization of the mammalian ISWI gene. Autoregulatory motifs AutoN and NegC are represented in orange and purple, respectively. The catalytic ATPase domain is shown in blue, and the C-terminal HAND-SANT-SLIDE domain in grey. Figure adapted from Goodwin and Picketts, 2018.

have long been known to display strikingly opposite expression patterns, both temporally and spatially. Snf2h is found throughout the organism but is highly expressed in the brain, whereas active Snf2l is only localized in neural tissue, as well as gonads and placenta[19,49]. Temporally, Snf2h expression is elevated in the embryonic brain while Snf2l remains lower until approximately P15 when it can be found enriched in the hippocampus and cerebellum[19,50]. These distinct expression patterns reveal an underlying role for Snf2h and Snf2l in the developing brain; Snf2h expression is prominent in proliferating progenitor cells, while Snf2l is elevated in differentiated cells[19,48,51,52].

Snf2h remodelling activity plays an indispensable role in development due to its presence in progenitor cell populations. Mice lacking active Snf2h resulting from Cre recombinase-mediated excision of the ATPase domain only survived to P25-P40, while heterozygous littermates have similar viability to wild-type animals. *Smarca5*$^{-/-}$ animals were embryonic lethal with death occurring between E5.5-E7.5[48], when the neural plate begins to form[53]. Unsurprisingly, *Smarca5*$^{-/-}$ blastocysts begin to display defective proliferation at the blastocyst stage[48]. *In situ* hybridization analysis of *Smarca5* suggests a critical early-developmental role for Snf2h in the brain; at E13.5 there is heightened *Smarca5* found in the cerebellum and neocortex with lower expression throughout the embryo[19]. This expression recedes postnatally in brain tissue[19]. In the post-natal mouse, Snf2l's expression, compared to the ubiquitous Snf2h expression, is more precisely limited to the hippocampus, the cerebellum and gonads[54,55]. In addition to Snf2l's expression towards the differentiation stage of neurodevelopment, Snf2l employs a splice site variant to control tissue-specific remodelling activity[49]. This variant includes an

additional exon (exon 13), adding 12 additional amino acids that disrupts the activity of the ATPase domain without preventing complex formation[49].

Snf2h's genomic binding sites are extensive, as ChIP-Seq experiments have uncovered that Snf2h binds to 46,614 sites, over half of which are located within genes and promoters[56]. A number of these genes are likely to be TFs. It has been roughly estimated that between 1,000-10,000 genes are involved in transcriptional regulation of neurons, many of which are transcription factors required for downstream effectors critical for both developing and adult neural tissues[57]. As ISWI proteins are prominent in both progenitor and differentiated cells in the brain and have been demonstrated to be recruited to a vast number of loci[58], a role for them as master regulators of the transcriptome during neurodevelopment is beginning to emerge.

1.3 Neurodevelopment

1.3.1 Early embryonic development

Shortly after conception, the embryo is formed and is composed of 3 main cellular compartments; the ectoderm, mesoderm and endoderm. These ultimately give rise to all organs as well as peripheral tissues required for embryo survival. In particular, the nervous system is derived from ectodermal cells[59]. Onset of gastrulation establishes the primitive streak in order to delineate the anterior-posterior axis of the embryo via signalling of a number of concerted signalling factors and gene expression changes[59]. In order to form the future brain and spinal cord, the neural plate of the ectoderm undergoes neurulation to create the neural tube by E9.0[60]. At this stage, the anterior region of the

neural tube goes on to form three further distinct regions of the brain; the forebrain, midbrain and hindbrain[61]. While the ISWI proteins are important to the development of all three brain regions this thesis will focus on the developing hindbrain, specifically cerebellar development.

1.3.2 The emerging cerebellum

The cerebellum is a distinct structure which emerges from the hindbrain region of the embryonic brain around E8.5[62]. Distinction of the borders of the cerebellum and establishment of patterning is ensured by tightly regulated expression of *Hoxa2*, *Otx2* and *Gbx2*, and loss of these expression patterns can significantly impair cerebellar expansion, growth and differentiation[63–65]. Shortly following the delimitation of the developing cerebellum, the rhombic lip located in the dorsal region begins to produce the main neuronal cell in the cerebellum, the granule neuron progenitors (GNPs)[62]. The second such germinal center of the developing cerebellum is the ventricular zone (VZ) wherein Purkinje cells are produced as early as E12.5[66,67]. These progenitors remain at the surface of the cerebellum forming the external germinal layer (EGL) and express Atoh1 which allows them to retain their proliferative capacity into post-natal stages[62,68] (Fig 3). Soon after birth (P4-P6), GNP pools undergo rapid expansion in the EGL which is followed by cell cycle exit and migration through the Purkinje cell layer into the internal germinal layer (IGL) where the differentiated GNPs, granule neurons (GNs) remain[62,67] (Fig 3). This controlled switch from proliferation to differentiation and migration is largely mediated by sonic hedgehog (Shh), a signalling factor which is released by Purkinje cells and regulates the proliferative state of GNPs *in vivo*[69,70].

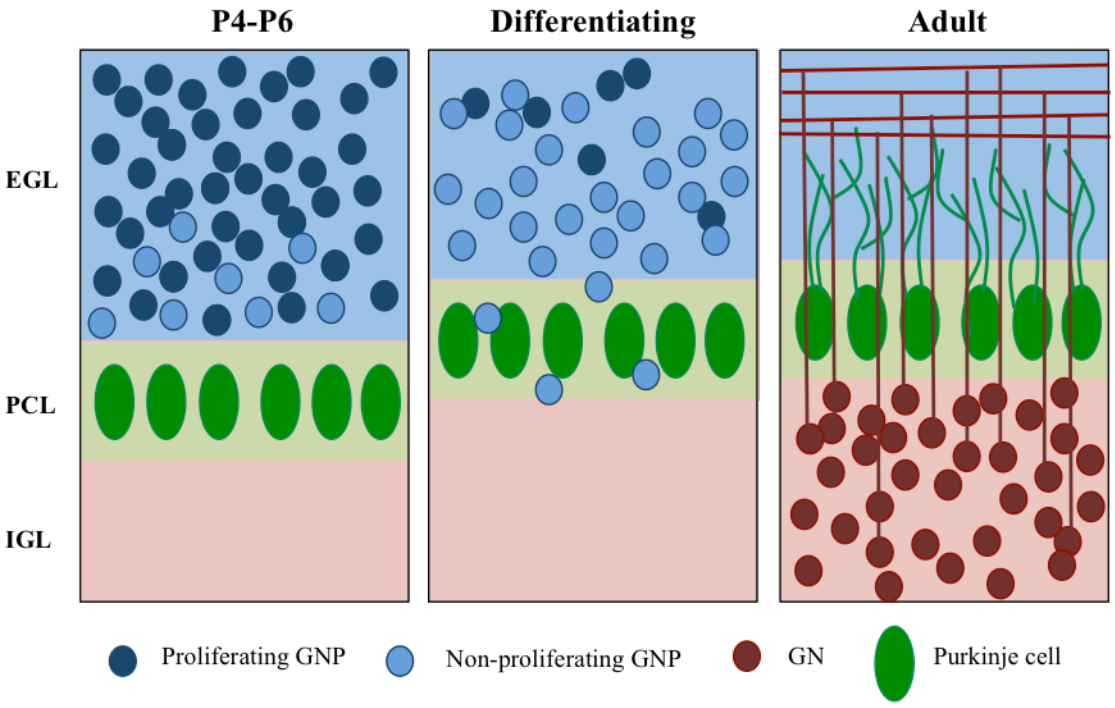


Figure 3. Granule neuron progenitor (GNP) maturation in post-natal cerebellar development. The proliferating external germinal layer (EGL) resides at the surfaces of the cerebellum after birth, where GNPs undergo rapid expansion. At the onset of differentiation, GNPs exit the cell cycle and begin to migrate towards the internal germinal layer (IGL). Differentiated granule neurons (GN) reside in the IGL and project their axons through the intermediary Purkinje cell layer (PCL). Figure adapted from Marzban *et al*., 2015 and Butts *et al*., 2014.

Generally, this process is complete by P21 in mice, and the adult cerebellum is central in synchronizing numerous neural processes involved in motor coordination, cognition and learning. Cerebellar defects have been tied to ataxia, but have now also been suspected to contribute to autism spectrum disorders (ASD) and cognitive deficiencies as well[71].

1.4 ISWI mouse models

1.4.1 Snf2h cKO mouse model

As Snf2h is most highly expressed in progenitors and has ubiquitous expression throughout the majority of tissues, complete knock-out (KO) of *Smarca5* has proven to be lethal at the implantation stage[48]. Therefore, a conditional KO (cKO) system was employed in order to preserve mouse viability by ablating *Smarca5* activity following critical embryonic stages. To achieve this, our group has previously developed a Snf2h cKO wherein loxP sites were placed on either side of exon 5 of the *Smarca5* gene (which allows for Snf2h's ATP-binding activity) and excised upon expression of Cre maintained by a *Nestin* promoter, which is expressed by E11 in cerebellar progenitors[50]. Resulting cKO mice were smaller than WT littermates, displayed ataxia due to a small, disorganized cerebellum and ultimately died around P40[50].

1.4.2 Ex6DEL Snf2l mouse model

In order to ablate Snf2l activity, a similar approach as for Snf2h was undertaken in this mouse model. Exon 6 of *Smarca1*, containing the SNF2 domain responsible for Snf2l ATP-binding was excised by *Gata1*-Cre (which provides ubiquitous expression of Cre

early in embryonic development[72]). The resulting Ex6DEL mice were viable, fertile and displayed no significant behaviour deficits[73]. Intriguingly, Ex6DEL mice were observed to have a larger head, and in particular an increase of brain to body mass ratio compared to WT mice. Coronal sections of the brains of Ex6DEL animals revealed increased cell numbers in cortical layers at multiple timepoints, and up-regulated proliferation and self-renewal of progenitor cells. While laminar positioning of cells in the cortex was not modified, cell fate determination was delayed as cells of layers I and VI were born around E12.5 in Ex6DEL, while in normal cortical development these layers begin to be established at E11.5[73]. Recently, our group has also noted a significant increase in the size of the cerebellum in these animals as well, reminiscent of the cortical phenotype observed previously (Fig 4).

1.5 ISWI proteins are the molecular motors for chromatin remodelling complexes

1.5.1 The importance of non-catalytic subunits

While capable of remodelling nucleosomes alone, chromatin remodelling proteins are typically found in chromatin remodelling complexes *in vivo*. In *Drosophila*, Isw1 is capable of forming two distinct chromatin remodelling complexes, Isw1a and Isw1b[74]. In mammals, the presence of multiple functionally redundant complexes, containing either Snf2h or Snf2l and varying in non-catalytic subunit composition can be a manner by which the organism can regulate specific modifications to the chromatin landscape. It

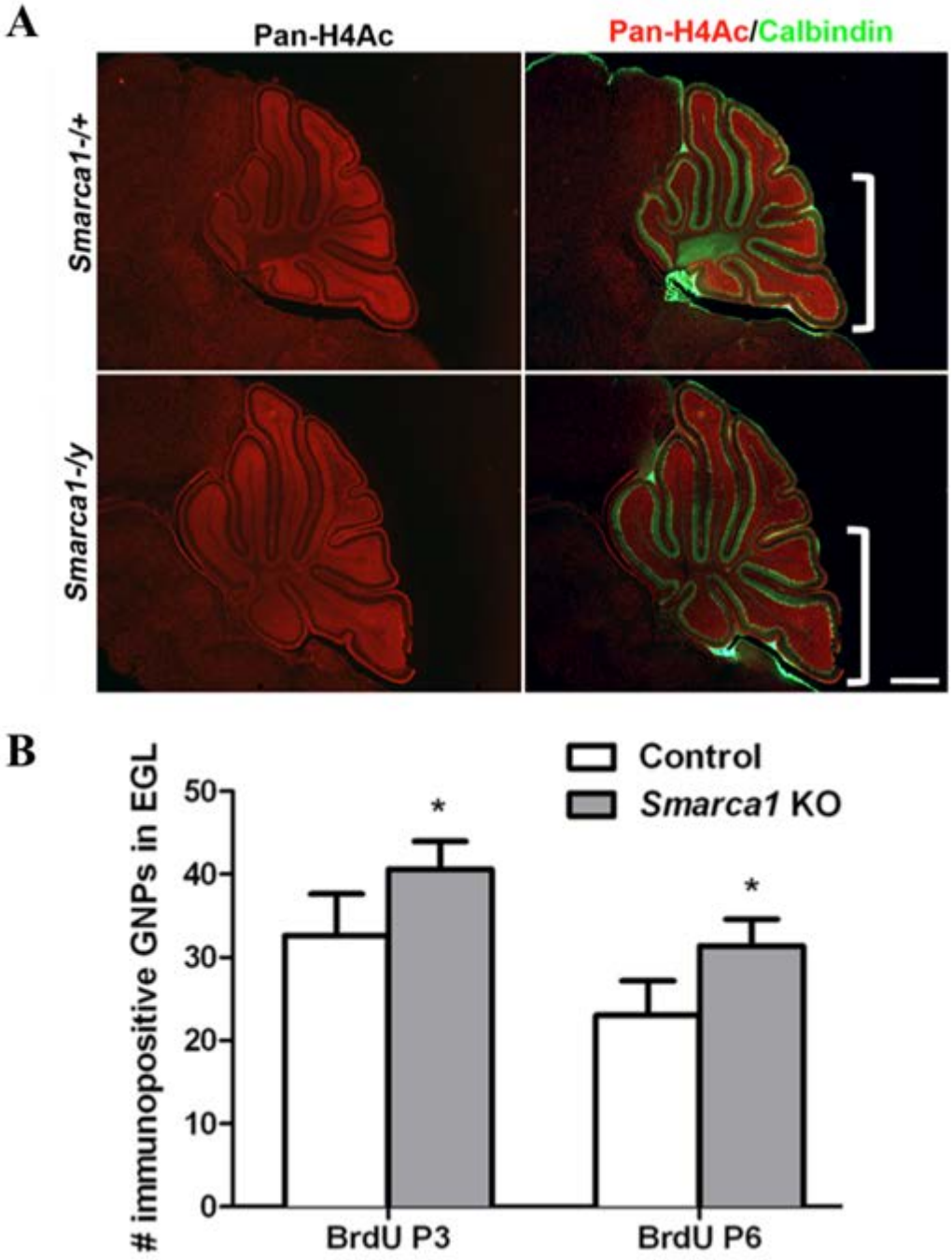


Figure 4. Loss of Snf2l activity results in increased cerebellar size. (A) Sagittal brain section of P9 WT (Smarca1-/+) and Ex6DEL (Smarca1-/y) stained with pan-H4ac to mark active transcription, and calbindin, a marker of Purkinje cells. Scale bar = 500 μM. **(B)** BrdU positive GNPs in the EGL of WT (control) and Ex6DEL (Smarca1 KO) cerebellum at P3 and P6. *p<0.05. Figures generated by Dr. Matias Alvarez-Saavedra.

then falls, in part, to the non-catalytic subunits to contribute to target specificity, activity and remodelling outcomes[17,26,75,76]. By sequestering ISWI into specific complexes, activity can be shifted to other targets[77], alter its functional remodelling of nucleosomes[78] or modify activity level compared to that of Snf2h or Snf2l alone[79]. A recent review highlights ISWI regulation via non catalytic interacting partners[22]. In general, many ISWI non-catalytic subunits contain bromodomain adjacent to zinc finger (BAZ) domains (with the exception of Rsf1 and Bptf), plant homeodomains (PHD) as well as AT hooks and DDT domains. There are five Snf2h-specific chromatin remodelling complexes identified, RSF (Rsf-1), ACF (Acf-1), CHRAC (Acf-1, CHRAC-15, CHRAC-17), WICH (Wstf) and NoRC (Tip5), as well as two Snf2l complexes, NURF (Bptf) and CERF (CECR2) (Fig 5). More recently, one study has indicated that Snf2h and Snf2l are interchangeable, thus doubling the total number of ISWI complexes[80].

1.5.2 Complex-specific activity during development

Numerous studies demonstrate the important role that ISWI chromatin remodelling complexes play in cell homeostasis including catalyzing positioning of nucleosome arrays and NFRs to modify transcriptional output[34–37], define heterochromatic regions and allow for their replication[38–40], mediate DNA repair[41–45] and rRNA regulation[46].

As cellular differentiation occurs, requirements for gene heterochromatinizion increases in order to restrict cell fate. In *Drosophila*, Nurf201 (BPTF) and ISWI are both required to maintain X chromosome chromatin and to regulate H1 deposition to suppress gene expression[81,82]. ISWI non-catalytic subunits ACF1 and RSF1 have been determined to be

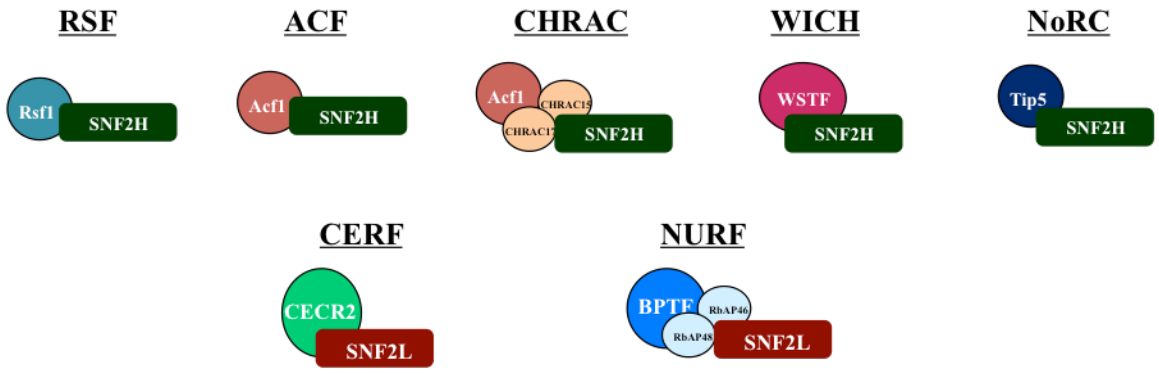


Figure 5. ISWI chromatin remodelling complexes. Complexes contain either Snf2h or Snf2l catalytic cores. Canonically, five Snf2h complexes have been described (RSF, ACF, CHRAC, WICH, NoRC) and two Snf2l complexes (CERF and NURF), each containing unique non-catalytic interacting partners (which themselves can interact with a number of non-ISWI proteins).

involved in nucleosome deposition and centromeric-specifc nucleosome repositioning, while NoRC activity represses rDNA[38,83–86]. Therefore, the ISWI proteins' ability to regulate replication and transcription through nucleosome sliding likely contributes to their importance in mediating differentiation in cells. ISWI proteins also exploit their nucleosome-sliding activity to generate or regulate NFRs. Studies have shown that yeast Isw2 mediates NFRs around promoters to reduce transcription of target genes, while the Isw1b complex re-establishes genomic nucleosome arrays following transcription[87–90]. To this end, they have been reported to bind both within genes as well as intergenic regions in order to remodel the nucleosomes immediately downstream from the TSS[31]. Analysis of mammalian SNF2H and SNF2L genomic binding sites indicate that these proteins are typically found near the TSS of genes in order to remodel nearby nucleosomes. While SNF2H efficiently remodels in proximity to CTCF (a TF and insulator protein), SNF2L only appears to play a minor role in modifying those arrays[36]. In this context, depletion of SNF2H drastically disrupted this nucleosome positioning while loss of ACF1, RSF-1, TIP5 and WSTF had less pronounced effects on chromatin adjacent to CTCF[36]. Therefore, there may be functional redundancy amongst SNF2H complexes which allows for one complex to compensate for the loss of another. Additionally, the NURF complex is able to regulate gene expression by binding TFs and sequestering them to target loci[35,37,54,91,92]. It is therefore likely that ISWI complexes are essential in neural progenitor pools to regulate gene expression both via nucleosome sliding to mediate NFRs and TF binding at promoters.

While both ACF and WICH hold a central role in mediating heterochromatic regions, they act in a complementary manner in S-phase. ACF acts downstream of replication forks to reduce condensation of chromatin to allow for strand separation and replication machinery positioning, while WICH re-establishes nucleosome arrays on nascent DNA following replication[93,94]. Therefore, Snf2h chromatin remodelling complexes appear to be highly involved in actively replicating cells, which may shed light on the requirement for high Snf2h expression in progenitor neurons of the forebrain in early development[19,48].

The NURF complex is involved in activating transcription of genes involved in the Notch pathway during development via interactions with the Putzig-TRF2-DREF complex[95]. Likely owing to these crucial interactions, *Bptf* knock-out models are embryonic lethal, due to gastrulation defects and insufficient development of certain embryonic tissues[91]. By approximately E6.5, most Bptf-deficient animals have insufficient trophoblast size[96]. A marked defect of the ectoplacental cone is also noted, resulting from reduced cellular proliferation[96]. Concomitantly, NURF has been reported to have many interactions with various TFs crucial for early development and patterning (reviewed in[20]). Studies have also delved into NURF's association to SMAD transcription factors[20]. SMAD-2 and NURF cooperate early in embryogenesis to regulate the patterning of the zebrafish ectoderm by means of regulating the wnt8a promoter[97]. In the absence of Bptf, anterior ectoderm proliferation is not curbed at the expense of the posterior neuroectoderm[97]. The influence of NURF in development, while critical, may vary according to cell populations[37,91] and likely has a part to play in cellular differentiation[52,91].

CECR2 expression is quite widespread in early embryonic stages, however it adopts a more restricted profile in neural tissue by E13.5[32,98]. In a study conducted with a CECR2^{Gt45Bic} genetrap construct in mouse in which the C-terminus of the protein is absent resulting in a loss-of-function model, homozygous progeny were found to have high perinatal mortality rates due to deficient neural tube closure resulting in embryonic exencephaly[32]. Work in a CECR2$^{tm1.1Hemc}$ null mutant line also reveals similar exencephaly paired with significant downregulation of transcription factors (*Alx1, Dlx5, Eya1, Six1, Epha7*) found in developing and differentiating neural tissue[99]. Collectively, these data suggest a crucial role for CERF in neurulation and transcriptional control of the brain in early development.

1.6 Intellectual disability (ID), neurodevelopmental disease (NDD) and autism spectrum disorder (ASD)

NDDs present as either ID, neuropsychiatric syndromes or ASD and have a high prevalence globally, with recent estimates of ID occurrence in 1% of the population, and this fraction increases drastically in lower-income countries[100]. Comorbidity of ASD in ID reaches 18%[101], suggesting similar underlying molecular mechanisms may be at play in both disorders. Identification of direct causes of NDD is difficult due to wide spectrums of clinical manifestations and abundant risk factors or contributors to disease. However, a recent systematic analysis has provided a database of 746 ID-associated genes within which there was enrichment for terms related to chromatin regulation and control[102]. Additionally, a meta-analysis of exome sequencing in ASD identified over a

hundred genes with high likelihood of mutation, in which there was significant enrichment for genes involved in chromatin regulation [103].

1.7 Emerging evidence for involvement of ISWI remodelling complexes in NDDs

1.7.1 Recent leads on a new suspect: Snf2l and ID

As ISWI proteins are powerful mediators of the regulation of brain development, mutations to these chromatin remodelling proteins are suspected in a number of neurodevelopmental disorders, in particular the X-linked gene *SMARCA1*. Previous work found that loss of ISWI in *Drosophila* leads to modifications in chromatin structure and transcriptome, however these effects are most severe on the male's single X chromosome at the TSS of a multitude of genes[31]. Early studies involving families whose ID was linked to Xq25-26, the location of the *SMARCA1* gene did not uncover any mutations [104]. When next generation sequencing methodologies were used to study 128 families affected by NDDs, a patient with microcephaly and intellectual disability was found to harbor a hemizygous deletion of *SMARCA1*[105]. Similar studies of Rett syndrome[106] and schizophrenia[107] patients revealed *de novo SMARCA1* mutations potentially underlying both pathologies.

Patients with Rett syndrome experience a range of symptoms and physical manifestations including the loss of acquired motor skills, language as well as autistic-like behaviour[108]. This X-linked neurodevelopmental disorder results in smaller brains, reduced cortical layer thickness and abnormal synapse formation[108]. While Rett syndrome is typically

known to be caused by a *MECP2* mutation, a 25 year old patient diagnosed as suffering from Rett syndrome was found to harbour a *SMARCA1* G966V *de novo* mutation[106]. Additionally, a sequencing study of families with schizophrenic-like symptoms identified one family with a deleterious V384M *SMARCA1* mutation shared between four siblings with schizophrenia, suggesting it was potentially causative[107]. The location of these *SMARCA1* mutations are summarized in Fig 6.

1.7.2 ISWI and the cerebellum in ASD

Symptoms and physical manifestations displayed by patients affected with ASD can be varied, ranging from hindered motor and language skills to an inability to maintain social interactions. The wide range of phenotypic variability amongst ASD patients is likely a reflection of the significant genetic heterogeneity of ASD etiology. Recent evidence is emerging suggesting ISWI dysfunction may be implicated in the onset of ASD due to Snf2h and Snf2l's critical roles in cerebellar development[71]. Purkinje cell populations are depleted and dysfunctional in ASD mouse models[71]. This is reminiscent of the phenotype resulting from cKO of Snf2h, wherein we have previously observed ataxia as well as marked cognitive defects[50].

Neurogenesis and maturation of the cerebellum is tightly regulated and mediated by numerous transcription and signalling factors[62]. Amongst these, Foxg1 has been recognized as a critical transcription factor in the regulation of numerous aspects of neurodevelopment. We have previously observed that mice lacking active Snf2l protein have hypercellularity of the cerebral cortex as well as the cerebellum[73]. Genomic



Figure 6. Schematic of reported disease-associated mutations in *SMARCA1*. Three distinct mutations in the *SMARCA1* gene have been reported in cases of ID, schizophrenia and Rett-like syndrome. Black lines indicate the approximate location of point mutations identified in the *SMARCA1* gene, with ATPase and HAND-SANT-SLIDE (HSS) domains identified.

analyses revealed a significant aberrant increase of *Foxg1* expression in this murine model. Further investigation determined that Snf2l negatively regulates Foxg1 levels via direct remodelling mechanisms and therefore plays a critical role in proper cerebellar development[73]. A recent study further probed the importance of FOXG1 in neurodevelopment while investigating neural cultures isolated from ASD patients. Their findings revealed misregulation of *FOXG1* expression. They suggested that this alteration leads to an increase of inhibitory GABAergic neurons which may contribute to the onset of ASD pathology[109]. In fact, individuals with FOXG1 syndrome (formerly congenital variant Rett syndrome) exhibit ID, epilepsy, dyskinesia, microcephaly and corpus callosum defects[110–115]. FOXG1 syndrome has been demonstrated to be caused by mutations or deletions of the FOXG1 gene[110–115] which is evolutionarily conserved for its key role in mediating neurodevelopment[116,117].

1.7.3 WICH complex and Williams-Beuren syndrome

The WICH complex, typically composed of Snf2h and Wstf has been identified as a contributing factor to Williams-Beuren syndrome, a hereditary disorder characterized by facial dysmorphia, ID and a range of motor limitations[118,119]. Genetic causes underlying this disorder stem from a 1.3 Mb deletion of chromosome 7 in these patients, which can ablate between 17-28 genes, including *WSTF*[118,119]. In particular, WSTF would appear to be contributing largely to the facial feature dysmorphia, a role which has been supported in a Wstf mutant mouse line as well as in *Xenopus*[118,120,121]. Additionally, the behavioural and intellectual deficiencies linked to Williams-Beuren syndrome may also be partially attributed to WICH's role in neural mechanisms. Up-regulation of Wstf in the nucleus

accumbens has been shown to be linked to increased resistance to social defeat stress tests, and up-regulation of both WICH complex subunits was observed in mice who self-administered cocaine dosages[122,123].

1.7.4 CECR2 and Cat eye syndrome

Cat eye syndrome results from a duplication of a large segment of chromosome 22 resulting in facial dysmorphia, ID and numerous organ defects[124]. Similarly to Williams-Beuren syndrome, the genomic region which undergoes duplication is variable, but a minimum of 2 Mb of 22q11.2 has been reported to be associated to the Cat eye syndrome features[125]. *CECR2* is found within this disrupted region and while etiology of this disorder is not yet clear, CECR2's involvement in embryonic and post-natal neurodevelopment as well as neurulation makes CERF activity a likely contributor to the clinical presentation of this genetic disorder[32,99,126].

1.7.5 Wnt deregulation and schizophrenia

Post-mortem studies have long revealed deregulation of neurogenesis and differentiation in adult brains of schizophrenia patients, defects which are suspected to originate from incorrect Wnt pathway signalling[127,128]. This pathway, which can often find itself mediating the switch between cell expansion and maturation during neurogenesis, may require ISWI non-catalytic subunits. Indeed, Wstf has been shown to co-localize with Frz-3 and Wnt-4 in the neural tube and midbrain, suggesting the possible regulation of members of the Wnt pathway by Wstf.[129]. In *Drosophila*, NURF and Acf1 were both found to maintain expression of members of the Wnt pathway, while NURF may also be

required for proper activity of the Notch signalling pathway with which it has significant crosstalk[130]. Extensive work studying gene expression in the prefrontal cortex of post-mortem schizophrenia brains has revealed a consistent increase of ACF1[131,132]. Thus, ACF and NURF activity may be required to promote proper Wnt signalling in early neurodevelopment, yet ACF appears to extend its role into adulthood.

1.8 Aims and rationale

Our group has previously demonstrated that the loss of Snf2l activity (Ex6DEL) leads to increased brain mass due to a thicker cortex as a result of additional rounds of replication of progenitor pools prior to differentiation. A recent finding has determined that the cerebellum of these animals is also significantly enlarged compared to WT mice (Fig 4). Recent discovery of mutations in the *SMARCA1* gene in the context of NDDs (Fig 6) has renewed interest in the potential role ISWI proteins may play in successfully mediating brain development, in particular in the cerebellum, a region of the brain which is being studied for its contribution to ASD[71]. While much is known about Snf2h genomic interactions and critical roles in development[48,50,56], the molecular function of Snf2l in mediating proper neurodevelopment largely remains to be understood. We **hypothesize** that Snf2l and its non-catalytic subunits are required to maintain critical chromatin states and regulate gene expression programs in the developing cerebellum. To this end, we have outlined three specific aims to begin to address this hypothesis;

1. Establish and characterize primary GNP cultures from both WT and Snf2l Ex6DEL mice

2. Assess changes in gene expression underlying the Ex6DEL GNP phenotype

3. Identify chromatin accessibility modifications resulting from the loss of active Snf2l.

2. Materials and Methods

2.1 Mouse Work

2.1.1 Animal Care

Mouse work was approved by the University of Ottawa's Animal Care committee and the Canadian Council on Animal Care and maintained compliance under the Ontario Animals for Research Act. Mice were housed at the University of Ottawa's Animal Care and Veterinary Services facility, and were exposed to regular light-dark cycles with food and water provided *ad libitum*. Matings were set up with one male in a cage with two females from which pups were removed between 4-6 days after birth for GNP isolation or cerebellum collection, or left until weaning age (21 days) for cerebellum collection.

2.1.2 Mouse lines

Snf2l Ex6DEL mouse line has been previously generated and described by our group[73]. Briefly, loxP sites were placed flanking exon 6 of *Smarca1* which contains the SNF2 domain that allows for ATP-binding activity of the gene product. *Smarca1*$^{y/f}$ mice were bred to *Gata1*-Cre (which express Cre globally early in embryonic development[72]) mice

on the FVB/N background in order to excise nucleic acids within the flanked region. The resulting Ex6DEL mice were viable and fertile and were thereafter bred independently of *Gata1*-Cre. *Smarca5*$^{f/f}$ mice were previously generated and described by our group[50]. Similarly to the generation of the Ex6DEL mice, loxP sites were positioned on either side of exon 5 of the *Smarca5* gene which encodes for Snf2h ATP-binding activity, analogous to exon 6 of *Smarca1*. *Smarca5*$^{f/f}$ on the FVB/N background were used as control animals in this study, and hereafter referred to as wild-type (WT).

2.1.3 Genotyping

Genotyping was performed from genomic DNA (gDNA) from freshly isolated GNPs following dissection (see 2.2.1 for GNPS isolation). To obtain genomic DNA, GNPs were placed in gDNA lysis buffer (100mM Tris pH 8, 5mM EDTA, 200 mM NaCl, 1% SDS) with 0.2% proteinase K (Thermo Scientific, cat # 17916) for at least 1 h on a 55°C heat block and then centrifuged to isolate supernatant. One volume 100% EtOH was added to the supernatant, mixed and then centrifuged at 13,300 RPM (accuSpin™ Micro17, Fisher Scientific) for 10 min. The pellet was washed in 70% EtOH and resuspended by heating at 55°C. PCR was then performed on 1.5 µL isolated gDNA by preparing a PCR reaction (0.25 µL Taq, 2.5 µL 2.5 mM dNTP, 0.75 µL 50 mM $MgCl_2$, 0.5 µL primers (Table 1) and 1X PCR buffer) and cycling under the following conditions: 94°C for 2 min, 39 PCR cycles (94°C for 30 sec, 60°C for 30 sec, 72°C for 45 sec) and a final cycle at 72°C for 10 min. PCR reactions were then run on a 1.5% agarose gel as described in 2.1.4.

Table 1. Genotyping primers

Primer	Sequence
Smarca1Intron6_R	GTATGGACAAGTGTGTGAAGCC
Smarca1Intron5_F	CCTGGGCTGGAACCATGATC
Smarca1Exon6_R	CCATGTGGGGTCCAGGAATG

2.1.4 Nucleic acid visualization

Agarose gels were prepared by melting 1.5% or 2% agarose (Thermo Fisher, cat # 16500500) in 100 mL 1X TAE in a microwave, and then cooling the flask slightly under running water. Diluted ethidium bromide solution was carefully added prior to solidifying the agarose in the gel casting tray. Samples were run alongside a DNA ladder (Invitrogen, cat # 10787-026) at 80V for approximately 20 min prior to UV visualization.

2.2 GNP

2.2.1 Isolation and *In vitro* Culture

GNPs were isolated from the cerebella of P4-P6 pups. This methodology has been published previously[133], and reported to result in GNP cultures 95-99% pure. Briefly, cerebella were collected and dissociated with papain (Worthington, cat # LS003126), followed by gentle shearing with a fire-polished glass pipette. Resuspended cells were separated from undigested debris and passed through an ovomucoid inhibitor (Worthington, cat # LS003087) gradient. Cells were then resuspended and passed through a 60%-35% Percoll gradient (Sigma, cat # P4937) wherein GNPs remained at the interphase between 60% and 35% Percoll. Once collected, the GNP pellet was resuspended in serum-containing Neurobasal™-A medium (Thermo Scientific, cat # 10888022) and preplated on a dish coated with 0.1 mg/mL Poly-D-lysine hydrobromide

(PDL) (Sigma, cat # P6407) for 20 min at 37°C. Remaining larger neurons and astroglia adhere to the surface, while GNPs are collected following being dislodged by gentle shaking. Cells are then seeded in serum-free Neurobasal™-A medium supplemented with B-27 supplement (Thermo Scientific, cat # 0080085-SA) at a density of $3x10^6$ cells/well in 6 well plates or $5.5x10^5$ cells/well of a 24 well plate previously coated with 1 mg/ml PDL in an incubator maintained at 37°C with 5% CO_2. Twenty-four hours following isolation, a partial media change is carried out, and repeated every 48h.

2.2.2 BrdU Pulse Labelling

GNPs plated on coverslips were pulsed for 2 h upon addition of 50 μM BrdU (Sigma, cat # B-5002) to the growth media at 37°C, and then washed carefully 3 times in PBS following pulse. Coverslips were then fixed, prepared and stained as described in section 2.2.3. An additional 10 min in 2.5M HCl incubation was required for detection of BrdU-labelling and was performed prior to blocking.

2.2.3 Immunostaining and Counting

Cells plated on round (VWR, cat # 89015-725) or square (VWR, cat # 48366-067) coverslips were gently washed twice in PBS and then fixed in 2% PFA for 10 min at room temperature (RT). PFA was then removed and coverslips were washed 3 times in PBS. Coverslips were permeabilized for 10 min at RT in PBS containing 0.03% triton followed by a brief PBS wash. A blocking solution comprised of 10% horse serum (Life Technologies, cat # 26050-088) in TBST with BSA was applied and allowed to incubate for 1 h RT. Primary antibodies were diluted in blocking solution (see Table 2 for

dilutions), applied to coverslips overnight at 4°C and then washed 3 times in PBS. Secondary Alexa Fluor® (Jackson Immunoresearch) antibody was diluted 1:4000 in PBS and applied to coverslips for 30 min RT, taking care to avoid light exposure. Coverslips were washed 3 times in PBS and incubated for 5 min in a 1:10000 bis-benzimide-Hoescht 33342 (Hoescht, DAPI) (Sigma, cat # B2261) solution in PBS. Following three PBS washes, coverslips were mounted onto slides with mounting medium (Agilent Technologies, cat # S3023). Coverslips were imaged with an Axio Imager M1 microscope (Zeiss) using either 20X or 40X objectives. Images were prepared with Fiji software[134] (version 2.0.0). All positive cell counts were performed relative to total nuclei and statistically analyzed by two-way ANOVA.

Table 2. Antibodies used for immunofluorescence and immunoblotting

Antibody	Species	Manufacturer	Western dilution	Immunofluorescence dilution
Snf2l	Rb	Abcam (ab37003)	1:2000	1:500
Snf2h	Rb	Abcam (ab72499)	1:2000	1:500
Vinculin	Rb	Abcam (ab129002)	1:2000	-
Tubulin	Rb	Sigma (T6199)	1:2000	-
β-actin	Ms	Sigma (A1978)	1:50000	1:500
Ki67	Rb	Abcam (ab16667)	1:2000	1:500
NeuN	Ms	Milipore (MAB377)	1:2000	1:500
BrdU	Ms	BD Biosciences (347580)	-	1:500
CECR2	Rb	Gift from Dr. H.E. McDermid	1:1000	-
Wstf	Rb	Gift from Dr. H.E. McDermid	1:500	-
BPTF	Rb	Thermo Fisher (ABE24)	1:1000	-
ERK	Rb	Santa Cruz (sc154)	1:2000	-
pERK	Ms	Santa Cruz (sc7383)	1:500	-
ELK1	Ms	Santa Cruz (sc365876)	1:500	-
pELK1	Ms	Santa Cruz (sc8406)	1:500	-
Tip5	Rb	Gift from Dr. H.E. McDermid	1:2000	-
Acf1	Rb	Gift from Dr. H.E. McDermid	1:12000	-
RbAp48	Ms	Upstate (05-524)	1:2000	-
GFAP	Rb	Stemcell Technologies (01415)	-	1:500
NF200	Rb	Sigma (N4142)	-	1:500
Tuj1	Ms	Stemcell Technologies (01409)	1:2000	-

2.2.4 Cell Viability

Media was removed from GNPs, and cells were resuspended in 500 μL ice-cold PBS with a cell scraper. GNPs were placed into a Beckman Coulter Vi-CELL™ XR Cell Viability Analyzer cell and run through default cell counting system (cell size 5-50 μM). Cell viability was assessed by trypan blue dye exclusion method, which was added to cells during the cell count analysis.

2.3 Protein Analysis

2.3.1 Cerebellar Protein Isolation

P5 and P21 pups were asphyxiated using CO_2 and decapitated using scissors. Cerebella were carefully removed with forceps, and placed on ice prior to being resuspended in 1 mL ice-cold lysis buffer (20 mM Tris-HCl pH 8, 137 mM NaCl, 1% NP-40, 2 mM EDTA) supplemented with protease inhibitor cocktail (Sigma, cat # P8340) or protease and phosphatase inhibitor cocktail (Fisher, cat # 78441). Tissue was sheared manually and then placed on a rotating platform for 10 min at 4°C. Lysates were centrifuged at 13,000 RPM in a microcentrifuge (Galaxy 20R, VWR) set at 4°C for 5 min, then added to 4X NuPage LDS sample buffer (Thermo Fisher, cat # NP0007) and boiled at 95°C for 5 min, followed by a 2 min incubation on ice.

2.3.2 GNP Protein Isolation

Cell lysates were prepared by removing media, rinsed cells twice in PBS and removed them from the plate surface with a cell scraper. Cells were pelleted briefly and

resuspended in ice-cold lysis buffer supplemented with protease inhibitor cocktail or protease and phosphatase inhibitor cocktail and placed on a rotating platform for 10 min at 4°C. Lysates were cleared of debris by centrifugation at 13,000 RPM in a microcentrifuge (Galaxy 20R, VWR) set at 4°C for 5 min, then added to 4X NuPage LDS sample buffer and boiled at 95°C for 5 min, followed by a 2 min incubation on ice.

2.3.3 Immunoblotting

An 8% polyacrylamide SDS-PAGE gel was loaded with boiled sample and 5 µL of Blueye Prestained Protein Ladder (FroggaBio Inc, cat # PM007-0500) and electrophoresed at 170V for 75 min in 1X running buffer (10X; 25 mM Tris, 192 mM glycine, 0.1% SDS). Protein was transferred onto a PVDF membrane (BioRad, cat # 162-0177) for 1 h at 100V in 1X transfer buffer (50mM Tris, 40 mM glycine, 20% MeOH). Membrane was rinsed in PBS and blocked with 5% milk powder in TBS-T (20mM Tris-HCl pH 7.5, 150mM NaCl, 0.1% Tween20) for 1 h RT on a rotating platform. The membrane was placed in TBS-T containing 5% BSA with 0.03% sodium azide and primary antibody-dependent concentration (Table 2) overnight at 4°C. Membrane was washed three times in TBS-T for 10 min each and incubated for 1h RT in TBS-T containing 5% skim milk with 1:25000 HRP-conjugated species-specific secondary antibody. Wash steps were repeated and membranes were incubated for 2 min in Clarity™ Western ECL Blotting Substrate (BioRad, cat # 170-5061) or SuperSignal West Femto Maximum Sensitivity Substrate (ThermoFisher Scientific, cat # 34095) solutions. Protein signals were detected with film (Harvard Apparatus Canada, cat # DV-E3012).

2.3.4 Protein Quantification by Densitometry

Films (section 2.3.3) were scanned and saved as .jpg images prior to being opened in Fiji. Measurements of identical areas were taken for each band based on 'grey mean value' setting. Relative protein expression was determined by subtracting background signal from bands, and calculating expression ratios to loading control.

2.3.5 Co-Immunoprecipitation (coIP)

Cerebellar lysates were prepared immediately following dissection as described above (section 2.3.1) and protein content from the supernatant was quantified by Bradford assay (BioRad, cat # 500-00006) in a cuvette at 595 nm. Each IP was prepared with 500 μg protein lysate, 1 μg antibody (either Snf2l, CECR2 or Rb IgG control) and lysis buffer supplemented with protease inhibitor was used to bring the total volume of the IP to 500 μL. IPs (including negative IgG control – NEB, cat # 2729S) were rocked overnight at 4°C. The following day, 30 μL of Protein A/G magnetic beads (Bioclone Inc, cat # MA-102) were aliquoted into a microcentrifuge tube and placed on a magnetized stand (Thermo Fisher) so they could be rinsed once with two volumes of non-denaturing lysis buffer. Buffer was removed and beads were resuspended at a 1:1 ratio in lysis buffer. The 30 μL bead slurry was added to each IP reaction. Capture occurred on a rocking platform at 4°C for 1 h. Beads were washed 5 times in 1 mL 0.3% triton-X in PBS, wherein tubes were placed on a rocking platform at 4°C for 5 min. Following the last wash, beads were resuspended in 0.1M glycine (pH 2.5) elution buffer and elution took place at RT for 10 min, shaking every few mins. Tubes were centrifuged briefly and eluate was recovered taking care to avoid pelleted beads. Elution was repeated 3 additional times, with total

volumes being pooled. Eluted samples were diluted 1:3 in 1X NuPAGE LDS Sample Buffer and 1.5% β-mercaptoethanol (Sigma, cat # M7522) was added to each sample. Diluted samples were boiled briefly at 95°C for 5 min prior to immunoblotting (section 2.3.3). Boiled eluates were stored short term at -20°C or long term at -80°C.

2.4 Sequencing

2.4.1 RNA Isolation

GNPs were pelleted and immediately resuspended in 1mL TRIzol (Life Technologies, cat # 15596018) and either stored in -80°C or proceeded directly to isolation. RNA isolation was performed according to manufacturer's instructions. Briefly, chloroform was added to TRIzol, mixed and centrifuged (12,000xg for 10 min at 4°C) to separate aqueous and organic phases. Aqueous phase was carefully removed and placed in a fresh 1.5 mL microcentrifuge tube containing 500 µL 100% isopropanol and 2 µL glycogen (Ambion, cat # 9510). RNA was pelleted at 4°C and washed once in 75% ethanol. RNA pellets were allowed to air dry and were resuspended in 20 µL nuclease-free water. RNA was stored at -80°C.

2.4.2 RNA-seq Preparation

RNA from GNPs was obtained as described above (section 2.4.1), however the aqueous phase was deposited directly in a PureLink RNA Mini kit silica cleanup tube (Thermo Fisher, cat # 12183020) for in-column cleanup in order to reduce RNA contaminants prior to sequencing. RNA cleanup was performed according to manufacturer's

instructions (Thermo Fisher, cat # 12183020) with addition of optional in-column DNAse digestion (Thermo Fisher, cat # AM1906). RNA was eluted into a sterile 1.5 mL microcentrifuge tube in a volume of 30 µL. A 5 µL aliquot was used to assess RNA integrity by agarose gel analysis (section 2.1.4) and RNA purity and concentration was determined with a 1 µL aliquot using a NanoDrop 2000 spectrophotometer (Thermo Fisher).

2.4.3 RNA-seq

RNA samples were submitted in triplicate to GenomeQuébec (Montréal). RNA integrity was confirmed upon arrival by Bioanalyzer prior to cDNA library generation. Paired RNA-seq was performed on HiSeq4000 PE 100 bp lane and a minimum of 35 million reads was obtained per sample.

2.4.4 RNA-seq Processing and Analysis

Quality control (QC) was carried out on all raw .fastq files obtained from Illumina HiSeq4000 to confirm successful and unbiased sequencing with FastQC (https://www.bioinformatics.babraham.ac.uk/projects/fastqc/) (version 0.11.5). Reads were pseudoaligned to GRCm38 (release 88) by kallisto[135] (version 0.44.0) with bootstraps option set to 50, and quantified by Sleuth[136] (version 0.29.0). Differentially expressed genes (DEGs) were determined with a fold-change threshold of ± 1.5 with qval (pvalue adjusted for false discovery rate (FDR)) ≥ 0.05. Data were visualized using Sleuth, and heatmaps were generated with pheatmap (version 1.0.10) and RColorBrewer (version 1.1-2). Gene Ontology (GO) enrichment analysis

(http://www.geneontology.org/) was performed on significant DEGs for biological process and molecular function terms, where terms were considered to be significantly enriched at fold enrichment ≥ 1.5 and FDR ≤ 0.05. To determine significantly enriched transcription factor binding sites (TFBS) governing up- or down-regulated DEGs, genes with absolute FC ≥ 2 were inputted into oPPOSUM3.0 (http://opossum.cisreg.ca/oPOSSUM3/) for Single Site Analysis with default parameters and enriched TFBS were sorted by Z-score.

2.4.5 ATAC-seq Sample and Library Preparation

Samples were prepared according to Buenrostro *et al.*[137], with slight modification in transposase reaction conditions. Briefly, 50 000 cells were resuspended in PBS and centrifuged at 500xg for 5 min at 4°C twice. Cell pellet was gently resuspended in 50 µL lysis buffer (10mM Tris-HCl pH 7.4, 10 mM NaCl, 3 mM $MgCl_2$, 0.1% IGEPAL) and centrifuged (500xg for 10 min at 4°C) from which the nuclei pellet was conserved and immediately put on ice. Transposition mix was prepared by combining 25 µL Nextera TD 2X reaction buffer and 5 µL Nextera TDE1 Tn5 Transposase (Illumina, cat # FC-121-1030) to 20 µL nuclease free H_2O. Transposition mix was used to resuspend the nuclei pellet, incubated for 40 min at 37°C, with gentle tapping every 10 min. Transposed DNA was purified and eluted in 10 µL Elution Buffer using Qiagen MinElute PCR Purification Kit (Qiagen, cat # 28004). Purified DNA was either stored at -20°C or immediately amplified. Amplification of purified DNA allows for the expansion of DNA fragments, as well as for the inclusion of the barcoded PCR primers to allow for Illumina sequencing and identification of samples. ATAC-seq primers are included in Table 3 and require one

common barcoded primer to all samples (primer Ad 1) as well as unique primers to distinguish samples (primers Ad 2.1-2.8). PCR amplification of libraries was carried out in three steps in order to avoid library complexity bias; first, limited PCR amplification was performed on the library, from which an aliquot was removed and used to run a qPCR side reaction to determine the number of additional PCR cycles required to avoid library bias. The PCR reaction was set up using 10 µL eluted tagmented DNA, 10 µL nuclease-free H_2O, 2.5 µL 25 µM ATAC PCR primers and 2X NEBNext High-Fidelity 2X PCR master mix (New England Biolabs, cat # M0541S) and amplified with one extension cycle (72°C for 5 min, 98°C for 30 sec) followed by 5 PCR cycles (98°C for 10 sec, 63°C for 30 sec, 72°C for 1 min). To set up the side qPCR reaction, 5 µL of the initial PCR reaction was combined with 0.25 µL 25 µM primers, 5 µL 2X NEBNext High-Fidelity 2X PCR master mix, 4.41 µL nuclease-free H_2O and 0.09 µL 100X SYBR Green I (Invitrogen, cat # S-7563). Cycling conditions were set as followed to run the qPCR side reaction: 1 cycle (98°C for 30 sec) and 20 cycles (98°C for 10 sec, 63°C for 30 sec, 72°C for 1 min) after which Rn was plotted versus cycle. Number of cycles remaining for PCR amplification was determined by the qPCR cycle which corresponds to ⅓ of the maximum signal. Amplified library was cleaned with Qiagen MinElute PCR Purification Kit, eluted in 20 µL Elution Buffer and verified by Bioanalyzer prior to sequencing (both performed by Stemcore, Ottawa Hospital Research Institute) .

Table 3. ATAC-seq primers[137]

Primer	Sequence
Ad1	AATGATACGGCGACCACCGAGATCTACACTCGTCGGCAGCGTCAGATGTG
Ad2.1	CAAGCAGAAGACGGCATACGAGATTCGCCTTAGTCTCGTGGGCTCGGAGATGT
Ad2.2	CAAGCAGAAGACGGCATACGAGATCTAGTACGGTCTCGTGGGCTCGGAGATGT
Ad2.3	CAAGCAGAAGACGGCATACGAGATTTCTGCCTGTCTCGTGGGCTCGGAGATGT
Ad2.4	CAAGCAGAAGACGGCATACGAGATGCTCAGGAGTCTCGTGGGCTCGGAGATGT

Ad2.5	CAAGCAGAAGACGGCATACGAGATAGGAGTCCGTCTCGTGGGCTCGGAGATGT
Ad2.6	CAAGCAGAAGACGGCATACGAGATCATGCCTAGTCTCGTGGGCTCGGAGATGT
Ad2.7	CAAGCAGAAGACGGCATACGAGATGTAGAGAGGTCTCGTGGGCTCGGAGATGT
Ad2.8	CAAGCAGAAGACGGCATACGAGATCCTCTCTGGTCTCGTGGGCTCGGAGATGT

2.4.6 ATAC-seq Processing and Analysis

Forward and reverse reads from each lane were combined separately and QC was carried out on all raw .fastq files obtained from Illumina NextSeq500 (PE 75 bp) to confirm successful and unbiased sequencing with FastQC (https://www.bioinformatics.babraham.ac.uk/projects/fastqc/) (version 0.11.6). Adapters were trimmed using atactk (http://atactk.readthedocs.io/en/latest/installation.html) (version 0.1.5) compiled by the Parker lab (based on Buenrostro *et al.* [137]) and alignment to mm10 was processed using Bowtie 2[138] (version 2.3.4). SAM files were sorted with samtools[139] to generate BAM files, from which duplicates were removed with Picard tools (https://broadinstitute.github.io/picard/) (version 2.17.0). Read files were filtered using samtools and peaks were called using macs2 –shift -100, --ext size 200 in --broad mode (qval < 0.1). Replicate files were merged with samtools and bigWig files were prepared for visualization with deepTools2 bamCoverage command, allowing for read normalization to reads per kilobase per million mapped reads (RPKM)[140]. deepTools2 was used to plot read abundance over TSS, transcription end site (TES) or scaled to a gene, as well as to generate accessibility heatmaps. Differentially accessible regions (DAR) were determined using DiffBind (http://bioconductor.org/packages/release/bioc/vignettes/DiffBind/inst/doc/DiffBind.pdf) (version 2.8.0) by generating consensus peaks for merged replicates without summits. GO terms for overlapping peaks between replicates were generated by ChIPpeakAnno[141]

(version 3.14.0), which was also used to annotate peaks and plot distribution over genomic features as well as identifying enriched GO terms for peak sets. ATACseqQC[142] (version 1.2.9) was used to separate reads based on length into NFRs, mononucleosomes, dinucleosomes and trinucleosomes. Previously generated dataset of mESC E14 merged control ATACseq was retrieved using GEO number GSE98390 and analyzed similarly to other samples using deepTools2.

2.5 Quantitative PCR (qPCR)

2.5.1 Reverse Transcription

Transcript quantification was performed by qPCR on complementary DNA (cDNA) generated from total RNA samples. RNA isolated as described in 2.4.1 following the Trizol protocol and bypassing column purification and DNaseI treatment. RNA was quantified by Nanodrop, and 1 µg RNA was used for cDNA generation. RNA was combined with 1 µL random hexamer primers (300 ng/µl) and brought to a final volume of 12 µL with water. Primer annealing was carried out at 65°C for 5 min, after which 4 µL Revertaid 5X buffer, 2 µL dNTPs, 1 µL Revertaid enzyme and 1 µL inhibitor (Thermo Fisher, cat # K1621) were added to each annealed sample. Reverse transcription was completed by thermocycler for 5 min at 25°C, 1 h at 42°C followed by 5 min at 70°C. cDNA was stored at -20°C.

2.5.2 qPCR

cDNA generated in 2.5.1 was diluted 1:20 in nuclease-free water prior to qPCR master mix preparation. A 20 µL total qPCR reaction was prepared by mixing 10 µL Lo-ROX 2X SYBR Master Mix (FroggaBio Inc, cat # BIO-94020) with 7.2 µL nuclease-free water, 0.4 µL 10 nM reverse primer, 0.4 µL 10 nM forward primer and 2 µL cDNA. Each qPCR reaction was performed in technical triplicates. Samples were loaded into a MicroAmp® Fast Optical 96-well Reaction Plate (Life Technologies, cat # 4346906), spun down briefly and run on the 7500 Applied Biosystems® Fast Real-Time PCR System using the following cycling settings: 95°C for 20 sec, 40 cycles (95°C for 3 sec, 60°C for 30 sec, 72°C for 20 sec), and 72°C for 1 min. Relative transcript abundance was determined against a control housekeeping gene (Eif4a2, Cyc1) for each sample. Fold change was calculated using the ΔΔCt method and significance determined by Student's t-test. Primers are listed in Table 4.

Table 4. qPCR primers

Primer	Sequence
Eif4a2_F2	TGGTGTCATCGAGAGCAACTG
Eif4a2_R2	GCAAATGTGGCTGTCTTGCC
Cyc1_F1	ATCGTTCGAGCTAGGCATGG
Cyc1_R1	GCCGGGAAAGTAAGGGTTGA
Fgf8_F[143]	AATCCAGCCCCAAACTACC
Fgf8_R[143]	GCTCTGCTCCCTCACATG
Faim2_F[144]	AGAAGACATCATGACCCAGGG
Faim2_R[144]	CTTTCTGGTCATCCCAGCTG
Anks1b_F	GGGAAAGGACTCTGTAGCGG
Anks1b_R	TCGCCAGATGCTTAGCAGATT
Foxr2_F	GGACTTGCCAAGAGCTATCAAAA
Foxr2_R	TCACTGGTCAGAGAAGCCAC
Cdc25b_F	CAGCCCCTGACTTGATGTGT
Cdc25b_R	GGGACCTTCTCGTCATCCTTTA

3. Results

3.1 Snf2l is required for timely differentiation of granule neurons *in vitro*

3.1.1 Wild-type cerebellar GNPs differentiate within 3 days

Inactivation of Snf2h and Snf2l in the cerebellum has resulted in a decrease or increase in cerebellar size, respectively, thereby suggesting a possible role for ISWI in cerebellum development[50,73]. We therefore employed isolated GNP cultures in order to more clearly establish the molecular roles of ISWI in the cerebellum. It has previously been shown by Lee *et al*. that isolation and culture of GNPs can be consistently achieved to a high degree of purity, and that functional mature GNs are obtained within 3 days *in vitro* (DIV) from this methodology[133]. We first confirmed the effectiveness of this protocol in our hands using P4-P6 WT mice (Fig 7). Cerebella from these animals were dissociated into single cell suspensions by enzymatic digestion followed by trituration, after which GNPs were enriched by passing cells through a Percoll density gradient, and contamination was further reduced by preplating in serum media. Purified GNPs were either immediately collected for cell lysates, or plated at a high density and allowed to differentiate for 72h *in vitro*. Immunoblot analysis of protein expression in undifferentiated (0h) and differentiated (72h) GNPs reveal a characteristic reduction of the proliferation marker Ki67, and concomitant up-regulation of NeuN and tuj1, markers of post-mitotic neurons (Fig 7A). Similarly we observed enrichment of Snf2h expression in the progenitor cells which was reduced in GNs with Snf2l adopting the opposite expression pattern, peaking in differentiated neurons, as previously reported in many CNS tissues[19,50] (Fig 7A). Moreover, we can confirm successful differentiation of GNPs by notable changes in cell

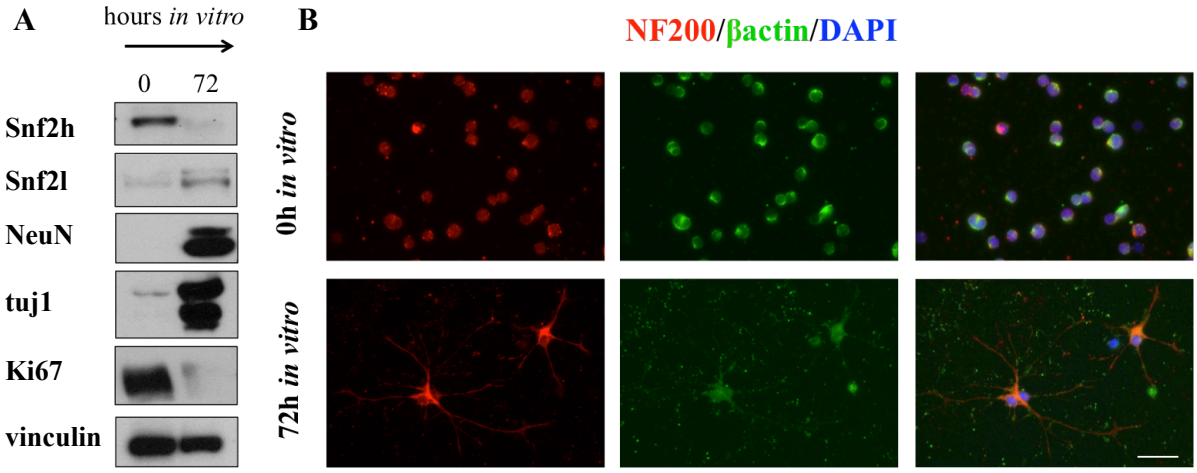


Figure 7. 72h GNP differentiation timecourse *in vitro*. GNPs isolated from P4-P6 WT cerebella were differentiated *in vitro* into GNs. (**A)** Characteristic reduction of the proliferation marker Ki67 and increased expression of differentiation markers (NeuN and tuj1), as well as changes in ISWI protein expression. **(B)** Cell imaging of GNPs and GNs showing morphology changes following differentiation. Scale bar = 25 μM.

morphology (Fig 7B), indicated by the round morphology of progenitor cells and typical neuron-like morphology with dendrites extending out from the cell body in the GNs following staining for the cytoskeletal proteins NF200 and β-actin.

While the above protocol ensures enrichment of GNPs via density gradients and preplating, the authors report culture purity between 95%-99%[133]. Contamination of GNPs by other cell types is possible under our culture conditions. Astrocytes represent the majority of glial cells in the brain[145], and are therefore the most likely contaminating cell type in GNP cultures. In order to verify our rate of contaminating glial cells in GNPs, we stained cultures for GFAP, a marker of glial cells (Fig 8). We detected $GFAP^+$ cells at 0h, 72h and up to 7 DIV (Fig 8A) but their presence was limited compared to $GFAP^-$ GNPs, with glial contamination rates below 10% (Fig 8B). In order to confirm the identity of the $GFAP^-$ cells we also attempted to discern Atoh1, a marker of GNPs. However no commercially available antibody was able to accurately detect Atoh1. We were later able to demonstrate a significant loss of *Atoh1* expression in WT cultures between 0h and 72h by RNA-seq (Appendix A), thereby confirming that cultured GNPs were indeed positive for Atoh1, and lost this specific marker as they differentiated into neurons.

3.1.2 Loss of Snf2l activity hinders GNP terminal differentiation

To begin to characterize the functional differences between WT and Ex6DEL GNPs, we first isolated and cultured GNPs from cerebella of P4-P6 Ex6DEL mice. We next verified

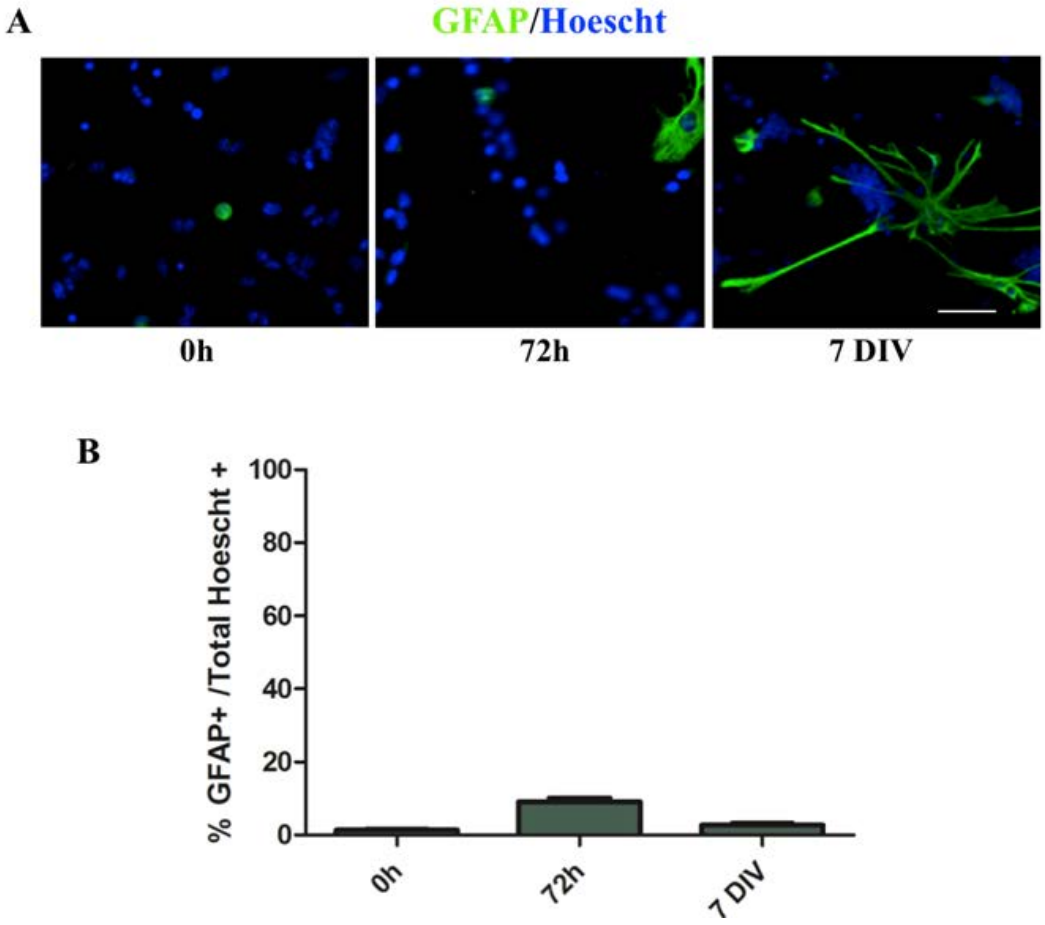


Figure 8. Cerebellar GNP cultures have limited glial contamination. Presence of glial cells was detected by GFAP staining **(A)** and quantified **(B)** relative to total nuclei, scale bar = 50 μM. at 0h, 72h or 7 days *in vitro* (DIV) (n=4) Mean ± SD.

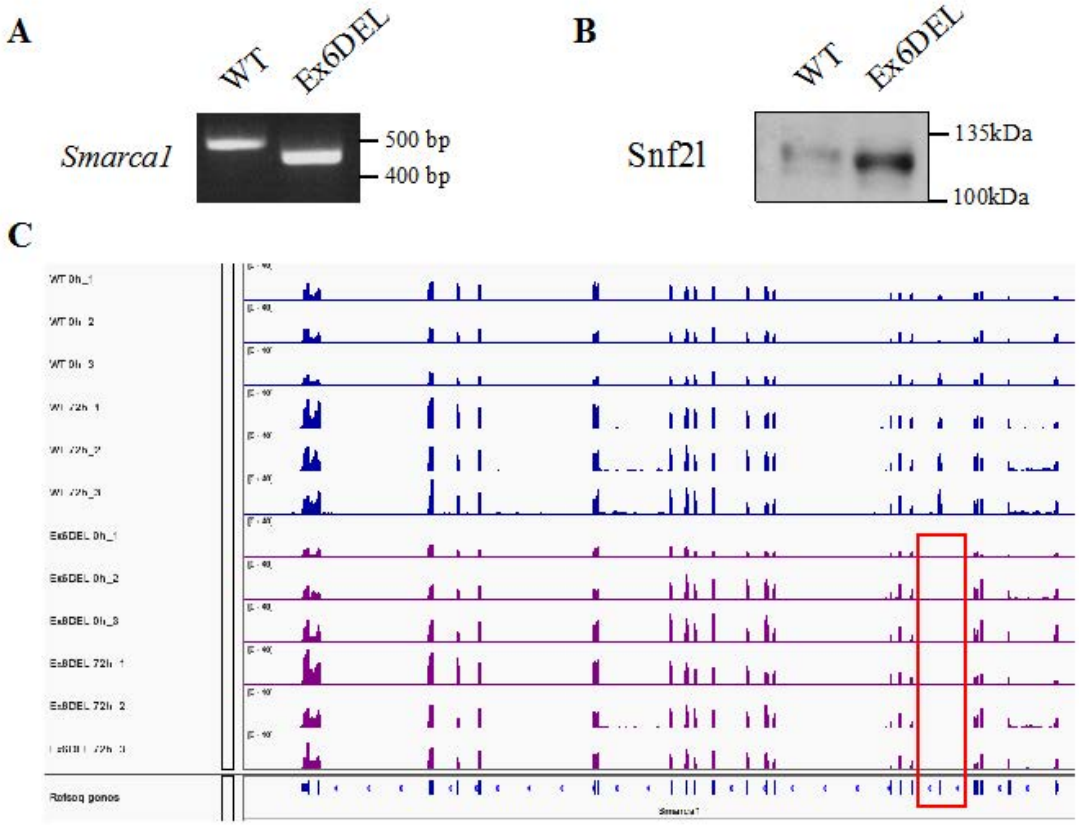


Figure 9. GNPs isolated from Ex6DEL mice express Snf2l isoform lacking ATP binding exon 6. (A) Genotyping for Snf2l in WT and Ex6DEL GNPs reveals a smaller band indicative of the absence of exon 6. **(B)** Immunoblots similarly indicate the expression of a smaller Snf2l protein product relative to WT. **(C)** RNA-seq analysis of WT and Ex6DEL confirms the absence of exon 6 in Snf2l transcripts.

the absence of exon 6 in *Smarca1* in GNPs by genotyping WT and Ex6DEL GNPs (Fig 9A) and confirmed that the resulting Snf2l protein is approximately 7 kDa smaller than WT Snf2l by immunoblotting (Fig 9B). We were later also able to confirm the specific excision of exon 6 of *Smarca1* in our Ex6DEL RNA-seq samples when reads were visualized on a genome browser (Fig 9C). Upon differentiation of Ex6DEL GNPs, we first noted a significant delay in the development of dendrites of these cells compared to WT cultures (Fig 10). Within the first 24h in culture, WT GNPs have already begun to lose their progenitor morphology while the majority of Ex6DEL GNPs do not begin to differentiate until 48 or 72h (Fig 10). Staining for Ki67 reveals that this proliferation marker is rapidly turned off following plating and differentiation of WT GNPs, however Ex6DEL cultures highly express this marker, with some cells continuing to be $Ki67^{+}$ until 7 DIV (Fig 11A). Concordantly, NeuN, which labels post-mitotic neurons is up-regulated by 72 h *in vitro* in WT cultures, but is largely reduced in Ex6DEL cells at all timepoints studied (Fig 11A-B). In order to quantify this delay, we pulsed WT and Ex6DEL GNP cultures with BrdU at 0, 24, 48 and 72h *in vitro* in order to distinguish differences in cell cycle. BrdU incorporates into replicating DNA during S-phase, and therefore $BrdU^{+}$/total cells represents the fraction of cells in this cell cycle phase at the time of the pulse. We used a 2h BrdU pulse prior to collecting the cells at each timepoint (Fig 12A-B). Ex6DEL cultures at 0, 24 and 48h have a significantly increased fraction of GNPs in S-phase compared to WT cells ($p<0.001$), while at 72h most cells appear to have begun to exit the cell cycle. GNPs cultured *in vitro* are generally known to be unable to actively replicate once plated and typically undergo a final cell cycle round[133]. As such, we reasoned that differences in the proportion of cells in S-phase could arise from increased cell death of

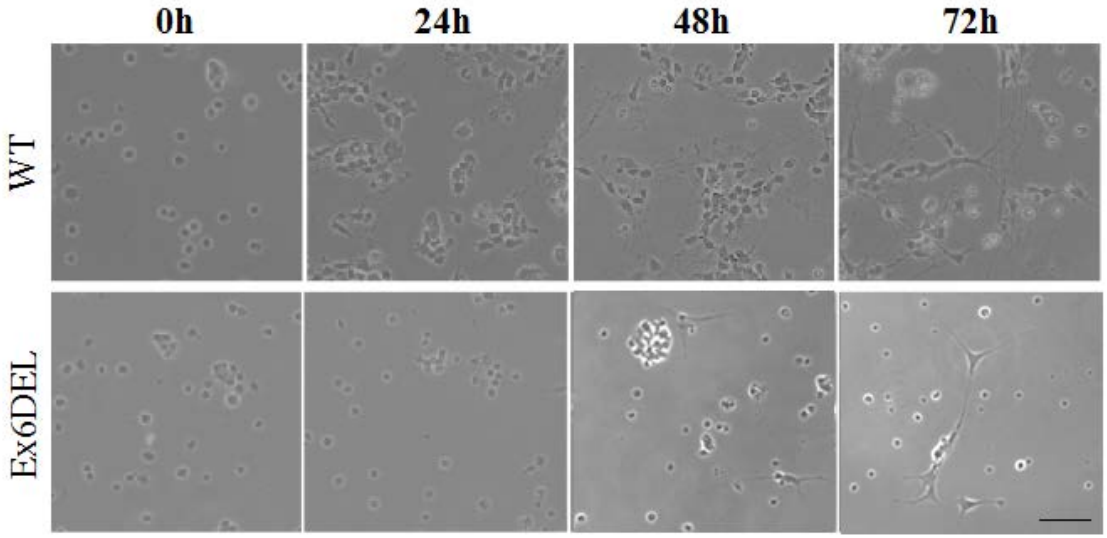


Figure 10. Terminal differentiation of Snf2l Ex6DEL GNPs is delayed *in vitro*. Phase-contrast imaging of WT and Ex6DEL GNP cultures reveal a delay in neuron morphology and neurite extension in Ex6DEL GNP cultures compared to WT after plating (0h) or following 24, 48 or 72h differentiation. Scale bar = 50 μM.

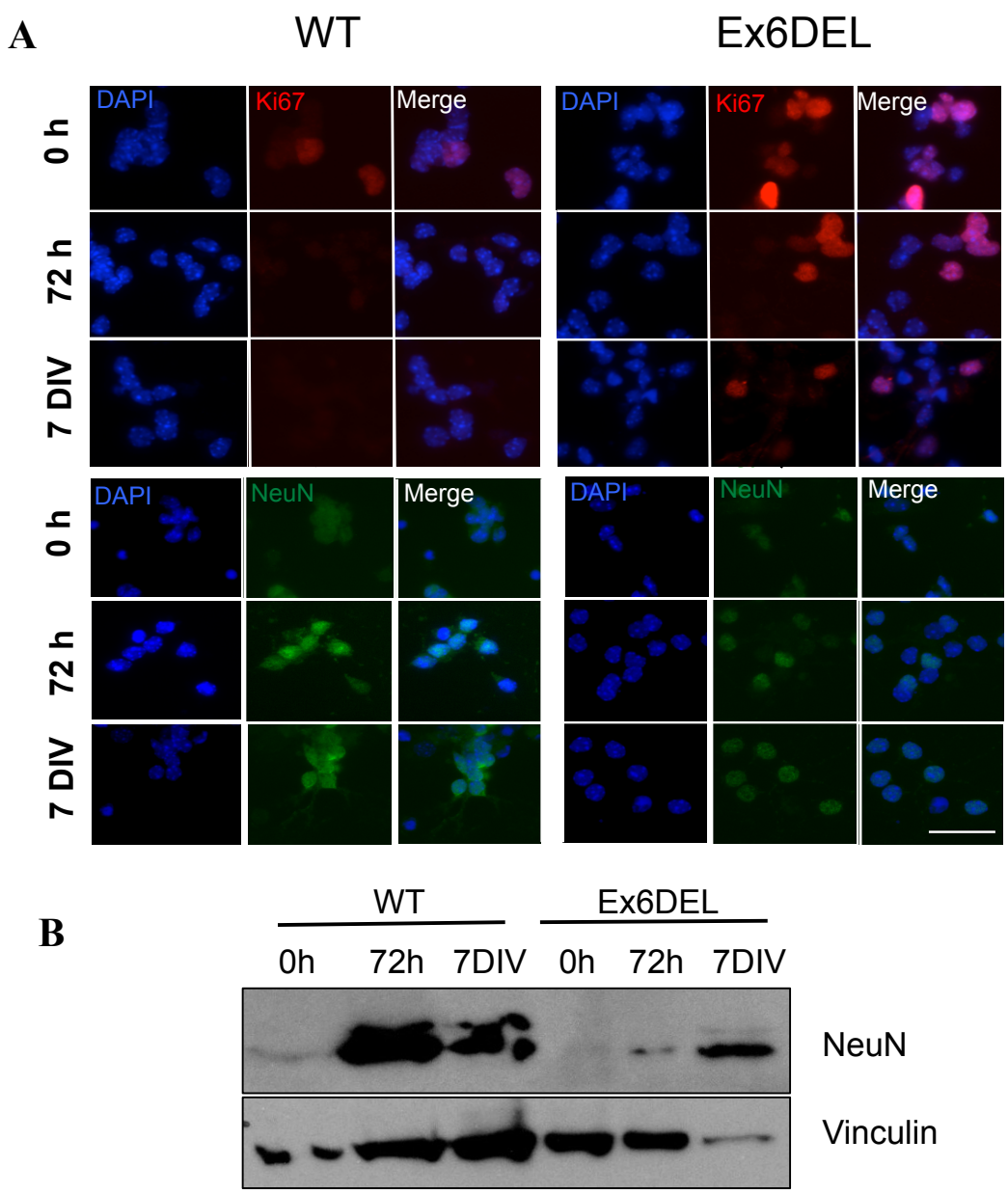


Figure 11. Ex6DEL cultures prolong expression of proliferation markers and delay expression of differentiation markers. (A) WT and Ex6DEL GNPs were stained with proliferation marker Ki67 (top panels) and differentiation marker NeuN (bottom panels) at 0h, 72h and 7 days in culture. Cells were counterstained with DAPI (blue). Scale bar = 25 μM. **(B)** Immunoblot for NeuN in WT and Ex6DEL cultures at 0h, 72h and 7 days *in vitro*.

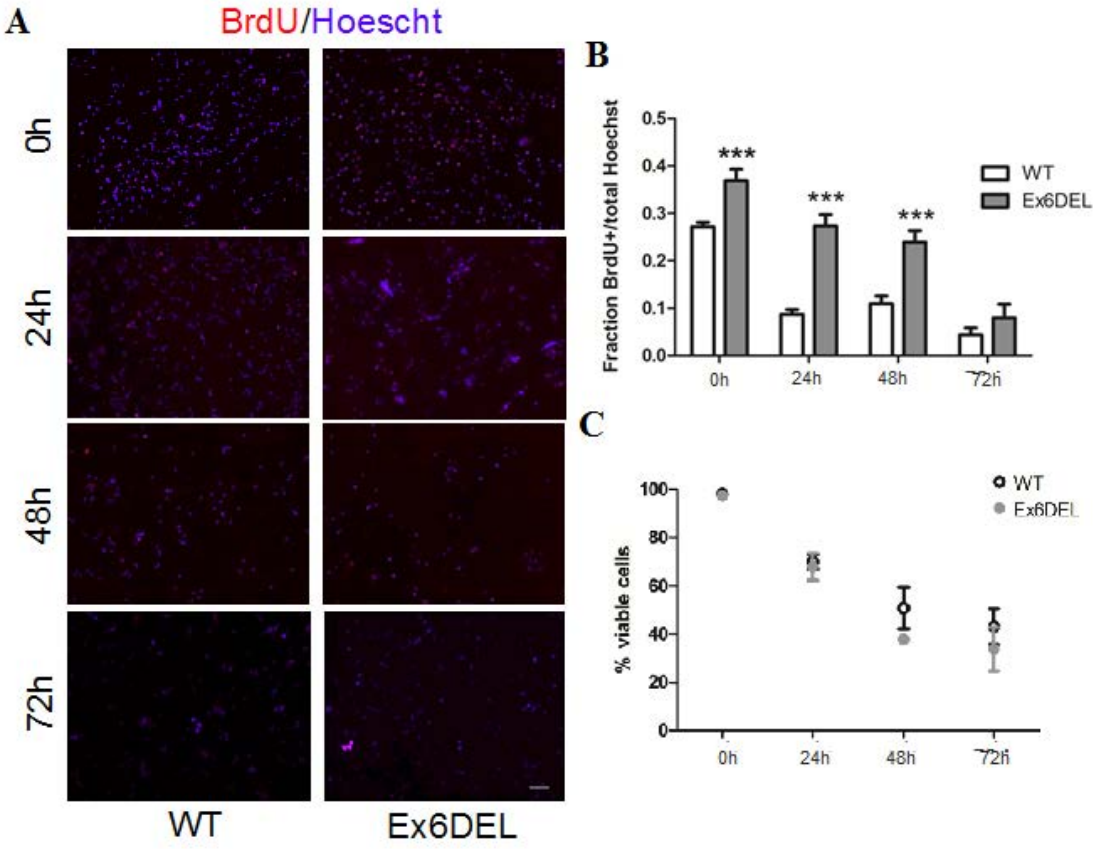


Figure 12. Ex6DEL GNPs remain in a prolonged S-phase during *in vitro* differentiation. (A) GNPs at 0h, 24h, 48 and 72h post-isolation were pulsed with BrdU for 2h, stained for BrdU and counterstained with Hoescht and **(B)** quantified relative to total nuclei, n=4 independent experiments; ***p<0.001. Scale bar = 40 μM. Mean ± SD **(C)** Trypan blue exclusion assay of viability of WT and Ex6DEL GNPs at 0h, 24h, 48 and 72h post-isolation. Percentage viable cells as a ratio of trypan blue negative cells over total collected cells , n=3 independent experiments,

differentiating neurons in the Ex6DEL cultures. To confirm that viability of Ex6DEL cultures was similar to that of WT cells we performed a trypan blue exclusion assay for viability. While we observed a sharp decrease in total numbers of viable cells through the differentiation timecourse, the viability of Ex6DEL cells was unchanged when compared to WT cells (Fig 12C).

3.1.3 Snf2l exon 6 is not required to mediate complex binding but complex hierarchy may be skewed

As we had previously observed that expression of both ISWI proteins changes throughout differentiation of WT GNPs (Fig 13A), we next asked whether the expression of non-catalytic subunits associated with either Snf2h or Snf2l chromatin remodelling complexes was similarly fluctuating with cell differentiation stage. There exists 5 Snf2h-specific complexes which are formed through specific interactions with Acf1, Tip5, Wstf, Rsf1 and RbAp48 subunits, and 2 Snf2l complexes which contain BPTF or CECR2. The majority of these subunits have conserved motifs required for DNA or histone interactions (Fig 13A). Assessment of protein abundance revealed an increased level of Wstf, RbAp48, Acf1 and CECR2 interacting proteins in differentiated WT cells compared to GNPs (Fig 13B). Tip5 protein showed no change in abundance levels after differentiation (Fig 9B).

We next assessed WT and Ex6DEL cultures at 0 and 72h timepoints for changes in abundance of ISWI proteins or Snf2l binding partners upon loss of Snf2l activity (Fig

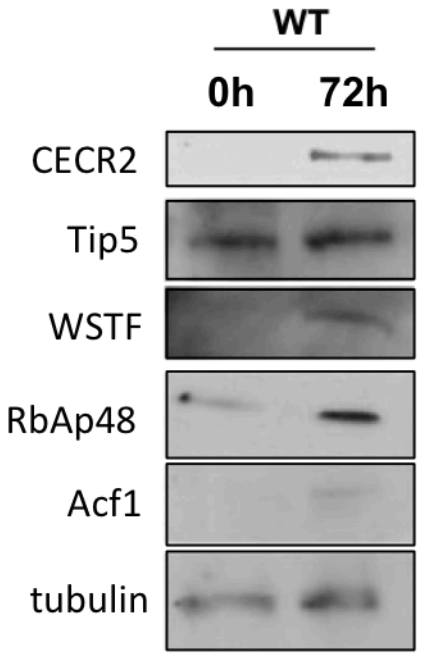


Figure 13. ISWI interacting partner protein abundance is dynamic during GNP differentiation. Immunoblots of WT GNPs at 0 and 72h post-isolation for Snf2h (Tip5, WSTF, RbAp48, Acf1) or Snf2l (CECR2) interacting partners relative to tubulin loading control.

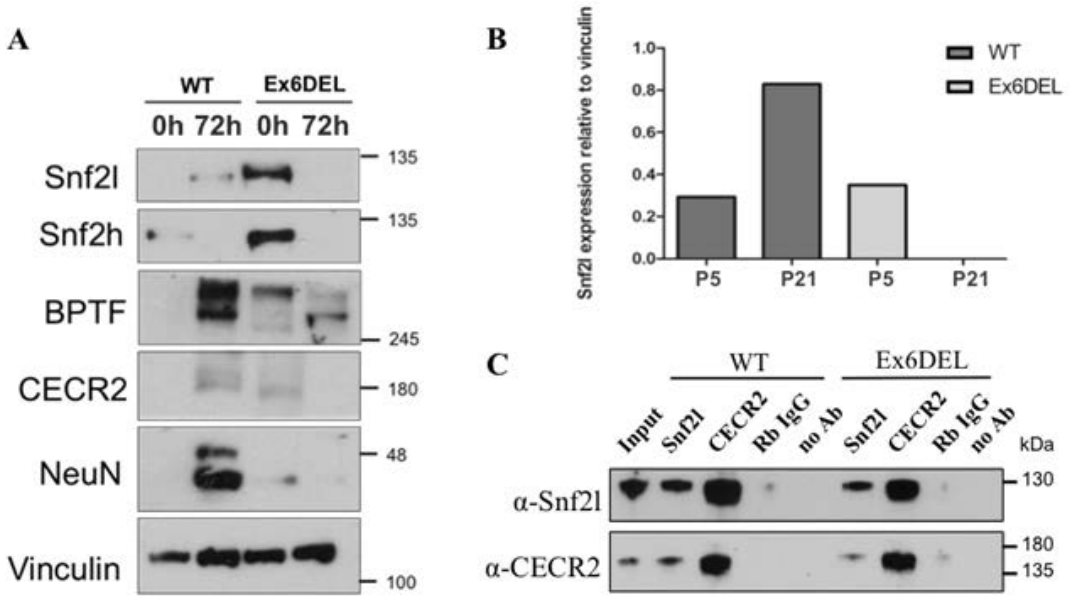


Figure 14. The Ex6DEL protein retains the ability to interact with CECR2. (A) Immunoblots of WT and Ex6DEL GNPs and GNs for ISWI, Snf2l binding partners BPTF and CECR2, differentiation marker NeuN and vinculin loading control. **(B)** Snf2l expression was quantified by densitometry in cerebellar lysates at proliferative (P5) and differentiated (P21) timepoints in both WT and Ex6DEL mice, n=1 **(C)** Reciprocal coIPs for Snf2l or CECR2 of P21 cerebellar lysates were then probed for Snf2l and CECR2 expression by immunoblotting along with input control as well as rabbit IgG and no antibody (no Ab) negative pulldown controls.

14A). While Snf2l is typically expressed in differentiated neurons, it was detected exclusively at the GNP stage, a pattern also observed in whole cerebellar extracts (Fig 14B). The Snf2h pattern remained the same in Ex6DEL cultures, but there appeared to be increased abundance at 0h in the Ex6DEL cultures. Intriguingly, we observed both Snf2l interacting partners BPTF and CECR2 in the progenitor cell lysates instead of being restricted to differentiated neurons (Fig 14A). To confirm Ex6DEL Snf2l retained the ability to form the chromatin remodelling complex CECR2, we performed reciprocal co-IPs for CECR2 and Snf2l in cerebellar lysates of P21 WT and Ex6DEL mice. Indeed, we observed reciprocal interactions between CECR2 and Snf2l in both Ex6DEL and WT cerebellar extracts (Fig 14C).

3.2 Widespread disruption of GNP transcriptome upon inactivation of Snf2l

3.2.1 Ex6DEL GNP differentiation is associated with altered transcription

To assess changes to the transcriptome underlying the Ex6DEL GNP phenotype, we performed RNA-seq analysis using freshly isolated GNPs (0h) and GNPs differentiated *in vitro* for 72h from both WT and Ex6DEL animals. Biological triplicates were sequenced for each timepoint, however after the initial analysis one 72h replicate from both WT and Ex6DEL cells appeared to contain significantly different transcript abundances compared to those of the other two replicates and thus was excluded these samples from further analysis (Appendix A). Heatmaps were generated for all differentially expressed transcripts with a fold-change threshold of ±1.5 and a qval < 0.05 for WT and Ex6DEL replicates at 0h and 72h (Fig 11A). DEGs were identified by pairwise analysis across samples, and resulted in 126 down-regulated and 407 up-

regulated genes at 0h in Ex6DEL compared to WT GNPs; 907 down-regulated and 3712 up-regulated genes at 72h in Ex6DEL compared to WT GNPs; 3880 down-regulated and 3027 up-regulated genes at 72h compared to 0h in WT cells and 2926 down-regulated; and 3360 up-regulated genes at 72h compared to 0h in Ex6DEL cells (Fig 15B). Intriguingly, DEGs that are either up or down regulated in Ex6DEL progenitors do not maintain their aberrant expression by 72h, with only 4 genes consistently up-regulated DEGs (*Kcnj15, Sox7, Ptprb, Lor*) and 2 remaining down-regulated (*Klhcd8a, Gm14305*) in the Ex6DEL cultures (Appendix B).

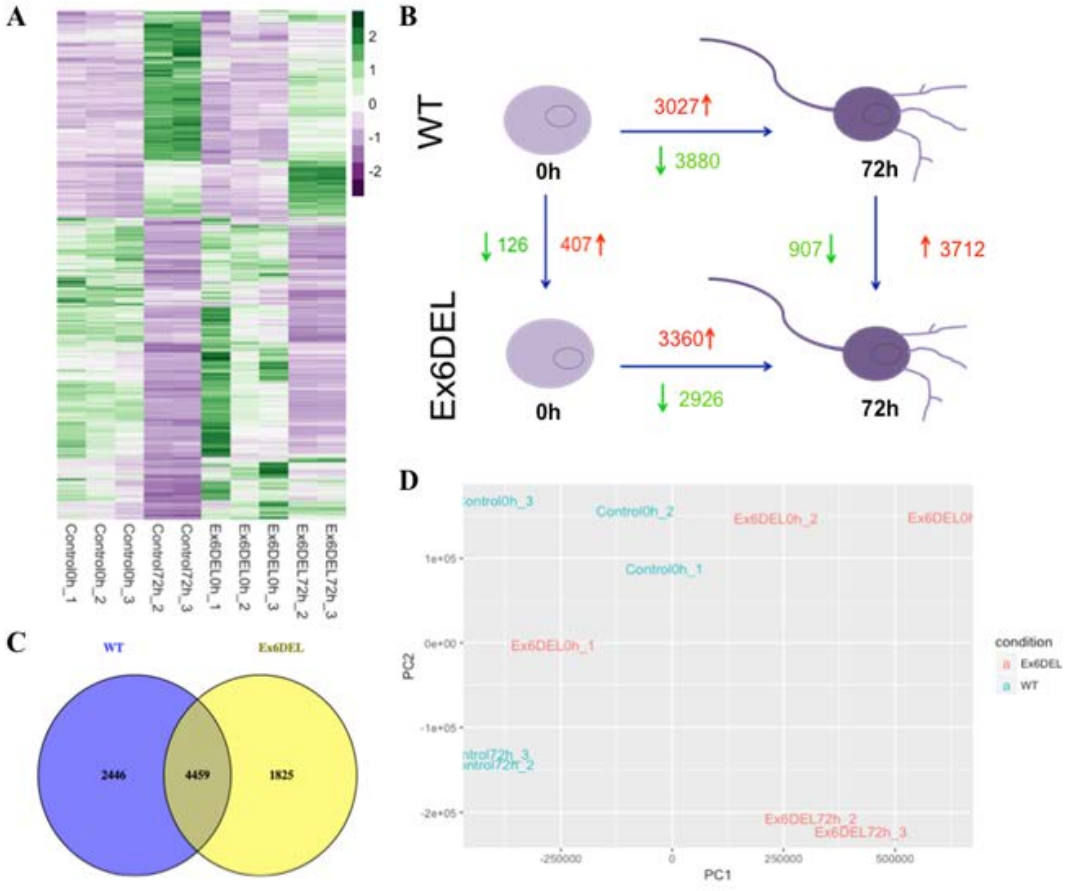


Figure 15. Loss of active Snf2l leads to widespread transcriptome disruptions during GNP differentiation. (A) RNA-seq heatmap of all transcripts with qval < 0.05 for WT (control) or Ex6DEL replicates at 0h or 72h of *in vitro* differentiation. **(B)** Schematic of differentially expressed genes (DEG) (fold change > 1.5 & qval < 0.05) in pairwise comparisons between genotypes at timepoints of 0h and 72h, as well as DEGs involved in differentiation pathways for WT and Ex6DEL. Up-regulated gene set annotated in red, and down-regulated genes in green. **(C)** Venn diagram of the overlapping gene sets involved in differentiation of WT (purple) and Ex6DEL (yellow) GNPs. **(D)** PCA plot grouping WT (blue) and Ex6DEL (orange) RNA-seq replicates between progenitor (0h) and differentiated (72h) timepoints.

3.2.2 WT and Ex6DEL DEGs undertake transcriptionally unique differentiation pathways

All DEGs involved in either WT or Ex6DEL differentiation were compared in order to determine if WT and Ex6DEL GNPs were undertaking transcriptionally similar differentiation pathways (Fig 15C). Indeed, 4459 DEGs were common to both WT and Ex6DEL differentiation, representing approximately two thirds (65% WT, 71% Ex6DEL) of total DEGs for each condition. Nonetheless, 2446 DEGs were involved in WT differentiation that were not modified in Ex6DEL cells, while 1825 DEGs were unique to Ex6DEL GNP differentiation. PCA plots of all four sample sets reveal that they are quite distinct, each residing in a separate quadrant (Fig 15D). The Venn and PCA plots together indicate that WT and Ex6DEL differentiation either utilize some distinct pathways or may represent distinct neuronal sub-types. WT differentiation appears to require nearly 7000 DEGs, with similar proportions of up- and down-regulated genes (Fig 16A,B). GO terms enriched in the subset of up-regulated genes involved in WT GNP differentiation (and not found in Ex6DEL GNP differentiation GO terms) relate to synapse maturation and regulation of G-protein signalling pathways (Fig 16C), while a similar list of down-regulated DEGs involve cell cycle control, proliferation regulation and the regulation of a number of pathways including Wnt, Notch, and Smoothened (Fig 16D). Alternatively, Ex6DEL GNP differentiation recruits a slightly lower number of total DEGs than WT differentiation, involving 2926 down- and 3360 up-regulated genes (Fig 17A,B). GO terms enriched amongst Ex6DEL

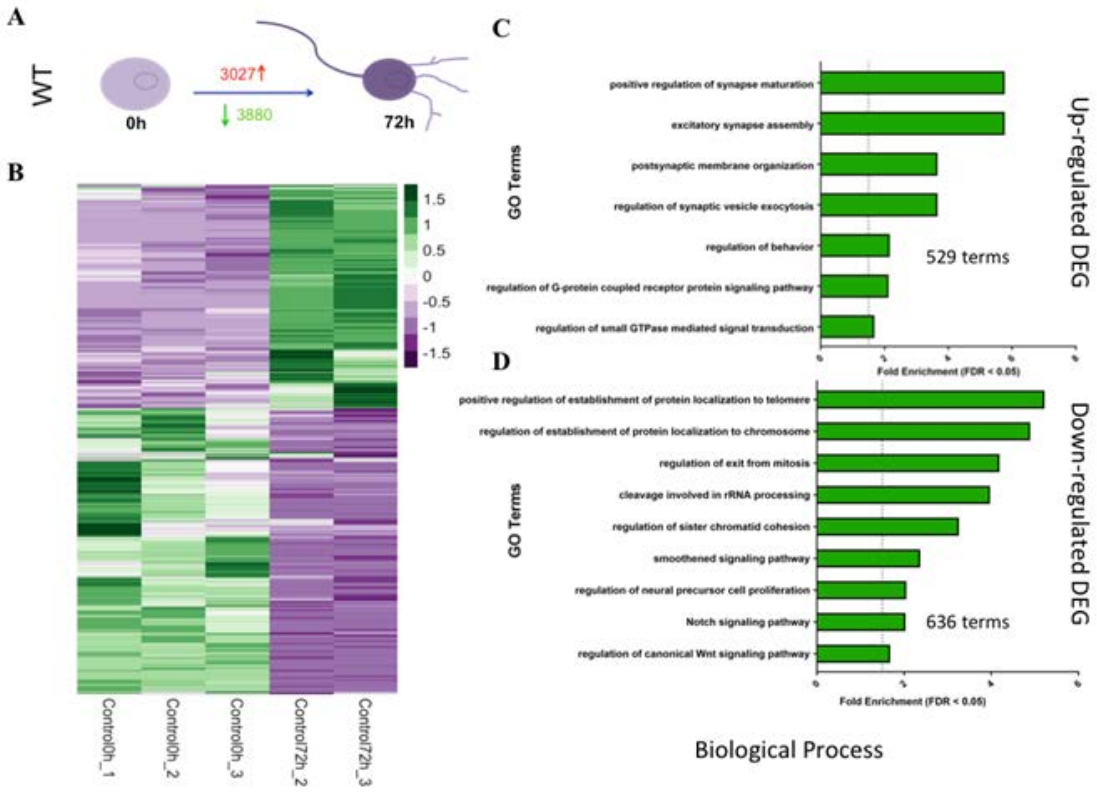


Figure 16. WT GNP differentiation requires substantial transcriptomic shifts to mediate cell cycle exit and neuron development. (A-B) 3027 DEGs are significantly up-regulated and 3880 DEGs down-regulated to mediate progenitor to neuron terminal differentiation. Select Gene Ontology (GO) terms associated exclusively with WT up-regulated **(C)** or down-regulated **(D)** sets of DEGs involved in WT GNP differentiation. Total number of significant (FDR < 0.05, fold enrichment > 1.5) GO terms listed.

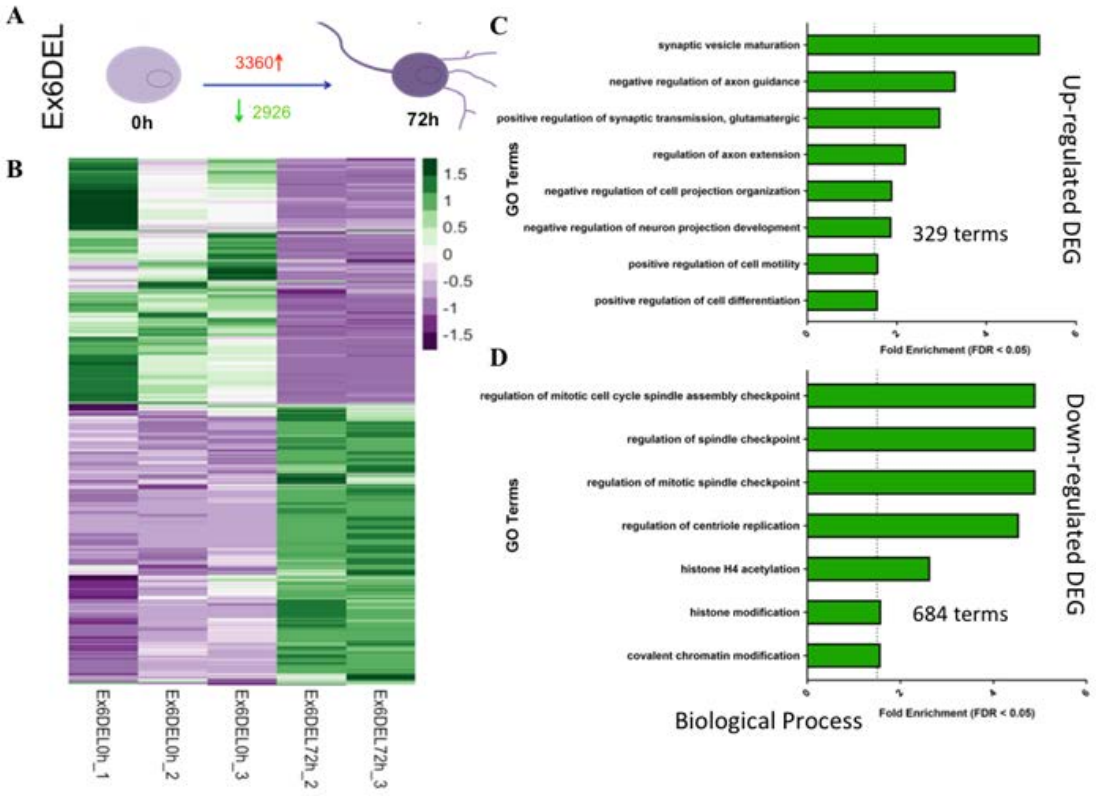


Figure 17. DEGs regulating Ex6DEL GNP differentiation indicate disruption of developmental pathways and reduced ability to differentiate. (A-B) 3360 DEGs are significantly up-regulated and 2926 DEGs down-regulated to mediate Ex6DEL cell progression between 0h and 72h *in vitro*. Select Gene Ontology (GO) terms associated exclusively with Ex6DEL up-regulated **(C)** or down-regulated **(D)** sets of DEGs involved in differentiation. Total number of significant (FDR < 0.05, fold enrichment > 1.5) GO terms listed.

differentiation up-regulated DEGs (and absent in WT differentiation) are regulation of synapses, negative regulation of neuronal projections and axon extension, and positive regulation of cell differentiation (Fig 17C), while similar analysis of down-regulated DEGs finds enrichment in GO terms relating to cell cycle checkpoints and histone modifications (Fig 17D).

3.2.3 Ex6DEL GNP and GN are transcriptionally distinct from their WT counterparts

We next sought to assess expression differences between WT and Ex6DEL cells at both progenitor and differentiated cell stages. GNPs have the smallest number of significant DEGs between WT and Ex6DEL; 126 down- and 407 up-regulated genes (Fig 18A-B). Select enriched GO terms in up-regulated DEGs reveal increased MAPK cascade regulation and increased protein phosphorylation (Fig 18C), while the down-regulated DEG subset indicates enrichment of genes required for regulation of synapses, neuron and cerebellum development and neuron differentiation (Fig 18D). At 72h there is a surprising increase of DEGs identified in Ex6DEL differentiated cells compared to WT; over 4000 DEGs were identified at this timepoint, the majority of which are down-regulated in mutant cells (Fig 19A-B). Amongst up-regulated DEGs, GO terms for positive regulation of proliferation, cell fate and regulation of ERK1 and ERK2, MAPK cascade as well as negative regulation of differentiation were identified (Fig 19C).

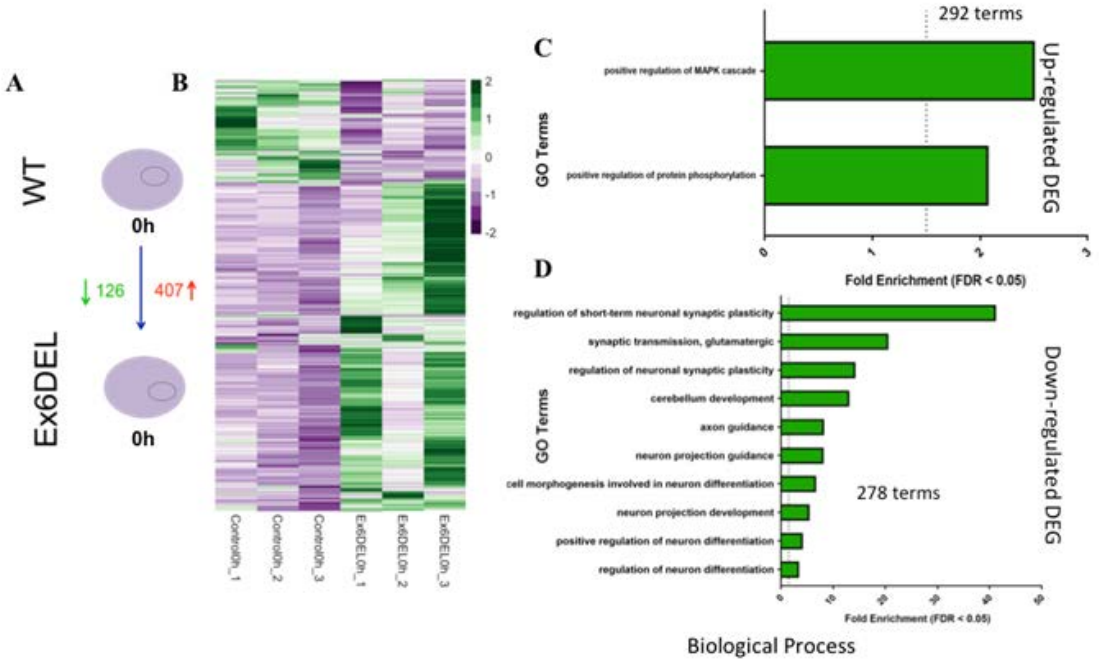


Figure 18. WT and Ex6DEL granule neuron progenitor cells are transcriptionally distinct. (A-B) 407 DEGs are significantly up-regulated and 126 DEGs down-regulated in the Ex6DEL progenitor pool compared to WT. Select Gene Ontology (GO) terms associated exclusively with Ex6DEL up-regulated **(C)** or down-regulated **(D)** sets of DEGs compared to WT progenitors. Total number of significant (FDR < 0.05, fold enrichment > 1.5) GO terms listed.

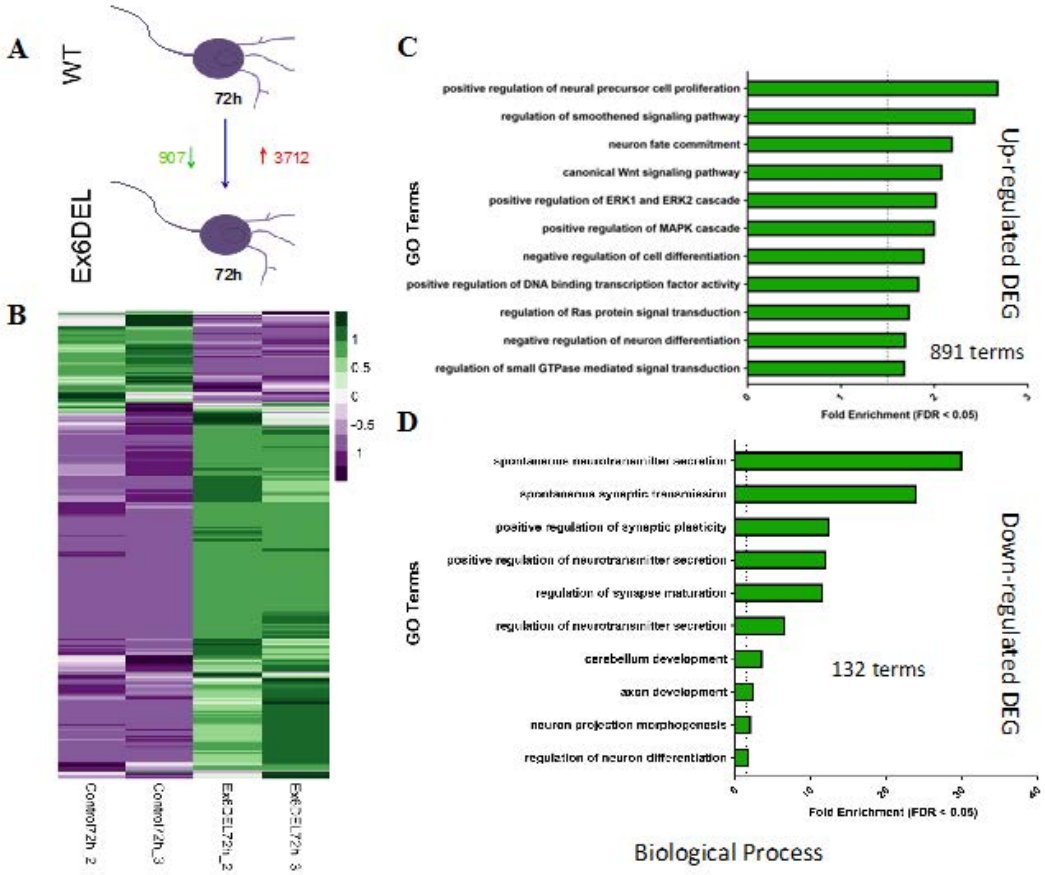


Figure 19. WT and Ex6DEL *in vitro* differentiation does not generate identical granule neuron populations. (A-B) 3712 DEGs are significantly up-regulated and 907 DEGs down-regulated in the Ex6DEL differentiated cells compared to WT. Select Gene Ontology (GO) terms associated exclusively with Ex6DEL up-regulated **(C)** or down-regulated **(D)** sets of DEGs compared to WT granule neurons. Total number of significant (FDR < 0.05, fold enrichment > 1.5) GO terms listed.

3.2.4 Differential expression of key genes mediating cerebellar development and cell cycle control

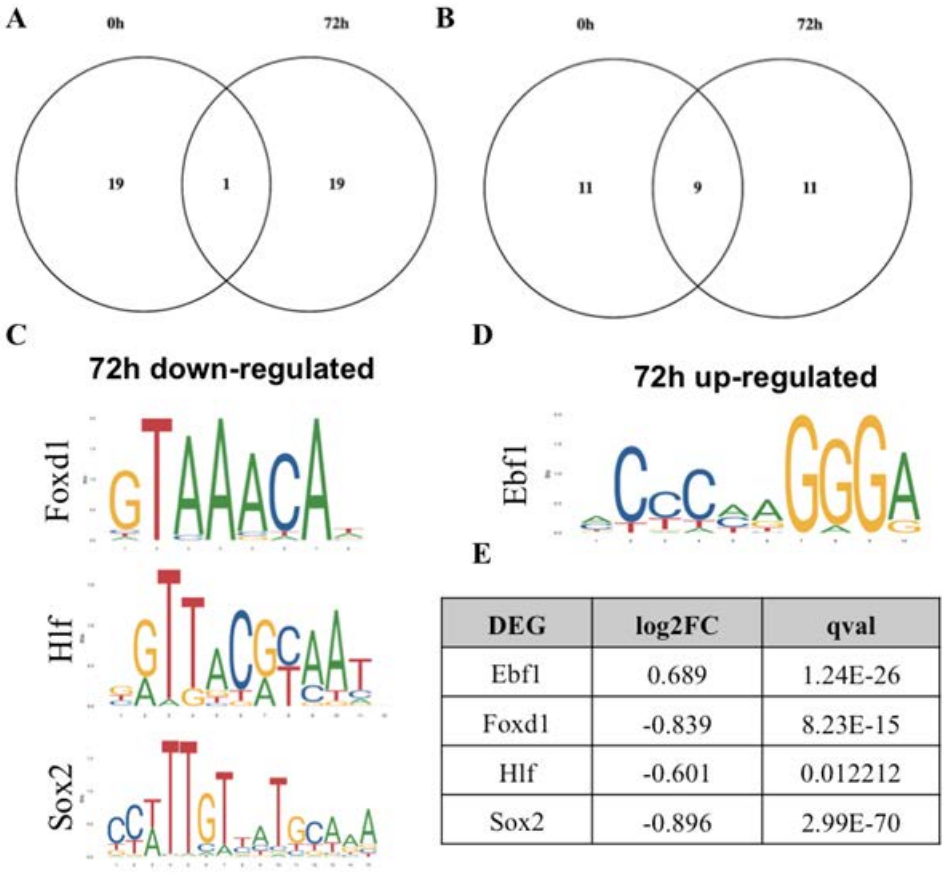
GNP differentiation is a carefully mediated cellular process, requiring changes to cell cycle and morphology, all of which rely on underlying transcriptomic shifts (Appendix C). We observed reduction of *Smarca5* expression in Ex6DEL (log_2FC -0.81) samples that was similar to the characteristic WT decrease (log_2FC-0.935) observed (Appendix C). Consistent with differentiation we observe decreased expression of Atoh1, a marker of GNPs in both WT and Ex6DEL cultures (log_2FC-3.685 and -2.93, respectively) thereby indicating the cells lost this GNP marker as they differentiated into GNs (Appendix C). In previous work, we've identified that Snf2h and Snf2l can mediate expression of *Engrailed-1* (*En1)*, an important mediator of cerebellum development and patterning[50,146]. The *En1* gene typically decreases upon GNP differentiation and we observed a log_2FC of -1.461 in WT cells but this decrease was significantly attenuated during Ex6DEL GNP differentiation (log_2FC -0.73) (Appendix C). Additionally, there is an increase in *Foxg1* expression in 72h Ex6DEL cultures (log_2FC 0.588) arising from the loss of Snf2l-mediated regulation of *Foxg1*[73] (Appendix C). Concomitantly, we were able to identify a significant increase by qRT-PCR in genes that mediate proliferation in the Ex6DEL cultures. Such genes include an increase in Cdc25b, a critical phosphatase for the entry into mitosis and a possible target of Shh signaling[147]; Foxr2, a proto-oncogene which promotes proliferation via the MYC pathway[148]; and Anks1b, a potential candidate gene in ASD and schizophrenia that is suggestive of altered GN function (Appendix C)[149,150].

3.2.5 Key transcription factors are associated to gene expression shifts in Ex6DEL cells

The mammalian ISWI genes have been demonstrated to control key TFs mediating neurodevelopment[50,73]. We reasoned that the loss of Snf2l activity could alter the expression of developmental TFs, or impair their activity leading to the large number of DEGs identified in Ex6DEL cultures. To investigate these possibilities, we first identified the top 20 TFBS governing expression of up- or down-regulated DEGs in Ex6DEL at 0h and 72h using oPOSSUM 3.0 (Appendix D-K). When comparing the highest 20 ranked TFBS for down- (Fig 20A) and up-regulated (Fig 20B) genes between 0h and 72h, only one TFBS of down-regulated genes remains consistent between both timepoints, whereas approximately half of the up-regulated genes are governed by the same TFBS at 0h and 72h *in vitro*. We then parsed our DEG lists at each time point for the presence of significant disruption of expression of TFs found in our TFBS lists (Appendix D-K). From these, no differentially expressed TFs were identified from our 0h *in vitro* TFBS lists. However, three TFs from the corresponding TFBS lists were identified as being down-regulated (*Foxd1, Hlf, Sox2*) in 72h Ex6DEL cultures (Fig 20C,E), while one was similarly identified in the up-regulated 72h Ex6DEL DEG list (*Ebf1*) (Fig 20D-E).

3.2.6 Up-regulation of ERK activation does not result in TF activity

Amongst enriched GO terms identified previously (section 3.2.3), we noted the involvement of the MAPK/ERK pathway in up-regulated genes at both 0h and 72h *in vitro*. The Ras-ERK (extracellular signal-regulated kinase, or MAPK, mitogen-activated protein kinase) pathway allows for the effective conversion of external signals via a



DEG	log2FC	qval
Ebf1	0.689	1.24E-26
Foxd1	-0.839	8.23E-15
Hlf	-0.601	0.012212
Sox2	-0.896	2.99E-70

Figure 20. Gene expression programs in Ex6DEL GNPs are temporally regulated and governed by unique TFs. Top 20 TFs regulating down- **(A)** and up- **(B)** regulated DEGs at 0h and 72h following TFBS analysis with oPOSSUM 3.0. **(C-E)** Following sorting of down-regulated DEGs against the top 20 TFs ruling down-regulated DEGs at 72h, Foxd1, Hlf and Sox2 were down-regulated in sets where their TFBS were required to mediate global transcription programs **(C)**, and similar analysis found one up-regulated TF at 72h which governs bulk gene expression programs **(D)**. **(E)** Summary of RNA-seq outputs for Foxd1, Hlf, Sox2 and Ebf1.

number of protein kinases and Ras GTPases, ultimately allowing for critical cellular decisions (proliferation, differentiation or apoptosis). We confirmed that certain mediators of the ERK pathway were indeed dysregulated in Ex6DEL cultures; Fgf8, an activator of ERK is up-regulated in 72h Ex6DEL cultures (Fig 21A), while Faim2, a repressor of the ERK pathway is up-regulated in Ex6DEL differentiation compared to WT (Fig 21B). We therefore sought to assess whether ERK pathway activation was being affected in Ex6DEL GNPs. When controlled for equal loading of vinculin, ERK protein expression was lower in Ex6DEL cultures at 72h compared to WT control (Fig 21C-D), however expression of active ERK, pERK, was markedly increased at this timepoint (Fig 21C) particularly when normalized to total ERK (Fig 21E).

Upon activation, ERK1/2 are capable of phosphorylating a wide variety of targets both in the cytoplasmic and nucleolar compartments[151,152]. A number of downstream ERK targets are TFs, making the potential effects of ERK activation quite widespread and context-specific[153]. A common ERK target is ELK1, which was identified once in our earlier TFBS analyses as having a binding site enriched in down-regulated DEGs found in Ex6DEL differentiation (Appendix D). However, densitometry analysis of ELK1 and pELK1 in Ex6DEL cerebella failed to indicate an increase in the activation levels of this TF (Fig 21F).

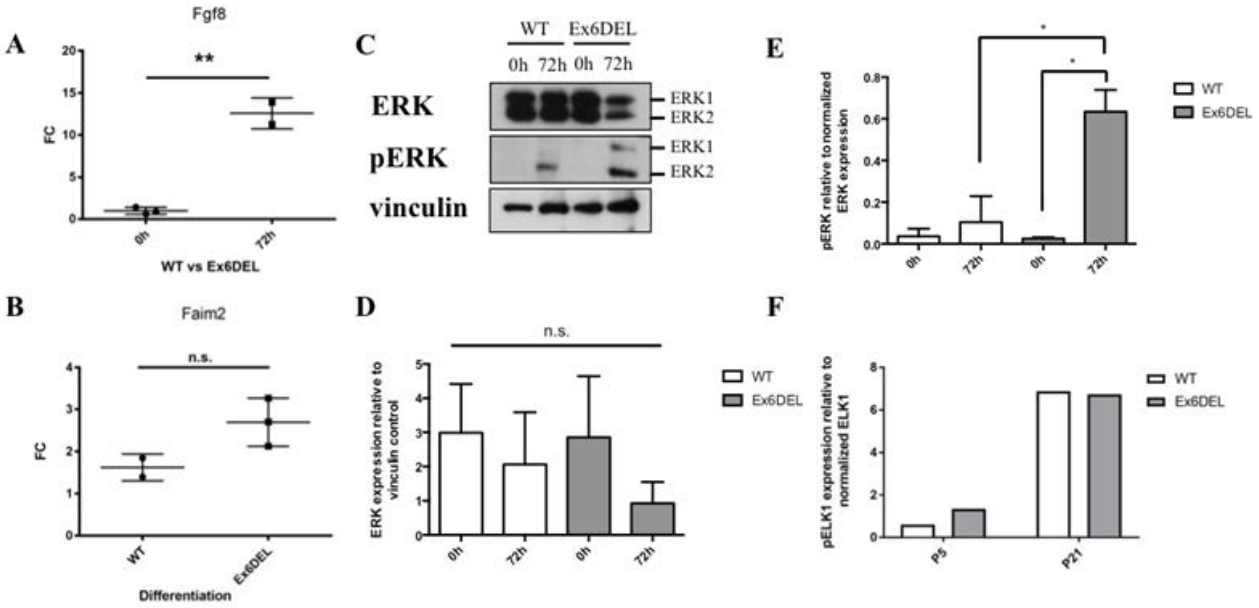


Figure 21. The ERK pathway is disrupted in Ex6DEL GNPs but it does not modify Elk1 TF activity. (A) ERK activity is assessed by immunoblotting of WT and Ex6DEL GNPs at 0h and 72h *in vitro*, and blotted for ERK, pERK and vinculin loading control. **(B)** Densitometry quantification of ERK relative to vinculin and **(C)** pERK densitometry relative to vinculin normalized ERK (n=2). **(D, E)** Fold change of Faim2 and Fgf8 (respectively) from RNA isolated from WT and Ex6DEL GNPs at 0h and 72h *in vitro*, determined by qPCR normalized according to housekeeping genes**.** Mean ± SD. **(F)** Normalized densitometry analyses of the expression of ELK1 and its active form, pELK1, in cerebellar lysates of P5 and P21 WT and Ex6DEL mice, n=1.

3.3 Loss of Snf2l activity results in increased chromatin accessibility

3.3.1 Accessibility at genomic features is not modified by Snf2l

As nucleosome remodelling proteins, Snf2h and Snf2l play an important role in regulating the chromatin landscape, with a particular role in development as demonstrated by the characterization of Snf2h-deficient and the Snf2l Ex6DEL mouse lines[50,73]. While much is known about Snf2h's promiscuous binding across the genome[36,56], little has been done regarding specific genomic interactions of Snf2l in mouse. We first attempted to perform ChIP-seq on WT and Ex6DEL GNPs in order to map Snf2l binding sites and identify Snf2l target genes. However, after thorough assessment of all commercially available mouse Snf2l antibodies, we failed to find one which provided sufficient enrichment with minimal background suitable for ChIP-seq (data not shown). Instead, we chose to employ a different sequencing methodology, Assay for Transposase-Accessible Chromatin sequencing (ATAC-seq). This technique utilizes a Tn5 transposase to cleave and attach adapters at regions of open chromatin thereby allowing for sequencing of NFRs, mono- di- and tri-nucleosomes. We sequenced biological duplicates of WT and Ex6DEL GNPs and GNs in this manner to help identify key loci which may be regulated by Snf2l. We confirmed that the resulting peaks from biological replicates had a high level of consensus peaks identical between both replicates, indicating a high level of technical reproducibility in ATAC-seq sample generation (Appendix L).

We first chose to assess the distribution of consensus accessible peaks across annotated genomic features of each timepoint in both WT and Ex6DEL samples (Fig 22). General

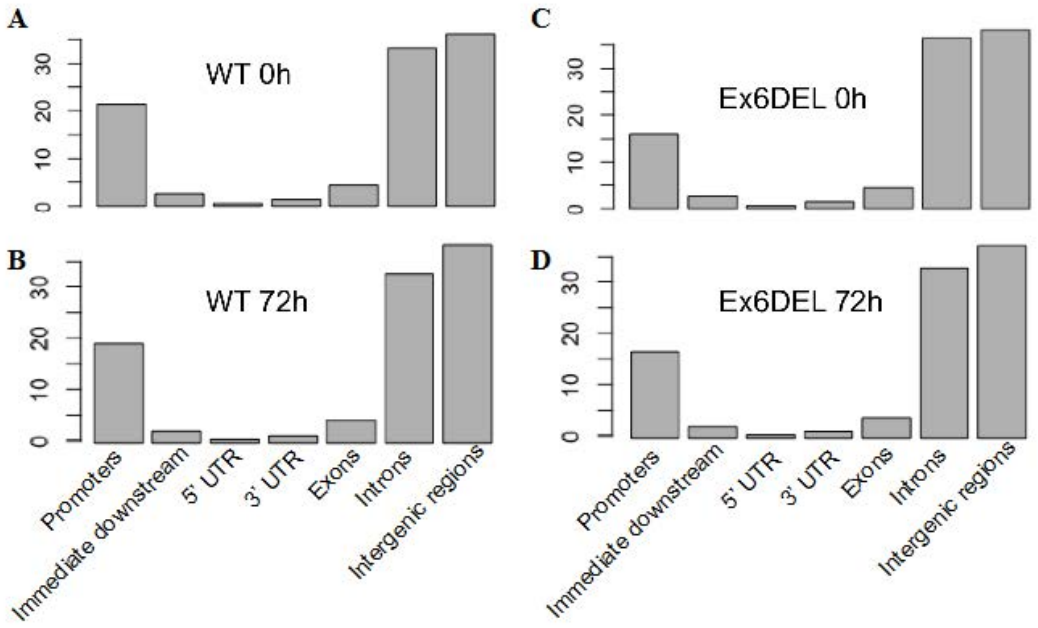


Figure 22. Chromatin accessibility distribution across genomic features is unchanged upon loss of active Snf2l. Distribution of peaks of accessibility across genomic features as a percentage of total peaks in WT **(A)** and Ex6DEL **(C)** progenitors, and differentiated neurons **(B, D).**

distribution of accessibility appears to be similar between timepoints and genotype, with the majority of accessible regions being located at promoters, introns and intergenic regions. However, a slight reduction of promoter accessibility can be noted in the Ex6DEL 0h promoter regions compared to WT (Fig 22A,C).

3.3.2 Genome wide chromatin accessibility is increased at TSS

ISWI chromatin remodellers are known to mediate nucleosome positioning immediately upstream and downstream of the TSS, as well as around the 3' end of genes. For this reason, we chose to separate ATAC-seq reads into NFR, mono-, di- and trinucleosome bins for each sample set, according to read length. This allowed us to more closely examine nucleosome positioning distribution at key features. Reads were then distributed and normalized across an average gene in order to generate accessibility profiles for WT and Ex6DEL samples (Fig 23A). Importantly, while accessibility peaks appear more distinct in Ex6DEL cultures, the location of these regions still remains similar to WT accessibility peaks. We next aimed to determine whether this averaged increase was due to increased accessibility at a subset of genes, or whether there was a greater number of genes with accessibility at the TSS. We therefore generated accessibility maps wherein reads for each gene (normalized to identical sizes) were organized vertically in order to represent accessibility at all genes (Fig 23B-E). While resolution becomes poor in the longer trinucleosome reads, the increase of accessibility of Ex6DEL cells observed in Fig 23A appears to be due to higher accessibility at genes which were already accessible in WT cultures as there was no clear increase in the number of genes with peaks at the TSS (Fig 23B-E).

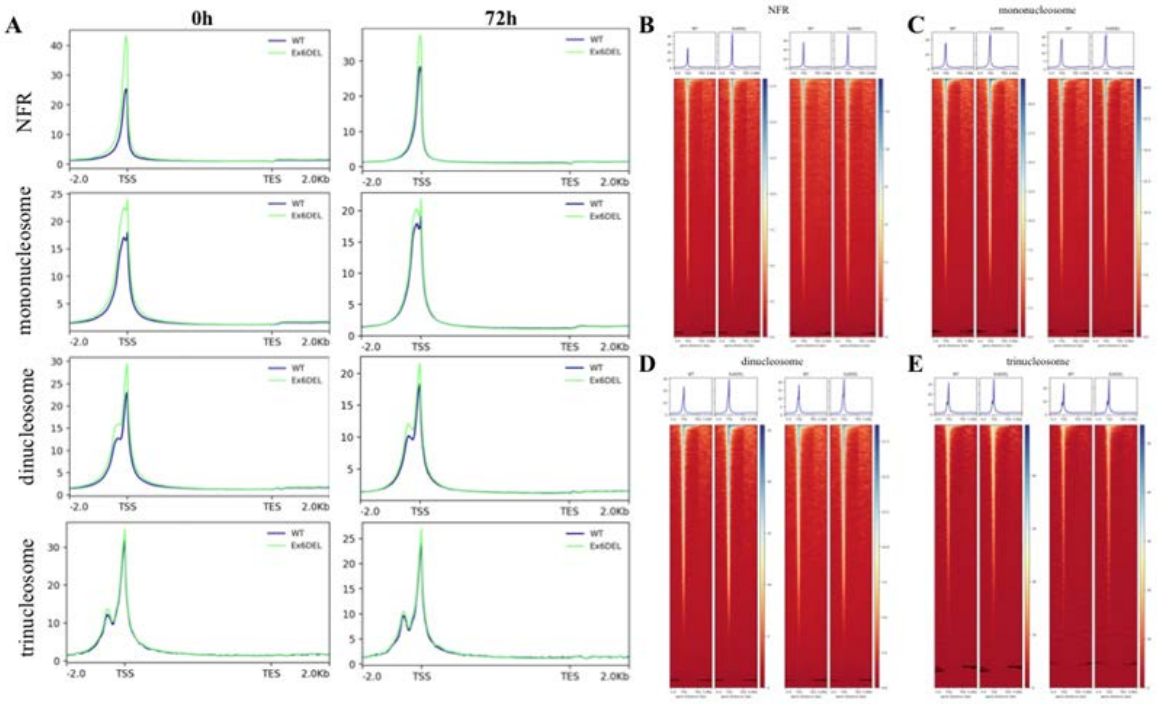


Figure 23. Snf2l mediates chromatin accessibility at the transcription start site (TSS). (A) Normalized accessibility (RPKM) across average gene from TSS to transcription end site (TES) for WT (blue) and Ex6DEL (green) at 0h and 72h of *in vitro* differentiation. ATAC-seq reads were binned into nucleosome-free regions (NFR), mononucleosome, dinucleosome and trinucleosome peaks. **(B-E)** Comparison of accessibility heatmaps and RPKM for NFR **(B)**, mononucleosome **(C)**, dinucleosome **(D)** and trinucleosome **(E)** peaks across an average gene at both 0h (left) and 72h. (right) Missing reads are annotated in black.

3.3.3 Ex6DEL chromatin landscape remains open in differentiated cells

Changes in open chromatin in Ex6DEL cells are notable when comparing total consensus peaks called for each timepoint; both 0h and 72h genotype comparisons yielded higher number of unique peaks in Ex6DEL than in WT (Fig 24C,D), from which the unique peaks at 0h are most remarkably high (approximately 33000 peaks, against only 2344 unique WT peaks). PCA analysis based on the accessibility profiles of each sample revealed that while both WT and Ex6DEL differentiated GNs are relatively similar to each other, both sets of progenitors remain in distinct areas of the plot (Fig 24A). This spatial arrangement is similarly shown by highlighting the number of DARs on a schematic diagram of the genotypes and differentiation status, as performed with the RNA-seq DEG comparisons (Fig 24B). In sum, there are 2758 DARs identified between WT and Ex6DEL progenitors while only 786 DARs distinguish both sets of differentiated cells. Further revealing the accessibility discrepancies in Ex6DEL GNPs, 8008 significant DARs mediated the WT differentiation process, while nearly 35000 are involved when lacking Snf2l activity, marking a large increase of accessibility in Ex6DEL cells not found in WT cells (Fig 24B-F), and supported by alignment of DARs and accessibility sites across the X chromosome (Fig 24G). Analysis of the significant DARs between WT and Ex6DEL samples at both 0h and 72h reveal a general increase of accessibility in the genome of Ex6DEL cells (Fig 25A-B). We then sought to establish whether changes in chromatin accessibility noted in Ex6DEL cells were correlated to DEGs obtained by RNA-seq. To this end, we searched up- and down-regulated DEGs resulting from the WT vs Ex6DEL 0h comparison for DARs in the gene and scored changes in accessibility associated to the DAR (Fig 25C,D).

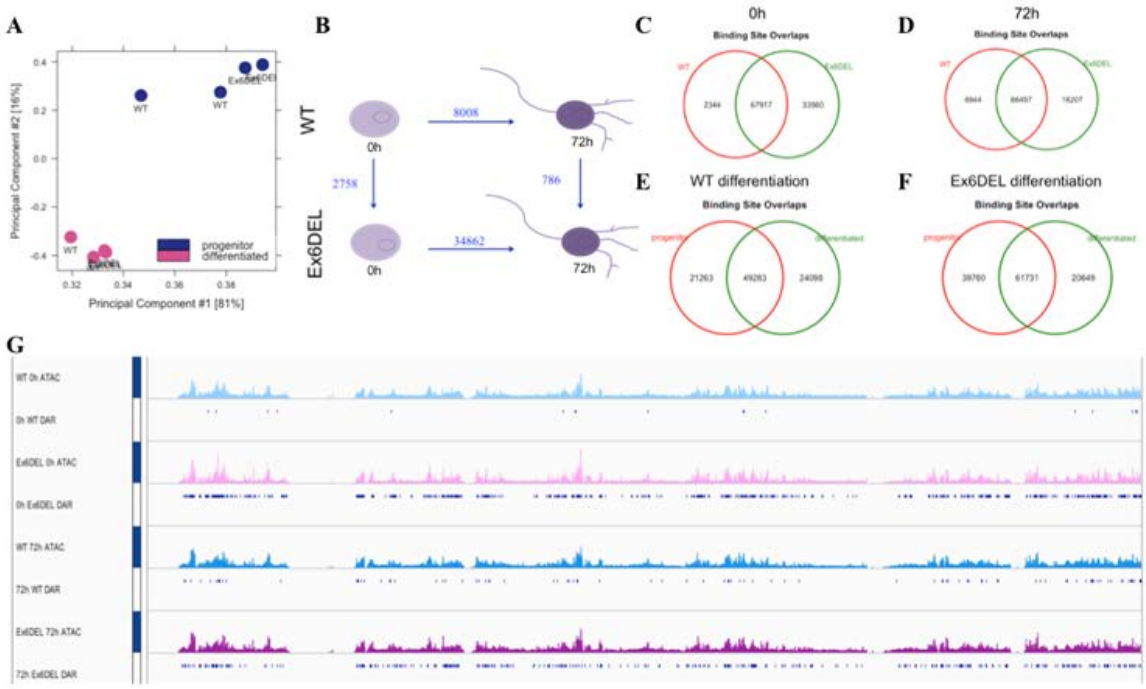


Figure 24. Snf2l Ex6DEL differentiation is associated with greater chromatin accessibility. (A) PCA plot of WT and Ex6DEL GNPs and GNs accessibility peaks. **(B)** Significantly differentially accessible regions (DAR) between pairwise comparisons (FDR < 0.05). Venn diagram grouping overlap between total consensus peaks of WT and Ex6DEL GNPs **(C)** and GNs **(D)**, and WT **(E)** and Ex6DEL **(F)** differentiation biological replicates. **(G)** Integrative genome viewer tracks along chromosome X of normalized ATAC-seq read; WT 0h (light blue), Ex6DEL 0h (light pink), WT 72h (dark blue), Ex6DEL 72h (dark pink). DARs resulting from genotype comparisons (WT vs Ex6DEL) designated with a single blue line below corresponding track.

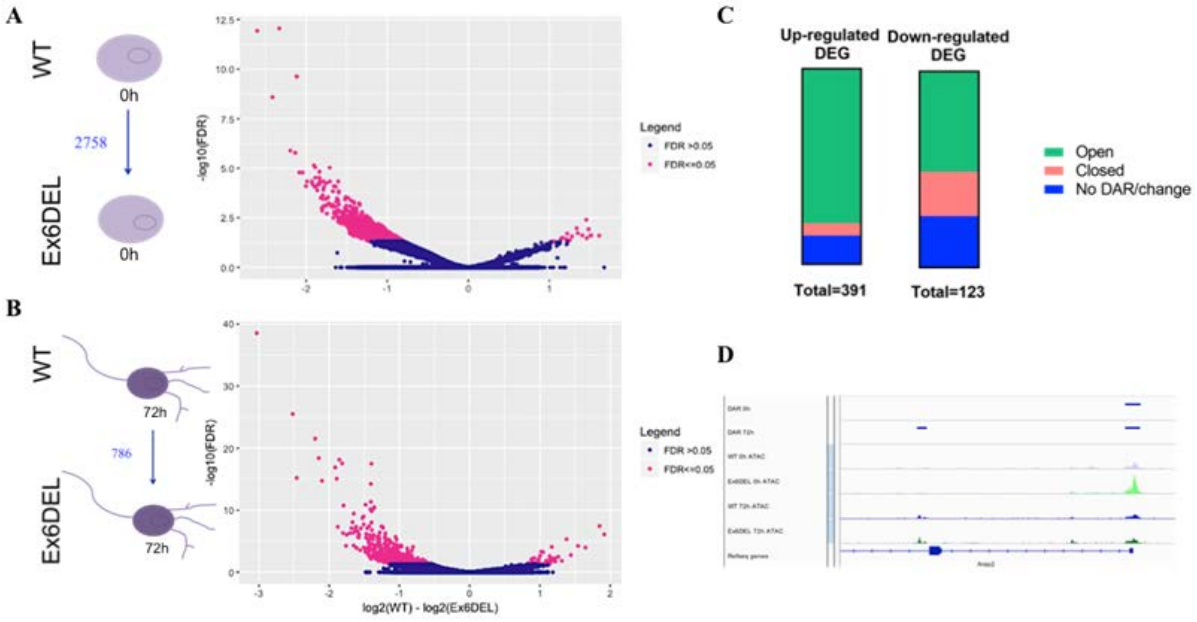


Figure 25. Loss of active Snf2l results in aberrantly open chromatin regions in both progenitors and differentiated cells. (A) Significant DARs (FDR < 0.05) plotted according to log2(Fold change) corresponding to increased accessibility in WT or Ex6DEL 0h ATAC-seq samples. **(B)** Significant DARs (FDR < 0.05) plotted according to log2(Fold change) corresponding to increased accessibility in WT or Ex6DEL 72h ATAC-seq samples. **(C)** In the subset of DEGs between WT and Ex6DEL 0h GNPs, DEGs were assessed for occupancy of at least one significant DAR in the gene, and whether the DAR increased (green) or decreased (pink) accessibility at that locus. Genes without significant DARs or accessibility changes were marked as No DAR/change (blue). **(D)** Integrated Genome Viewer tracks of increased accessibility at TSS of an up-regulated DEG, which contains a significant DAR (DAR 0h track) indicated with a blue line. Normalized ATAC-seq tracks for WT (blue) and Ex6DEL (green) progenitor (light) and differentiated (dark) GNPs on a linear scale 0-55.

In this subset of DEGs, the majority of up-regulated DEGs were accompanied by at least one DAR (79%) leading to increased accessibility, whereas this fraction is reduced in down-regulated DEGs (51%) and closed chromatin is increased (23% compared to 6%) (Fig 25C,D). An example of a DEG with increased accessibility in Ex6DEL cells is shown in Fig 25D. Moreover, Ex6DEL differentiation recruits a greater number of accessibility sites in differentiation compared to the similar WT process, and the fraction of sites shared between progenitor and differentiated cells is increased in Ex6DEL cultures (Fig 24E,F, Fig 26).

3.3.4 DARs from Ex6DEL GNPs resemble earlier progenitor cell populations

As multipotent progenitors commit towards a particular cell lineage, the chromatin landscape becomes increasingly restricted. Given that we noted a significant increase in chromatin accessibility in the Ex6DEL cultures compared to the WT cultures, and in particular at the GNP stage, we hypothesized that the loss of Snf2l slows chromatin condensation in progenitor cells, suggesting that Ex6DEL GNPs have a more "open" chromatin state that is comparable to a more pluripotent (or less committed) progenitor. To address this possibility, we made use of publicly available ATAC-seq data (GEO#: GSE98390) from E14 mouse embryonic stem cells (mESCs) and generated matching accessibility profiles as described previously (section 3.3.2) (Fig 27A,C). The mESC data was chosen for comparison as similar ATAC-seq data was not available for NSCs. As predicted, the mESCs had higher chromatin accessibility across the normalized gene, and similar accessibility at the TSS to the Ex6DEL GNPs compared to WT GNPs (Fig 27A).

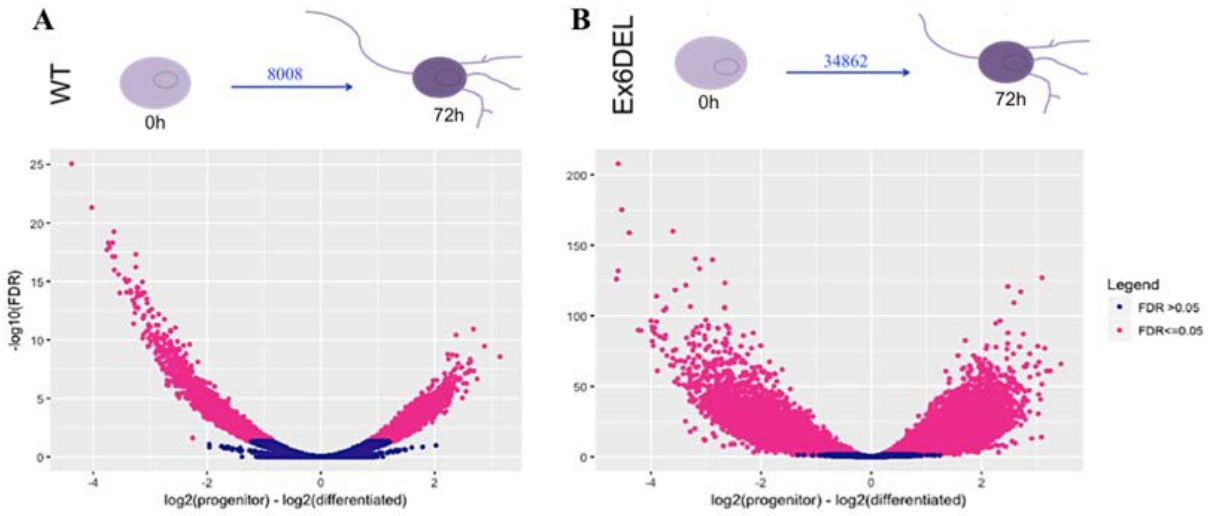


Figure 26. Ex6DEL GNP differentiation requires increased number of DARs compared to WT process. (A) Significant DARs (FDR < 0.05) plotted according to log2(Fold change) corresponding to increased accessibility in progenitor or differentiated ATAC-seq samples. **(B)** Significant DARs (FDR < 0.05) plotted according to log2(Fold change) corresponding to increased accessibility in progenitor or differentiated ATAC-seq samples.

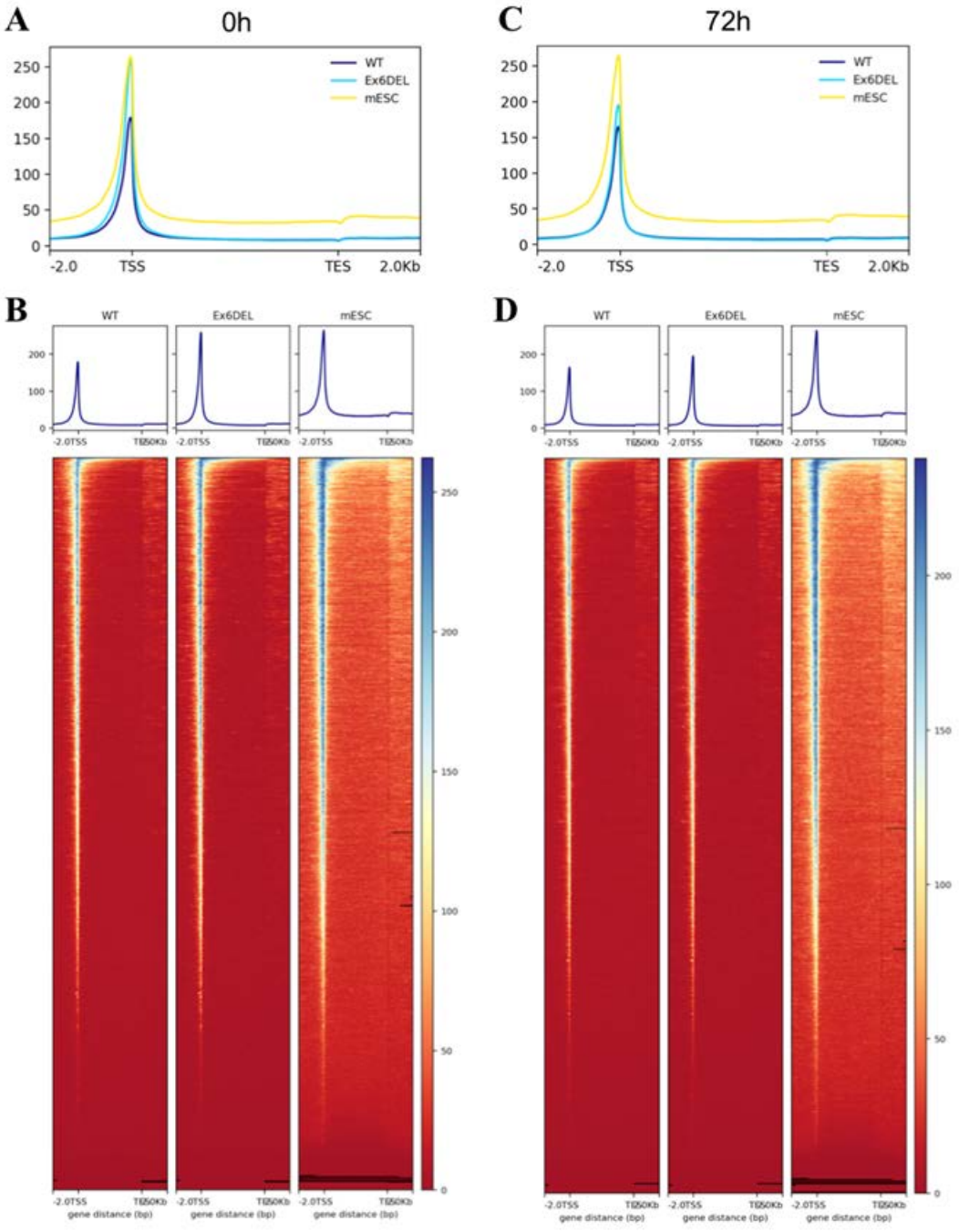


Figure 27. Ex6DEL accessibility at TSS is similar to earlier lineage mouse embryonic stem cells (mESC). (A-B) 0h WT (dark blue) Ex6DEL (light blue) and mESC (yellow) (GEO GSE98390) total averaged accessibility across a normalized gene **(A)**, and **(B)** accessibility heatmaps for WT, Ex6DEL progenitors and mESC. **(C-D)** 72h WT (dark blue) Ex6DEL (light blue) and mESC (yellow) (GEO GSE98390) total averaged accessibility across a normalized gene **(C)**, and **(D)** accessibility heatmaps for WT, Ex6DEL differentiated cells and mESC. Missing reads are annotated in black.

Accessibility heatmaps revealed that this increase was due to global reduction of chromatin condensation in mESCs (Fig 27B,D).

4. Discussion

4.1 Snf2l activity is required for timely differentiation of GNPs

In vivo, GNP differentiation begins after P6 and is mostly complete by P21 in the mouse[62]. *In vitro* however, isolated GNPs are cultured without the Shh mitogen that is produced by Purkinje cells in the cerebellum[133]. This signal maintains the proliferative state of the GNPs in the EGL *in vivo*[154,155]. Therefore, the GNPs initiate differentiation immediately upon plating in the culture conditions we have described previously (section 2.2.1). While WT cultures begin differentiating by 24h in *vitro* and complete differentiation by 3 DIV (Figs 7,10), the majority of Ex6DEL GNPs remain undifferentiated at 3 DIV (Fig 10). Actively proliferating cells are positive for Ki67 staining, while differentiated neurons lose this proliferative marker and instead express NeuN, present in post-mitotic neurons. Accordingly, WT GNPs are initially $Ki67^{+}NeuN^{-}$, and this marker identity switches by 3 DIV (Fig 11). However, Ex6DEL cells retain the $Ki67^{+}NeuN^{-}$ progenitor expression pattern and are drastically delayed in expressing NeuN (Fig 11). This staining pattern suggests that loss of Snf2l activity hinders the ability of GNPs to initiate terminal differentiation at the same rate as WT GNPs. Snf2l has been known to be required for cell differentiation processes, as loss of Snf2l in Hela cells results in increased culture proliferation[51] and Ex6DEL mice show increased numbers of intermediate progenitor cells leading to a larger brain[73]. BrdU pulse labelling

of GNP cultures also suggests that Ex6DEL cells are remaining in a proliferative state for an extended period of time; BrdU incorportation remains significantly increased compared to WT cells between 0 and 48h *in vitro* (Fig 12). GNPs in culture do not actively replicate due to culture conditions[133] (Fig 12C), yet Ex6DEL maintain a GNP state for several days *in vitro* without differentiating with no notable change in levels of caspase-3, a marker of apoptosis[156] (data not shown). Our data suggests that Ex6DEL GNPs retain progenitor marker expression and remain in the cell cycle for a delayed period, whether due to prolonged cell cycle or failure to promptly exit the cell cycle. As such, GNPs appear to be delayed in losing their progenitor identity and initiating terminal differentiation without Snf2l activity, which has been previously reported in other model systems[51,55,92,157].

4.2 Terminal differentiation without Snf2l remodelling occurs according to a distinct mechanism compared to WT GNPs

Differentiation of a progenitor into a committed cell requires extensive restructuring of gene expression programs in order to accommodate cellular demands of the mature cell. This broad transcriptome shift is regulated in large part by chromatin remodelling proteins. As ISWI proteins are known to have extensive binding sites, in particular to promoter regions and the TSS of genes[31,36,56], we reasoned that Snf2l may be responsible for mediating expression of key genes required for the transition from progenitor to differentiated state. We undertook RNA-seq analysis between WT and Ex6DEL GNPs

and GNs in an attempt to uncover key pathways and mechanisms of GNP differentiation that were misregulated upon loss of Snf2l remodelling activity.

Significantly enriched GO terms amongst genes upregulated in Ex6DEL GNs relative to WT revealed several terms such as Positive Regulation of ERK1 and ERK2 cascade and Positive Regulation of MAPK cascade (Fig 19C). While the ERK pathway has been studied extensively in the context of cancers[158], renewed interest in these signalling factors has been sparked by potential involvement in neurodevelopmental and intellectual disability disorders[159,160]. In neurons, ERK signalling may be responsible for neuroplasticity and synaptic function, but also long-term memory[161]. Culture of rat-derived GNPs allowed for study of the role of the ERK pathway in synaptic potential and neurite outgrowth, yet activation of this pathway has also been associated with proliferation and survival in these cells[162].

Chromatin remodelling proteins can mediate TFs and signalling cascades in order to govern drastic cell changes[36,37,50,51,73]. Therefore, we reasoned that Snf2l may be capable of mediating the expression of an important regulator or member of the ERK pathway in order to regulate the cell cycle exit and promote neuron differentiation. Careful search of our RNA-seq datasets revealed an up-regulation of Fgf8 (Fig 21A), a fibroblast growth factor which is critical for cerebellar development[163–165]. Loss of *Fgf8*, as well as *Fgf17*, leads to reduced precursor proliferation at E11.5 in the hindbrain and disrupts cerebellar patterning and ataxia[164]. Fgf8 expression is also responsible for the maintenance of proliferative and undifferentiated pools of neural crest cells and spermatogonial stem

cells *in vivo*[166,167]. Mechanistically, Fgf8 is an activator of the Ras-ERK pathway in the early cerebellum[163,165], and therefore its increased expression in Ex6DEL mice would suggest heightened activation of ERK signalling. We were able to confirm an increase of activation of the ERK pathway through up-regulation of phosphorylation of ERK in the 72h cultures of Ex6DEL cells (Fig 21C-E).

Upon investigation of the numerous targets of ERK1/2 activity, phosphorylation of histone H3 at ser10 was identified as a commonly phosphorylated target[168]. During interphase, phosphorylation of H3 (pH3) is associated with increased transcription of key target genes[152,168]. While we have found an increase of pH3 in both WT and Ex6DEL P5 cerebellar lysates due to the abundance of cycling progenitors at this timepoint, we were not able to distinguish significant differences in pH3 expression in P21 Ex6DEL cerebella (data not shown).

Analysis of the TFBS governing DEGs at 72h allowed for the identification of three TFs (*Foxd1, Hlf, Sox2*) which may regulate Ex6DEL down-regulated genes. Interestingly, these three TFs were themselves down-regulated in our RNA-seq data. Similarly, one up-regulated TF, *Ebf1*, governed up-regulated DEGs in Ex6DEL cells (Fig 20C-E). This suggests that Snf2l may be regulating key TFs which are critical to maintain extended gene expression programs. TFBS analysis also revealed that down-regulated DEGs in Ex6DEL differentiation (Appendix D) and up-regulated DEGs in Ex6DEL GNPs (Appendix I) were both significantly enriched for Elk1 TFBSs. Elk1 is a TF which is phosphorylated (pElk1) downstream of the ERK pathway and has been shown to regulate

neuronal differentiation[151,169–171]. However, we were unable to uncover changes in Elk1 activation in P5 or P21 cerebellar lysates from Ex6DEL animals (Fig 21F).

However, regulation of the Ras-ERK pathway appears to extend beyond rudimentary activation by phosphorylation or feedback loops. In fact, the manner of activation, and duration of activation of the ERK pathway owing to regulatory feedback mechanisms also significantly impacts the cellular outcome of pathway recruitment. In a differentiation PC12 *in vitro* model, Santos *et al*. were able to induce or avert neurite outgrowth by treatment with NGF or EGF, respectively, and inversed these effects when they modified the topology of both activation pathways suggesting that the timing and duration of ERK activation is critical to determine biological outcomes[169]. This remains an unexplored aspect of the present study.

4.3 A role for Snf2l in mediating chromatin compaction underlying cell differentiation

Little is known about the chromatin remodelling targets of Snf2l in development. We endeavoured to employ our catalytically inactive Snf2l mouse model to probe the Snf2l-specific remodelling contributions to the chromatin landscape. We first opted to perform ChIP-seq on WT and Ex6DEL GNPs in order to discern binding sites of Snf2l across the genome, however this proved difficult; commercially available Snf2l antibodies were not suitable for ChIP-seq (data not shown), and the added complication that Ex6DEL Snf2l complexes are still recruited to chromatin despite being inactive (Fig 14C, discussed in section 4.4) we decided to abandon this approach. Instead, we turned to methodology

developed by Buenrostro *et al*., ATAC-seq. ATAC-seq enables efficient sequencing of regions of open chromatin which encompass NFRs, mono-, di- and trinucleosomes[137]. We first explored chromatin organization across genes, as ISWI proteins are known to remodel nucleosomes at the TSS and 3' region of target genes[31]. There was no significant change in chromatin accessibility at genomic features in both WT and Ex6DEL (Fig 22) as well as in the positioning of NFRs or small nucleosome arrays across genes (Fig 23A). However, we observed a surprising increase of accessibility at the TSS of genes in the Ex6DEL genome, most pronounced at 0h *in vitro* (Fig 23,24). Elevated numbers of DARs representing increased chromatin accessibility in Ex6DEL GNPs also revealed a potential role for Snf2l in mediating chromatin compaction and gene expression in these cells (Fig 24,25). In fact, when the subset of DEGs between WT and Ex6DEL GNPs was evaluated for presence of DARs in the gene, we found that the majority of up-regulated genes in Ex6DEL cells (79%) had at least one DAR in which chromatin was more accessible. Inversely, within down-regulated DEGs we found that the proportion of associated DARs indicating increased accessibility was decreased (51%) and closed chromatin increased from 6% to 23% (Fig 25). DEGs with DARs reflecting changes in chromatin accessibility corresponding to their change in expression may in fact represent direct targets of Snf2l remodelling.

Next-generation sequencing has allowed for increasingly precise investigation of cell behaviour in specific cell populations. This has advanced our understanding of the complexity and dynamism of the chromatin landscape throughout early development and cell lineage establishment. The earliest stages of pre-implantation development implicate

rapid expansion of accessible chromatin regions[172–174]. The distribution of accessibility is also quickly modified in the first stages of the embryo; while 1-, 2- and 4-cell embryo accessibility is restricted to promoters, ESCs have a high proportion of accessible sites at intergenic regions at the expense of earlier promoter accessibility[174]. Later cell fate decisions require gradual restriction of gene expression profiles leading the cell to express genes proper to only one branch of terminally differentiated cells[4,175]. This specification requires certain progenitor transcripts to be down-regulated by decreasing chromatin accessibility, while genes required to direct the developmental fate become more accessible[4]. As we had observed that Ex6DEL GNPs exhibited increased open chromatin compared to WT cells prior to *in vitro* differentiation (Fig 25A-B), we reasoned that loss of Snf2l may cause isolated GNPs to be delayed in their differentiation trajectory. We thus compared accessibility of WT and Ex6DEL cultures to published E14.5 mESC ATAC-seq data. Without Snf2l remodelling, average chromatin accessibility in Ex6DEL GNPs was similar to that of mESCs (Fig 27). Snf2l therefore plays an important role in reducing chromatin accessibility prior to differentiation, whereby GNPs are primed to terminally differentiate into GNs. This finding was somewhat unexpected as Snf2l is known to be most highly expressed in differentiated neurons[19,50,73], yet the other member of the NURF complex, Bptf, is critical in embryonic development[91,96,97,176]. It is therefore possible that the NURF complex may be required earlier in cerebellar development in order to begin to restrict the chromatin landscape in progenitors. Snf2l has previously been shown to be required for proper cell fate delineation in the cerebral cortex of Ex6DEL mice, again indicating that Snf2l may be required at earlier developmental stages where it may be less abundant[73].

However, differentially accessible loci data are not necessarily a direct reflection of Snf2l remodelling activity, but rather a global snapshot of all open chromatin at the moment of tagmentation. In this manner, we cannot exclude the possibility that increased chromatin accessibility could be caused by increased transcription triggered by a number of direct Snf2l targets such as TFs instead of the loss of direct Snf2l remodelling or maintenance.

4.4 Compensation by chromatin remodelling complexes

While the present study was able to establish a role for Snf2l catalytic activity in GNP differentiation, regulation and compensation by Snf2h and non-catalytic subunits cannot be excluded. Historically, the seven mammalian ISWI complexes have been known as Snf2h- or Snf2l-specific[46]. Evidence has recently begun to emerge indicating that ISWI complex composition may indeed be more fluid than previously believed[80,177]. In this manner, any given complex could incorporate either Snf2l or Snf2h to mediate catalytic activity[80]. This is not surprising, as mammalian ISWI proteins share approximately 86% identity[19]. The specificity of remodelling which is conferred by the particular ISWI proteins is not yet clear. Within Snf2h complexes, remodelling activity has been shown to be modified by the individual subunits with which Snf2h is associated[77]. However, the main catalytic core of remodelling complexes may still impart some level of regulation in its activity. Switching only the ATPase domains of BRG1 and Snf2h modified remodelling activity and partially altered remodelling loci in accordance to the origin ATPase, and not of the remaining protein[178]. Similar differences may be expected when Snf2l is substituted for Snf2h within an ISWI complex.

Our study employed a Snf2l mouse model which was not a total protein KO but rather a catalytic dead isoform, Ex6DEL, which produced a smaller protein following the excision of exon 6 (Fig 9). This mutant is functionally similar to the naturally-occurring *SMARCA1* splice variant, SNF2L+13 which is present in all non-neuronal and reproductive tissues[34,49,104]. Although inactive, this variant still has the capacity to be included in its chromatin remodelling complexes[49,80]. We therefore confirmed that the Ex6DEL Snf2l isoform was also still able to interact with CERC2 from the CERF complex (Fig 14C). Thus, it is reasonable to assume that the Ex6DEL complexes are still being recruited to the genome. It has been shown that ISWI's genomic interactions can occur independently of catalytic activity. Indeed, immobilization times of the Snf2l+13 catalytically inactive splice variant on specific loci of the genome are similar to those of WT Snf2h and Snf2l[30,75]. This may be particularly relevant in the context of complexes such as NURF, where Bptf has been shown to be able to independently recruit TFs to the genome[37]. Harmful effects of inactive Snf2l may be mitigated by remodelling-independent properties of Cecr2 and Bptf. The loss of Bptf or Cecr2 in the mouse results in embryonic lethality, neural tube defects, exencephaly and facial clefts[32,47,91,99], while the Ex6DEL mouse has a very mild phenotype in comparison, suggesting that Bptf and Cecr2 can counteract some of the effects of the loss of Snf2l but not vice-versa.

Aside from potential compensation by non-catalytic subunits, partial recovery of Snf2l-specific remodelling activity may be carried out by Snf2h. Snf2h has been reported to be the main ISWI protein interacting with Cecr2 in the testis[177], and both Bptf and Cecr2 can

be purified associated to Snf2l or Snf2h at a 1:1 ratio[80]. Our group has previously demonstrated that upon cKO of Snf2h, Snf2l was upregulated at an early stage[50], which is supported by previous literature[51]. This shift was able to partially recover regulation of the *En1* locus, typically governed in progenitors by Snf2h[50]. Embryonic lethality of Snf2h KO mice[48] may be indicative of the compensation potential between ISWI members; Snf2l may not be sufficiently abundant at embryonic timepoints to replace Snf2h's catalytic activity. A double cKO (cDKO) of both Snf2l and Snf2h in which no ISWI compensation was possible resulted in animals which died at birth[50]. However, our study has found that there is an up-regulation of Snf2h expression upon loss of Snf2l activity in GNPs relative to WT cells, as well as premature Snf2l expression (Fig 14A). This suggests attempts at recovery of ISWI remodelling in the absence of Snf2l-mediated remodelling. In fact, analysis of the catalytic activity of purified recombinant Snf2l- and Snf2h-containing complexes revealed that Snf2h is a more effective remodelling catalyst in the presence of a nucleosome array[80]. It is thus possible that Snf2h may be more readily capable of compensating for lacking Snf2l activity, while Snf2l's lower remodelling rate may not be able to completely recover for loss of Snf2h in the case of the Snf2h cKO model[50]. Additionally, we observed aberrant Bptf and Cecr2 expression in Ex6DEL GNPs (Fig 14A), further indicating attempts at compensation of remodelling in these cells. Oppikofer *et al*. have suggested that non-catalytic subunit assembly choice may be heavily dictated by the relative abundance of each protein, indicating that transcriptional control mediates complex composition and therefore, ISWI activity[80]. Snf2l complexes may therefore be critical even in stages of low protein abundance in order to begin restricting transcription and drive the cell towards terminal differentiation,

as previously discussed (section 4.3). Lack of Snf2l remodelling at key differentiation genomic targets may therefore be partially recovered by Snf2h activity, which is already abundant in progenitor cells.

4.5 Future Directions

This study has determined that Ex6DEL cultures recruit increased activation of the ERK signalling pathway compared to WT cells (Fig 21). However, while we have suggested that up-regulated Fgf8 expression may be causing this aberrant signalling, we are still uncertain how this pathway contributes to the Ex6DEL *in vitro* and *in vivo* phenotypes observed. Analysis of DEGs in Ex6DEL cells revealed that a small number of TFs could be mediating large transcriptomic shifts (Fig 20), and in particular we have proposed Elk1 as a potential deregulated target downstream of ERK in the Ex6DEL mouse model (Fig 21). Unfortunately, changes in protein expression of Elk1 and pElk1 at the level of cerebellar lysates were not supportive of this hypothesis (Fig 21). The cerebellum is composed of a number of cell types[62] which may obscure changes of activation strictly in GNPs. For this reason, we suggest studying GNP-specific Elk1 activation levels.

While our group has previously generated a catalytic dead Snf2l mouse model[73], our findings have suggested that Ex6DEL Snf2l is still capable of interacting with CECR2 from the CERF chromatin remodelling complex (Fig 14C). As discussed previously, there is potential for compensation of inactivation of Snf2l *in vivo* by Snf2h and/or non-catalytic subunits (Fig 14 and [50,80,177]). This study highlights the need for a Snf2l KO mouse model, wherein Snf2l remodelling complexes would not be able to form without

associating to Snf2h instead[80,177]. In this manner, ISWI compensation would be more readily discernable in order to determine the molecular underpinnings of Snf2h- and Snf2l-mediated remodelling, and potential activity overlap between both. This KO model would also allow us to more clearly outline the role of Snf2l in neurodevelopment. While Snf2h KO models are not viable and cKO models suffer from significant impairment and reduction of lifespan[48,50], loss of Snf2l activity does not appear to hinder motor or behavioural capacities[73]. It is therefore of interest whether complete abrogation of Snf2l expression would result in a more severe phenotype than the Ex6DEL mouse model.

The potential for compensation between ISWI proteins, and within ISWI remodelling complexes, renders studies of these proteins difficult. As previously discussed, the presence of Snf2l-interacting non-catalytic subunits may muddle analysis of the role of this molecular motor. Therefore, this underlines the need for the generation of specific KOs of individual subunits in order to assess specific roles carried out by each complex[47]. In fact, there may be important functions for individual chromatin remodelling complexes in mediating neurodevelopment. The related NuRD chromatin remodelling complexes are composed of either CHD3, CHD4 or CHD5 ATPase-dependent remodellers, as well as various non-catalytic subunits. Recent work carefully limiting activity of each of these catalytic subunits in neuronal progenitors has revealed that particular complexes are exclusively required to mediate different stages of cortical development (proliferation, migration or differentiation)[179].

We have determined that a subset of DEGs identified by RNA-seq have associated DARs which dictate their change of expression (Fig 25C). This subset of genes may represent

direct targets of Snf2l chromatin remodelling. It will be of interest to further investigate whether these changes in accessibility are directly caused by absence of Snf2l activity. Analysis of Snf2l binding at these loci by ChIP could be valuable in determining direct interaction of Snf2l at the sites of the DARs. As discussed earlier in this thesis, the lack of suitable Snf2l antibodies for ChIP-seq experiments prevented us from generating Snf2l binding site data. No mouse-specific Snf2l binding data exists to date, and this information could be useful in trying to discern direct targets of Snf2l remodelling. As an alternative to antibody generation, we suggest generating a CRISPR-Cas9-mediated tag knock-in that generates a tagged recombinant Snf2l protein in order to be able to perform ChIP-seq by immunoprecipitating the tag, thereby avoiding the need for antibody optimization. In combination with the previously discussed ATAC-seq data, ChIP-seq analysis of Snf2l genomic binding sites would provide powerful insight into the roles of Snf2l and its associated chromatin remodelling complexes. In addition, the degree of similarity of Snf2l and Snf2h[56] binding sites would be telling of their ability to co-regulate key loci in development[50].

References

1. Venkatesh, S. & Workman, J. L. Histone exchange, chromatin structure and the regulation of transcription. *Nature* **16,** (2015).
2. Perrod, S. & Gasser, S. M. Long-range silencing and position effects at telomeres and centromeres: parallels and differences. *Cell. Mol. Life Sci.* (2003). doi:10.1007/s00018-003-3246-x
3. Rego A, Sinclair PB, Tao W, Kireev I, B. A. The facultative heterochromatin of the inactive X chromosome has a distinctive condensed ultrastructure. *J. Cell Sci.* (2008). doi:10.1242/jcs.026104
4. Cusanovich, D. A. *et al.* The cis-regulatory dynamics of embryonic development at single-cell resolution. *Nat.* **555,** (2018).
5. Bannister, A. J. & Kouzarides, T. Regulation of chromatin by histone modifications. *Cell Res.* **21,** 381–395 (2011).
6. Tekel, S. J. & Haynes, K. A. Molecular structures guide the engineering of chromatin. *Nucleic Acids Res.* **45,** 7555–7570 (2017).
7. Lorzadeh, A., Bilenky, M., Hammond, C. & et al. Nucleosome Density ChIP-Seq Identifies Distinct Chromatin Modification Signatures Associated with MNase Accessibility. *Cell Rep.* **17,** 2112–2124 (2016).
8. Flaus, A. & Owen-Hughes, T. Mechanisms for ATP-dependent chromatin remodelling: The means to the end. *FEBS J.* (2011). doi:10.1111/j.1742-4658.2011.08281.x
9. Narlikar, G. J., Sundaramoorthy, R. & Owen-Hughes, T. Mechanisms and Functions of ATP-Dependent Chromatin-Remodeling Enzymes. *Cell* (2013). doi:10.1016/j.cell.2013.07.011
10. Clapier, C. R., Iwasa, J., Cairns, B. R. & Peterson, C. L. Mechanisms of action and regulation of ATP-dependent chromatin-remodelling complexes. *Nat. Rev.* **18,** (2017).
11. Neigeborn, L. & Carlson, M. Genes affecting the regulation of Suc2 gene expression by glucose repression in Saccharomyces cerevisiae. *Genetics* (1984).
12. Wang, W. *et al.* Diversity and specialization of mammalian SWI/SNF complexes. *Genes Dev.* (1996).
13. Peterson, C. L. & Herskowitz, H. Characterization of the Yeast SW/l, SW2, and SW13 Genes, Which Encode a Global Activator of Transcription. *Cell* **68,** 573–583 (1992).
14. Hargreaves, D. C. & Crabtree, G. R. ATP-dependent chromatin remodeling: genetics, genomics and mechanisms. *Cell Res.* **2132,** (2011).
15. Tsukiyama, T. & Wu, C. Purification and Properties of an ATP-Dependent Nucleosome Remodeling Factor. *Cell* **83,** (1995).
16. Tsukiyama, T., Daniel, C., Tamkun, J. & Wu, C. ISWI, a Member of the SWI2/SNF2 ATPase Family, Encodes the 140 kDa Subunit of the Nucleosome Remodeling Factor. *Cell* **83,** 1021–1026 (1995).
17. Guschin, D. *et al.* Multiple ISWI ATPase Complexes from Xenopus laevis. *J. Biol. Chem.* (2000). doi:10.1074/jbc.M006041200
18. Ocampo, J., Azvan, R., Chereji, V., Eriksson, P. R. & Clark, D. J. The ISW1 and CHD1 ATP-dependent chromatin remodelers compete to set nucleosome spacing

in vivo. *Nucleic Acids Res.* **44,** 4625–4635 (2016).
19. Lazzaro, M. A. & Picketts, D. J. Cloning and characterization of the murine Imitation Switch (ISWI) genes: Differential expression patterns suggest distinct developmental roles for Snf2h and Snf2l. *J. Neurochem.* **77,** 1145–1156 (2001).
20. Alkhatib, S. G. & Landry, J. W. The nucleosome remodeling factor. *FEBS Lett.* **585,** 3197–3207 (2011).
21. Strohner, R. *et al.* NoRC - a novel member of mammalian ISWI-containing chromatin remodeling machines. *EMBO J.* **20,** 4892–4900 (2001).
22. Toto, M., D'Angelo, G. & Corona, D. E. V. Regulation of ISWI chromatin remodelling activity. *Chromosoma* 91–102 (2014).
23. Grüne, T. *et al.* Crystal Structure and Functional Analysis of a Nucleosome Recognition Module of the Remodeling Factor ISWI. *Mol. Cell* **12,** 449–460 (2003).
24. Aalfs, J. D., Narlikar, G. J. & Kingston, R. E. Functional Differences between the Human ATP-dependent Nucleosome Remodeling Proteins BRG1 and SNF2H. *J. Biol. Chem.* **276,** 34270–34278 (2001).
25. Zofall, M., Persinger, J. & Bartholomew, B. Functional Role of Extranucleosomal DNA and the Entry Site of the Nucleosome in Chromatin Remodeling by ISW2. *Mol. Cell. Biol.* **24,** 10047–57 (2004).
26. Yang, J. G., Madrid, T. S., Sevastopoulos, E. & Narlikar, G. J. The chromatin-remodeling enzyme ACF is an ATP-dependent DNA length sensor that regulates nucleosome spacing. *Nat. Struct. Mol. Biol.* **13,** 1078–1083 (2006).
27. Blosser, T. R., Yang, J. G., Stone, M. D., Narlikar, G. J. & Zhuang, X. Dynamics of nucleosome remodelling by individual ACF complexes. *Nature* **462,** 1022–1027 (2009).
28. Hwang, W. L., Deindl, S., Harada, B. T. & Zhuang, X. Histone H4 tail mediates allosteric regulation of nucleosome remodelling by linker DNA. *Nature* **512,** 213–217 (2014).
29. Tallant, C. *et al.* Molecular Basis of Histone Tail Recognition by Human TIP5 PHD Finger and Bromodomain of the Chromatin Remodeling Complex NoRC. *Structure* (2015). doi:10.1016/j.str.2014.10.017
30. Erdel, F. & Rippe, K. Quantifying transient binding of ISWI chromatin remodelers in living cells by pixel-wise photobleaching profile evolution analysis. *Proc. Natl. Acad. Sci.* **109,** E3221-30 (2012).
31. Sala, A. *et al.* Genome-wide characterization of chromatin binding and nucleosome spacing activity of the nucleosome remodelling ATPase ISWI. *EMBO J.* **30,** 1766–1777 (2011).
32. Banting, G. S. *et al.* CECR2, a protein involved in neurulation, forms a novel chromatin remodeling complex with SNF2L. *Hum. Mol. Genet.* **14,** 513–524 (2005).
33. Clapier, C. R. & Cairns, B. R. The Biology of Chromatin Remodeling Complexes. *Annu. Rev. Biochem.* (2009). doi:10.1146/annurev.biochem.77.062706.153223
34. Ye, Y. *et al.* Singular v dual inhibition of SNF2L and its isoform, SNF2LT, have similar effects on DNA damage but opposite effects on the DNA damage response, cancer cell growth arrest and apoptosis. *Oncotarget* **3,** 475–89 (2012).
35. Kwon, S. Y., Grisan, V., Jang, B., Herbert, J. & Badenhorst, P. Genome-Wide

Mapping Targets of the Metazoan Chromatin Remodeling Factor NURF Reveals Nucleosome Remodeling at Enhancers, Core Promoters and Gene Insulators. *PLoS Genet.* **12,** 1–26 (2016).
36. Wiechens, N. *et al.* The Chromatin Remodelling Enzymes SNF2H and SNF2L Position Nucleosomes adjacent to CTCF and Other Transcription Factors. *PLoS Genet.* **12,** 1–25 (2016).
37. Qiu, Z. *et al.* Functional Interactions between NURF and Ctcf Regulate Gene Expression. *Mol. Cell. Biol.* **35,** 224–37 (2015).
38. Guetg, C. *et al.* The NoRC complex mediates the heterochromatin formation and stability of silent rRNA genes and centromeric repeats. *EMBO J.* **29,** 2135–46 (2010).
39. Culver-Cochran, A. E. & Chadwick, B. P. Loss of WSTF results in spontaneous fluctuations of heterochromatin formation and resolution, combined with substantial changes to gene expression. *BMC Genomics* **14,** 740 (2013).
40. Hanai, K., Furuhashi, H., Yamamoto, T., Akasaka, K. & Hirose, S. RSF governs silent chromatin formation via histone H2Av replacement. *PLoS Genet.* **4,** (2008).
41. Dowdle, J. A. *et al.* Mouse BAZ1A (ACF1) Is Dispensable for Double-Strand Break Repair but Is Essential for Averting Improper Gene Expression during Spermatogenesis. *PLoS Genet.* **9,** (2013).
42. Kubota, Y., Shimizu, S., Yasuhira, S. & Horiuchi, S. SNF2H interacts with XRCC1 and is involved in repair of H2O2-induced DNA damage. *DNA Repair (Amst).* **43,** 69–77 (2016).
43. Lan, L. *et al.* The ACF1 Complex Is Required for DNA Double-Strand Break Repair in Human Cells. *Mol. Cell* **40,** 976–987 (2010).
44. Barnett, C. & Krebs, J. E. WSTF does it all: a multifunctional protein in transcription, repair, and replication. *Biochem. Cell Biol.* **89,** 61–73 (2011).
45. Atsumi, Y. *et al.* ATM and SIRT6/SNF2H Mediate Transient H2AX Stabilization When DSBs Form by Blocking HUWE1 to Allow Efficient gH2AX Foci Formation. *Cell Rep.* **13,** 2728–2740 (2015).
46. Erdel, F. & Rippe, K. Chromatin remodelling in mammalian cells by ISWI-type complexes - Where, when and why? *FEBS J.* **278,** 3608–3618 (2011).
47. Goodwin, L. R. & Picketts, D. J. The role of ISWI chromatin remodeling complexes in brain development and neurodevelopmental disorders. *Mol. Cell. Neurosci.* 1–10 (2018). doi:10.1016/j.mcn.2017.10.008
48. Stopka, T. & Skoultchi, A. I. The ISWI ATPase Snf2h is required for early mouse development. *Proc. Natl. Acad. Sci. U. S. A.* **100,** 14097–102 (2003).
49. Barak, O., Lazzaro, M. A., Cooch, N. S., Picketts, D. J. & Shiekhattar, R. A tissue-specific, naturally occurring human SNF2L variant inactivates chromatin remodeling. *J. Biol. Chem.* **279,** 45130–45138 (2004).
50. Alvarez-Saavedra, M. *et al.* Snf2h-mediated chromatin organization and histone H1 dynamics govern cerebellar morphogenesis and neural maturation. *Nat. Commun.* **5,** 4181 (2014).
51. Eckey, M. *et al.* Nucleosome remodeler SNF2L suppresses cell proliferation and migration and attenuates Wnt signaling. *Mol. Cell. Biol.* **32,** 2359–71 (2012).
52. Koludrovic, D. *et al.* Chromatin-Remodelling Complex NURF Is Essential for Differentiation of Adult Melanocyte Stem Cells. *PLoS Genet.* **11,** e1005555

(2015).
53. Hitoshi, S. *et al.* Primitive neural stem cells from the mammalian epiblast differentiate to definitive neural stem cells under the control of Notch signaling. *Genes Dev.* 1806–1811 (2004).
54. Barak, O. *et al.* Isolation of human NURF: a regulator of Engrailed gene expression. *EMBO J.* (2003).
55. Pépin, D., Paradis, F., Perez-Iratxeta, C., Picketts, D. J. & Vanderhyden, B. C. The imitation switch ATPase Snf2l is required for superovulation and regulates Fgl2 in differentiating mouse granulosa cells. *Biol. Reprod.* **88,** 142 (2013).
56. Morris, S. A. *et al.* Overlapping chromatin-remodeling systems collarborate genome wide at dynamic chromatin transitions. *Nat. Struct. Mol. Biol.* **21,** 73–83 (2014).
57. Pérez-Cadahia, B., Drobic, B. & Davie, J. R. Activation and function of immediate-early genes in the nervous system. *Biochem. Cell Biol.* **89,** 61–73 (2011).
58. Morris, S. A. *et al.* Overlapping chromatin-remodeling systems collaborate genome wide at dynamic chromatin transitions. *Nat. Struct. Mol. Biol.* **21,** 73–81 (2013).
59. Rossant, J. & Tam, P. P. L. Emerging Asymmetry and Embryonic Patterning in Early Mouse Development. *Dev. Cell* **7,** 155–164 (2004).
60. Copp, Andrew J., N. D. E. G. and J. N. M. The genetic basis of mammalian neurulation. *Nat. Rev. Genet.* **784,** (2003).
61. Adnani, L., Han, S., Li, S., Mattar, P. & Schuurmans, C. *Mechanisms of Cortical Differentiation*. *International Review of Cell and Molecular Biology* **336,** (Elsevier Inc., 2017).
62. Butts, T., Green, M. J. & Wingate, R. J. T. Development of the cerebellum : simple steps to make a ' little brain '. *Development* 4031–4041 (2014). doi:10.1242/dev.106559
63. Gavalas, A; Davenne, M; Lumsden, A. et al. Role of Hoxa-2 in axon pathfinding and rostral hindbrain patterning. *Development* (1997).
64. Katahira, T. *et al.* Interaction between Otx2 and Gbx2 defines the organizing center for the optic tectum. *Mech. Dev.* (2000).
65. Su, C.-Y., Kemp, H. A. & Moens, C. B. Cerebellar development in the absence of Gbx function in zebrafish. *Dev. Biol.* **386,** 181–190 (2014).
66. Mizuhara, E. *et al.* Purkinje cells originate from cerebellar ventricular zone progenitors positive for Neph3 and E-cadherin. *Dev. Biol.* **338,** 202–214 (2010).
67. Marzban, H. *et al.* Cellular commitment in the developing cerebellum. *Front. Cell. Neurosci.* (2015). doi:10.3389/fncel.2014.00450
68. Klisch, T. J. *et al.* In vivo Atoh1 targetome reveals how a proneural transcription factor regulates cerebellar development. *PNAS* (2011). doi:10.1073/pnas.1100230108
69. Corrales, JD; Blaess, S; Mahoney, E. et al. The level of sonic hedgehog signaling regulates the complexity of cerebellar foliation. *Development* (2006). doi:10.1242/dev.02351
70. Corrales, JMD; Rocco, GL; Blaess, S. et al. Spatial pattern of sonic hedgehog signaling through Gli genes during cerebellum development. *Development* (2004).

doi:10.1242/dev.01438
71. Reeber, S. L., Otis, T. S., Sillitoe, R. V, Watson, T. C. & Watson, C. R. New roles for the cerebellum in health and disease. *Front. Syst. Neurosci.* **7,** 1–11 (2013).
72. Mao, X., Fujiwara, Y. & Orkin, S. H. Improved reporter strain for monitoring Cre recombinase- mediated DNA excisions in mice. *Dev. Biol.* **96,** 5037–5042 (1999).
73. Yip, D. J. *et al.* Snf2l regulates Foxg1-dependent progenitor cell expansion in the developing brain. *Dev. Cell* **22,** 871–8 (2012).
74. Vary, J. C. *et al.* Yeast Isw1p Forms Two Separable Complexes In Vivo. *Mol. Cell. Biol.* **23,** 80–91 (2003).
75. Erdel, F., Schubert, T., Marth, C., Längst, G. & Rippe, K. Human ISWI chromatin-remodeling complexes sample nucleosomes via transient binding reactions and become immobilized at active sites. *Proc. Natl. Acad. Sci. U. S. A.* **107,** 19873–19878 (2010).
76. He, X., Fan, H. Y., Narlikar, G. J. & Kingston, R. E. Human ACF1 alters the remodeling strategy of SNF2h. *J. Biol. Chem.* **281,** 28636–28647 (2006).
77. He, X., Fan, H. Y., Garlick, J. D. & Kingston, R. E. Diverse regulation of SNF2h chromatin remodeling by noncatalytic subunits. *Biochemistry* **47,** 7025–7033 (2008).
78. Längst, G., Bonte, E. J., Corona, D. F. V & Becker, P. B. Nucleosome Movement by CHRAC and ISWI without Disruption or trans-Displacement of the Histone Octamer. *Cell* **97,** 843–852 (1999).
79. Ito, T. *et al.* ACF consists of two subunits, Acf1 and ISWI, that function cooperatively in the ATP-dependent catalysis of chromatin assembly. *Genes Dev.* **13,** 1529–1539 (1999).
80. Oppikofer, M. *et al.* Expansion of the ISWI chromatin remodeler family with new active complexes. *EMBO Rep.* **18,** e201744011 (2017).
81. Badenhorst, P., Voas, M., Rebay, I. & Wu, C. Biological functions of the ISWI chromatin remodeling complex NURF. *Genes Dev.* **16,** 3186–3198 (2002).
82. Deuring, R. *et al.* The ISWI Chromatin-Remodeling Protein Is Required for Gene Expression and the Maintenance of Higher Order Chromatin Structure In Vivo. *Mol. Cell* **5,** 355–365 (2000).
83. Fyodorov, D. V & Kadonaga, J. T. Binding of Acf1 to DNA involves a WAC motif and is important for ACF-mediated chromatin assembly. *Mol. Cell. Biol.* **22,** 6344–53 (2002).
84. Loyola, A., Leroy, G., Wang, Y.-H. & Reinberg, D. Reconstitution of recombinant chromatin establishes a requirement for histone-tail modifications during chromatin assembly and transcription. (2001).
85. Perpelescu, M., Nozaki, N., Obuse, C., Yang, H. & Yoda, K. Active establishment of centromeric cenp-a chromatin by rsf complex. *J. Cell Biol.* **185,** 397–407 (2009).
86. Fyodorov, D. V., Blower, M. D., Karpen, G. H. & Kadonaga, J. T. Acf1 confers unique activities to ACF/CHRAC and promotes the formation rather than disruption of chromatin in vivo. *Genes Dev.* **18,** 170–183 (2004).
87. Whitehouse, I., Rando, O. J., Delrow, J. & Tsukiyama, T. Chromatin remodelling at promoters suppresses antisense transcription. *Nature* (2007). doi:10.1038/nature06391

88. Zentner, G. E., Tsukiyama, T. & Henikoff, S. ISWI and CHD Chromatin Remodelers Bind Promoters but Act in Gene Bodies. *PLoS Genet.* **9,** (2013).
89. Maltby, V. E. *et al.* Histone H3 Lysine 36 Methylation Targets the Isw1b Remodeling Complex to Chromatin. *Mol. Cell. Biol.* (2012). doi:10.1128/MCB.00389-12
90. Morillon, A. *et al.* Isw1 Chromatin Remodeling ATPase Coordinates Transcription Elongation and Termination by RNA Polymerase II. *Cell* **115,** 425–435 (2003).
91. Landry, J. *et al.* Essential role of chromatin remodeling protein Bptf in early mouse embryos and embryonic stem cells. *PLoS Genet.* **4,** (2008).
92. Lazzaro, M. a *et al.* The imitation switch protein SNF2L regulates steroidogenic acute regulatory protein expression during terminal differentiation of ovarian granulosa cells. *Mol. Endocrinol.* **20,** 2406–17 (2006).
93. Collins, N. *et al.* An ACF1-ISWI chromatin-remodeling complex is required for DNA replication through heterochromatin. *Nat. Genet.* **32,** 627–32 (2002).
94. Poot, R. A. *et al.* The Williams syndrome transcription factor interacts with PCNA to target chromatin remodelling by ISWI to replication foci. *Nat. Cell Biol.* **6,** 1236–1244 (2004).
95. Kugler, S. J. & Nagel, A. C. A Novel Pzg-NURF Complex Regulates Notch Target Gene Activity. *Mol. Biol. Cell* **21,** 3443–3448 (2010).
96. Goller, T., Vauti, F., Ramasamy, S. & Arnold, H. H. Transcriptional regulator BPTF/FAC1 is essential for trophoblast differentiation during early mouse development. *Mol Cell Biol* **28,** 6819–6827 (2008).
97. Ma, Y. *et al.* The Chromatin Remodeling Protein Bptf Promotes Posterior Neuroectodermal Fate by Enhancing Smad2-Activated wnt8a Expression. *J. Neurosci.* **35,** 8493–8506 (2015).
98. Chen, J., Morosan-Puopolo, G., Dai, F., Wang, J. & Brand-Saberi, B. Molecular cloning of chicken Cecr2 and its expression during chicken embryo development. *Int. J. Dev. Biol.* **54,** 925–929 (2010).
99. Fairbridge, N. A. *et al.* Cecr2 Mutations Causing Exencephaly Trigger Misregulation of Mesenchymal/Ectodermal Transcription Factors. *Birth Defects Res. (Part A)* (2010). doi:10.1002/bdra.20695
100. Maulik, P. K., Mascarenhas, M. N., Mathers, C. D., Dua, T. & Saxena, S. Prevalence of intellectual disability: A meta-analysis of population-based studies. *Res. Dev. Disabil.* **32,** 419–436 (2011).
101. Tonnsen, B. L. *et al.* Prevalence of Autism Spectrum Disorders Among Children With Intellectual Disability. *Am. J. Intellect. Dev. Disabil.* **121,** 487–500 (2016).
102. Kochinke, K. *et al.* Systematic Phenomics Analysis Deconvolutes Genes Mutated in Intellectual Disability into Biologically Coherent Modules. (2016). doi:10.1016/j.ajhg.2015.11.024
103. Ben-David, E. & Shifman, S. Combined analysis of exome sequencing points toward a major role for transcription regulation during brain development in autism. *Mol. Psychiatry* **18,** (2013).
104. Lazzaro, M. a *et al.* Characterization of novel isoforms and evaluation of SNF2L/SMARCA1 as a candidate gene for X-linked mental retardation in 12 families linked to Xq25-26. *BMC Med. Genet.* **9,** 11 (2008).
105. Ender Karaca, Tamar Harel, Davut Pehlivan, Shalini N. Jhangiani, Tomasz

Gambin, Zeynep Coban Akdemir, Claudia Gonzaga-Jauregui, Serkan Erdin, Yavuz Bayram, Ian M. Campbell, Jill V. Hunter, Mehmed M. Atik, Hilde Van Esch, Bo Yuan, Wojciech Wiszniewski, Sed, M. O. & Donna M. Muzny, David R. Adams, Eric Boerwinkle, Wendy K. Chung, R. A. G. and J. R. L. Genes that Affect Brain Structure and Function Identified by Rare Variant Analyses of Mendelian Neurologic Disease. *Neuron* (2015).

106. Lopes, F. *et al.* Identification of novel genetic causes of Rett syndrome-like phenotypes. *J. Med. Genet.* 190–199 (2016). doi:10.1136/jmedgenet-2015-103568
107. Homann, O. R. *et al.* Whole-genome sequencing in multiplex families with psychoses reveals mutations in the SHANK2 and SMARCA1 genes segregating with illness. *Mol Psychiatry* **21,** 1690–1695 (2016).
108. Johnston, M. V, Jeon, O.-H., Pevsner, J., Blue, M. E. & Naidu, S. Neurobiology of Rett syndrome: a genetic disorder of synapse development. *Brain Dev.* (2001).
109. Mariani, J. *et al.* FOXG1-Dependent Dysregulation of GABA/Glutamate Neuron Differentiation in Autism Spectrum Disorders. *Cell* **162,** 375–390 (2015).
110. Byun, C. K. *et al.* FOXG1 Mutation is a Low-Incidence Genetic Cause in Atypical Rett Syndrome. *Child Neurol. Open* (2015). doi:10.1177/2329048X14568151
111. Le Guen, T. *et al.* A FOXG1 mutation in a boy with congenital variant of Rett syndrome. *Neurogenetics* (2011). doi:10.1007/s10048-010-0255-4
112. Zhang, Q. *et al.* Novel FOXG1 mutations in Chinese patients with Rett syndrome or Rett-like mental retardation. *BMC Med. Genet.* (2017). doi:10.1186/s12881-017-0455-y
113. Pratt, D. W., Warner, J. V & Williams, M. G. Genotyping FOXG1 Mutations in Patients with Clinical Evidence of the FOXG1 Syndrome. *Mol Syndr.* **3,** 284–287 (2012).
114. Kortüm, F. *et al.* The core FOXG1 syndrome phenotype consists of postnatal microcephaly, severe mental retardation, absent language, dyskinesia, and corpus callosum hypogenesis. *J. Med. Genet.* (2011). doi:10.1136/jmg.2010.087528
115. Mitter, D. *et al.* FOXG1 syndrome: genotype-phenotype association in 83 patients with FOXG1 variants. *Genet. Med.* **20,** (2018).
116. Roth, M., Bonev, B., Lindsay, J. & et al. FoxG1 and TLE2 act cooperatively to regulate ventral telencephalon formation. *Development* (2010). doi:10.1242/dev.044909
117. Kumamoto, T. & Hanashima, C. Evolutionary conservation and conversion of Foxg1 function in brain development. *Dev. Growth Differ.* (2017). doi:10.1111/dgd.12367
118. Fusco, C. *et al.* Smaller and larger deletions of the Williams Beuren syndrome region implicate genes involved in mild facial phenotype, epilepsy and autistic traits. *Eur. J. Hum. Genet.* **22,** 64–70 (2013).
119. Meng, X., Lu, X., Morris, C. A. & Keating, M. T. A novel human gene, WSTF, is deleted in Williams syndrome. *Genomics* **52,** 130–137 (1998).
120. Ashe, A. *et al.* A genome-wide screen for modifiers of transgene variegation identifies genes with critical roles in development. *Genome Biol* **9,** R182 (2008).
121. Barnett, C. *et al.* Williams Syndrome Transcription Factor is critical for neural crest cell function in Xenopus laevis. *Mech. Dev.* **129,** 324–38 (2013).
122. Sun, H. *et al.* Regulation of Baz1a and nucleosome positioning in the nucleus

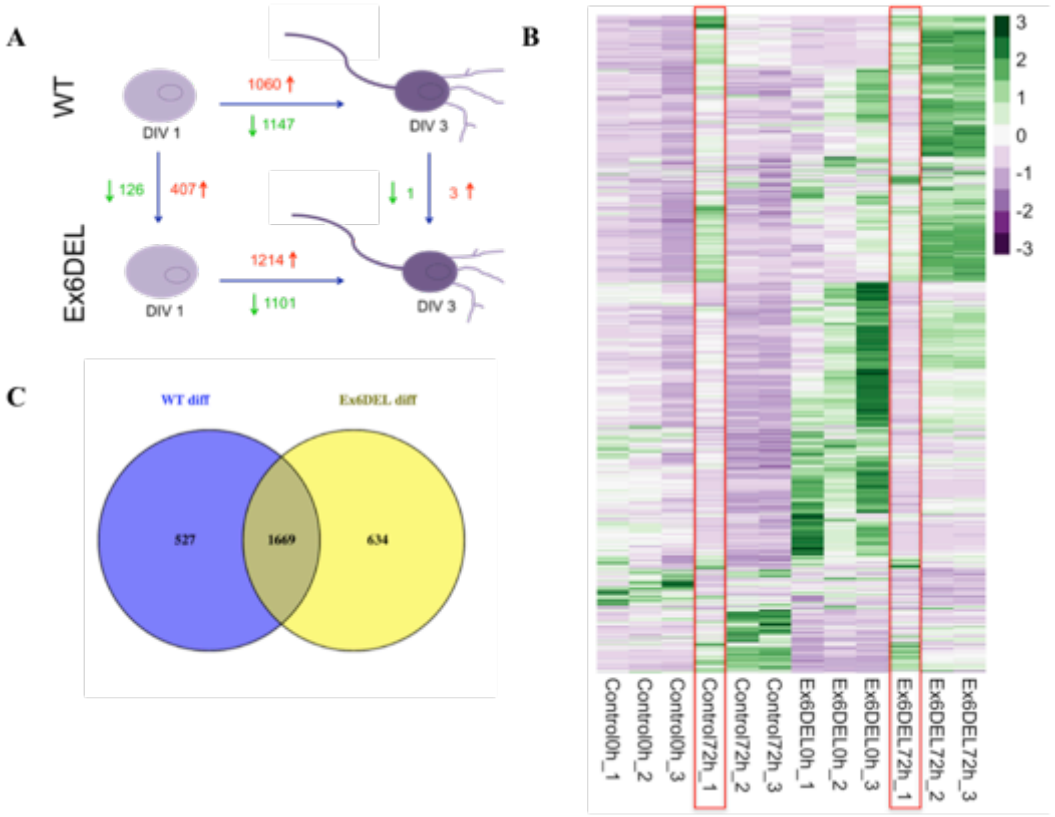
accumbens in response to cocaine. *Neuroscience* **353,** 1–6 (2017).
123. Sun, H. *et al.* BAZ1B in Nucleus Accumbens Regulates Reward-Related Behaviors in Response to Distinct Emotional Stimuli. *J. Neurosci.* **36,** 3954–3961 (2016).
124. Footz, T. K. *et al.* Analysis of the Cat Eye Syndrome Critical Region in Humans and the Region of Conserved Synteny in Mice: A Search for Candidate Genes at or near the Human Chromosome 22 Pericentromere. *Genome Res.* (2001).
125. Mears, A. J., El-Shanti, H., Murray, J. C., Mcdermid, H. E. & Patil2, S. R. Minute Supernumerary Ring Chromosome 22 Associated with Cat Eye Syndrome: Further Delineation of the Critical Region. *Am. J. Hum. Genet* **57,** 667–673 (1995).
126. Dawe, C. E., Kooistra, M. K., Fairbridge, N. A., Pisio, A. C. & McDermid, H. E. Role of chromatin remodeling gene Cecr2 in neurulation and inner ear development. *Dev. Dyn.* **240,** 372–383 (2011).
127. Cotter, D. *et al.* Abnormalities of Wnt signalling in schizophrenia – evidence for neurodevelopmental abnormality. *Clin. Neurosci.* **9,** 1379–1383 (1998).
128. Panaccione, I. *et al.* Neurodevelopment in Schizophrenia: The Role of the Wnt Pathways. *Curr. Neuropharmacol.* **11,** 535–558 (2013).
129. Cus, R., Maurus, D. & Kühl, M. Cloning and developmental expression of WSTF during Xenopus laevis embryogenesis. *Gene Expr. Patterns* **6,** 340–346 (2006).
130. Liu, Y. I. *et al.* The chromatin remodelers ISWI and ACF1 directly repress Wingless transcriptional targets. *Dev. Biol.* **323,** 41–52 (2008).
131. Mistry, M., Gillis, J. & Pavlidis, P. Meta-analysis of gene coexpression networks in the post-mortem prefrontal cortex of patients with schizophrenia and unaffected controls. *BMC Neurosci.* **14,** 105 (2013).
132. Meeta Mistry, Jesse Gillis, and P. P. Genome-wide expression profiling of schizophrenia using a large combined cohort. *Mol Psychiatry* **18,** 215–225 (2013).
133. Lee, H. Y., Greene, L. A., Mason, C. A. & Chiara Manzini, M. Isolation and Culture of Post-Natal Mouse Cerebellar Granule Neuron Progenitor Cells and Neurons. *JoVE* **23,** (2009).
134. Schindelin J, Arganda-Carreras I, Frise E, Kaynig V, Longair M, Pietzsch T, Preibisch S, Rueden C, Saalfeld S, Schmid B, Tinevez JY, White DJ, Hartenstein V, Eliceiri K, Tomancak P, C. A. Fiji - an Open Source platform for biological image analysis. *Nat. Methods* (2013).
135. Bray, N. L., Pimentel, H., Melsted, P. & Pachter, L. Near-optimal probabilistic RNA-seq quantification. *Nat. Biotechnol.* **34,** 525–527 (2016).
136. Pimentel, H., Bray, N. L., Puente, S., Melsted, P. & Pachter, L. Differential analysis of RNA-seq incorporating quantification uncertainty. *Nat. Methods* **14,** 687–690 (2017).
137. Buenrostro, J. D., Giresi, P. G., Zaba, L. C., Chang, H. Y. & Greenleaf, W. J. Transposition of native chromatin for fast and sensitive epigenomic profiling of open chromatin, DNA-binding proteins and nucleosome position. *Nat. Methods* **10,** 1213–1218 (2013).
138. Langmead, B. & Salzberg, S. L. Fast gapped-read alignment with Bowtie 2. *Nat. Methods* **9,** 357–359 (2012).
139. Li, H. *et al.* The Sequence Alignment/Map format and SAMtools. *Bioinforma. Appl. NOTE* **25,** 2078–2079 (2009).

140. Ramírez, F. *et al.* deepTools2: a next generation web server for deep-sequencing data analysis. *Nucleic Acids Res.* **44,** (2016).
141. Zhu, L. J. *et al.* ChIPpeakAnno: a Bioconductor package to annotate ChIP-seq and ChIP-chip data. *BMC Bioinformatics* (2010). doi:10.1186/1471-2105-11-237
142. Ou, J. *et al.* ATACseqQC: a Bioconductor package for post-alignment quality assessment of ATAC-seq data. *BMC Genomics* **19,** (2018).
143. Inman, K. E., Purcell, P., Kume, T. & Trainor, P. A. Interaction between Foxc1 and Fgf8 during Mammalian Jaw Patterning and in the Pathogenesis of Syngnathia. *PLoS Genet.* **9,** (2013).
144. Tauber, S. C. *et al.* Modulation of hippocampal neuroplasticity by Fas/CD95 regulatory protein 2 (Faim2) in the course of bacterial meningitis. *J. Neuropathol. Exp. Neurol.* **73,** 2–13 (2014).
145. García-Martín, E., Majewska, A. K., Guizzetti, M., Jäkel, S. & Dimou, L. Glial Cells and Their Function in the Adult Brain: A Journey through the History of Their Ablation. *Front. Cell. Neurosci.* (2017). doi:10.3389/fncel.2017.00024
146. Wilson, S. L., Kalinovsky, A., Orvis, G. D. & Joyner, A. L. Spatially Restricted and Developmentally Dynamic Expression of Engrailed Genes in Multiple Cerebellar Cell Types. *Cerebellum* 356–372 (2011).
147. Bénazéraf, B. *et al.* Identification of an unexpected link between the Shh pathway and a G2/M regulator, the phosphatase CDC25B. *Dev. Biol.* (2006). doi:10.1016/j.ydbio.2006.02.035
148. Li, X. *et al.* FOXR2 Interacts with MYC to Promote Its Transcriptional Activities and Tumorigenesis. *Cell Rep.* **12,** 487–497 (2016).
149. Kang, S., Chee, I., Lee, | Kwanghun & Lee, J. rs7968606 polymorphism of ANKS1B is associated with improvement in the PANSS general score of schizophrenia caused by amisulpride. *Hum. Psychopharmacol. Exp.* (2016). doi:10.1002/hup.2562
150. Li, J. *et al.* Integrated systems analysis reveals a molecular network underlying autism spectrum disorders. *Mol Syst Biol* **10,** (2014).
151. Yoon, S. & Seger, R. The extracellular signal-regulated kinase: Multiple substrates regulate diverse cellular functions. *Growth Factors* (2006). doi:10.1080/02699050500284218
152. Courcelles, M. *et al.* Phosphoproteome dynamics reveal novel ERK1/2 MAP kinase substrates with broad spectrum of functions. *Mol. Syst. Biol.* **9,** (2013).
153. Ramos, J. W. The regulation of extracellular signal-regulated kinase (ERK) in mammalian cells. *Int. J. Biochem. Cell Biol.* **40,** 2707–2719 (2008).
154. Wallace, V. A. Purkinje-cell-derived Sonic hedgehog regulates granule neuron precursor cell proliferation in the developing mouse cerebellum. *Curr. Biol.* **9,** 445–448 (1999).
155. Haldipur, P., Sivaprakasam, I., Periasamy, V., Govindan, S. & Mani, S. Asymmetric cell division of granule neuron progenitors in the external granule layer of the mouse cerebellum. *Biol. Open* (2015). doi:10.1242/bio.009886
156. Porter, A. G. & Janicke, R. U. Emerging roles of caspase-3 in apoptosis. *Cell Death Differ.* (1999). doi:10.1038/sj.cdd.4400476
157. Li, Y. *et al.* Setd1a and NURF mediate chromatin dynamics and gene regulation during erythroid lineage commitment and differentiation. *Nucleic Acids Res.* **44,**

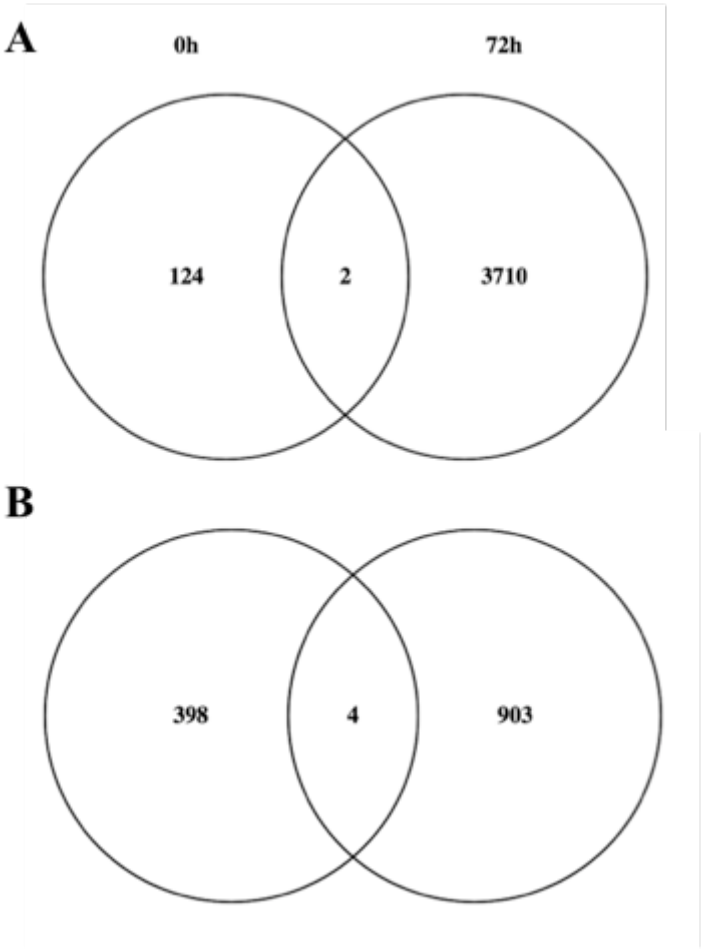
(2016).
158. Roberts, P. J. & Der, C. J. Targeting the Raf-MEK-ERK mitogen-activated protein kinase cascade for the treatment of cancer. *Oncogene* **26,** 3291–3310 (2007).
159. Faridar, A. *et al.* Mapk / Erk activation in an animal model of social deficits shows a possible link to autism. 1–12 (2014). doi:10.1186/2040-2392-5-57
160. Samuels, I. S., Saitta, S. C. & Landreth, G. E. MAP'ing CNS Development and Cognition: An ERKsome Process. doi:10.1016/j.neuron.2009.01.001
161. Obara, Y., Horgan, A. M. & Stork, P. J. S. The requirement of Ras and Rap1 for the activation of ERKs by cAMP, PACAP, and KCl in cerebellar granule cells. *J. Neurochem* **101,** 470–482 (2007).
162. Borodinsky, L. N., Coso, O. A. & Fiszman, M. L. Contribution of Ca2+ calmodulin-dependent protein kinase II and mitogen-activated protein kinase kinase to neural activity-induced neurite outgrowth and survival of cerebellar granule cells. *J. Neurochem.* **80,** 1062–1070 (2002).
163. Sato, T. & Nakamura, H. The Fgf8 signal causes cerebellar differentiation by activating the Ras-ERK signaling pathway. *Development* (2004). doi:10.1242/dev.01281
164. Xu, J., Liu, Z. & Ornitz, D. M. Temporal and spatial gradients of Fgf8 and Fgf17 regulate proliferation and differentiation of midline cerebellar structures. *Development* 1833–1843 (2000).
165. Suzuki-Hirano, A., Harada, H., Sato, T. & Nakamura, H. Activation of Ras-ERK pathway by Fgf8 and its downregulation by Sprouty2 for the isthmus organizing activity. *Dev. Biol.* **337,** 284–293 (2010).
166. Hasegawa, K. & Saga, Y. FGF8-FGFR1 Signaling Acts as a Niche Factor for Maintaining Undifferentiated Spermatogonia in the Mouse. *Biol. Reprod.* **91145,** 1–8 (2014).
167. Shao, M. *et al.* FGF8 signaling sustains progenitor status and multipotency of cranial neural crest-derived mesenchymal cells in vivo and in vitro. *J. Mol. Cell Biol.* (2015). doi:10.1093/jmcb/mjv052
168. Prigent, C. & Dimitrov, S. Phosphorylation of serine 10 in histone H3, what for? *J. Cell Sci.* **116,** 3677–3685 (2003).
169. Santos, S. D. M., Verveer, P. J. & Bastiaens, P. I. H. Growth factor-induced MAPK network topology shapes Erk response determining PC-12 cell fate. *Nat. Cell Biol.* **9,** (2007).
170. Ronique Sgambato, V., Pagè, C., Rogard, M., Besson, M.-J. & Caboche, J. Extracellular Signal-Regulated Kinase (ERK) Controls Immediate Early Gene Induction on Corticostriatal Stimulation. *J. Neurosci.* (1998).
171. Vanhoutte, P. *et al.* Opposing Roles of Elk-1 and Its Brain-specific Isoform, Short Elk-1, in Nerve Growth Factor-induced PC12 Differentiation*. *J. Biol. Chem.* (2000). doi:10.1074/jbc.M006678200
172. Gao, L. *et al.* Chromatin Accessibility Landscape in Human Early Embryos and Its Association with Evolution. *Cell* **173,** 248–259.e15 (2018).
173. Wu, J. *et al.* The landscape of accessible chromatin in mammalian preimplantation embryos. *Nature* (2016).
174. Lu, F. *et al.* Establishing Chromatin Regulatory Landscape during Mouse Preimplantation Development. *Cell* (2016).

175. Li, D. *et al.* Chromatin Accessibility Dynamics during iPSC Reprogramming. *Cell Stem Cell* (2017).
176. Xu, B. *et al.* The Chromatin Remodeler BPTF Activates a Stemness Gene-Expression Program Essential for the Maintenance of Adult Hematopoietic Stem Cells. *Stem Cell Reports* (2018). doi:10.1016/j.stemcr.2018.01.020
177. Thompson, P. J., Norton, K. A., Niri, F. H., Dawe, C. E. & McDermid, H. E. CECR2 is involved in spermatogenesis and forms a complex with SNF2H in the testis. *J. Mol. Biol.* **415,** 793–806 (2012).
178. Fan, H.-Y., Trotter, K. W., Archer, T. K. & Kingston, R. E. Swapping Function of Two Chromatin Remodeling Complexes. *Mol. Cell* **17,** 805–815 (2005).
179. Nitarska, J. *et al.* A Functional Switch of NuRD Chromatin Remodeling Complex Subunits Regulates Mouse Cortical Development. *Cell Rep.* (2016). doi:10.1016/j.celrep.2016.10.022

Appendix



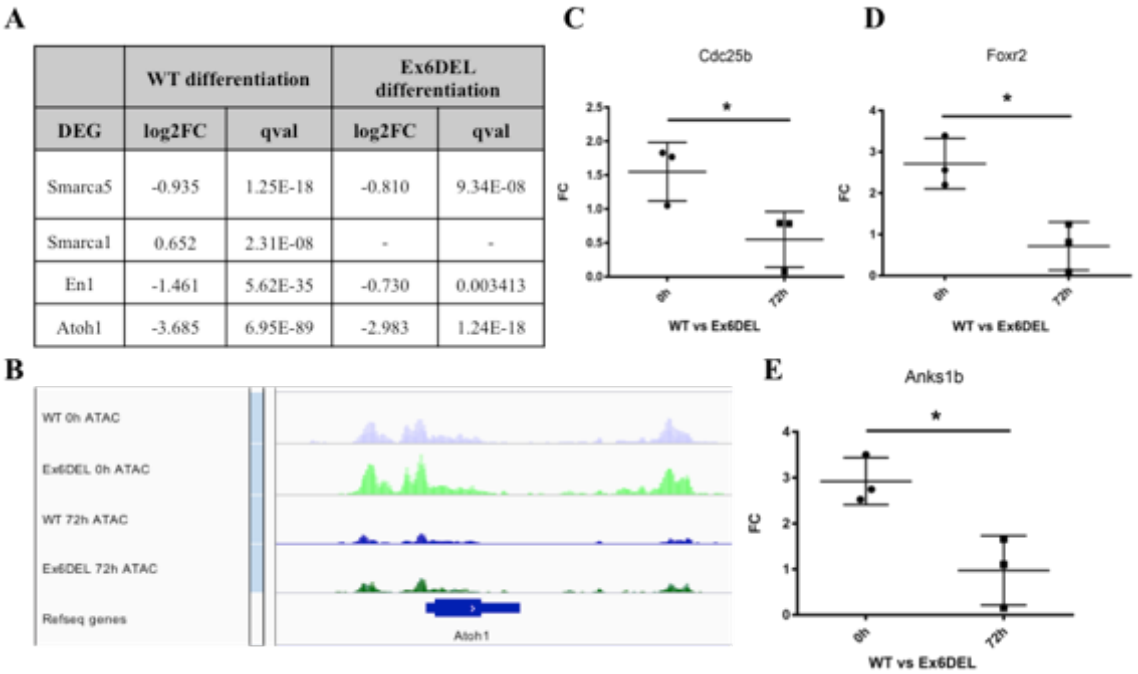
Appendix A. Loss of active Snf2l leads to widespread transcriptome disruptions in GNP differentiation. (A) RNA-seq heatmap of all transcripts with qval < 0.05 for WT (control) or Ex6DELtriplicates at 0h or 72h of *in vitro* differentiation. **(B)** Schematic of differentially expressed genes (DEG) (fold change > 1.5 & qval < 0.05) in pairwise comparisons between genotypes at timepoints of 0h and 72h, as well as DEGs involved in differentiation pathways for WT and Ex6DEL. Up-regulated gene set annotated in red, and down-regulated genes in green. Red box identifies two replicate samples which were removed from analysis. **(C)** Venn diagram of the overlapping gene sets involved in differentiation of WT (purple) and Ex6DEL (yellow) GNPs.



Appendix B. Ex6DEL DEGs are not consistent between progenitor and differentiated cells. (A) Down- and **(B)** up-regulated significant DEGs (FC > 1.5, qval < 0.05) resulting from WT vs Ex6DEL comparisons at 0h and 72h in vitro have been grouped in overlapping Venn diagrams.

A

	WT differentiation		Ex6DEL differentiation	
DEG	log2FC	qval	log2FC	qval
Smarca5	-0.935	1.25E-18	-0.810	9.34E-08
Smarca1	0.652	2.31E-08	-	-
En1	-1.461	5.62E-35	-0.730	0.003413
Atoh1	-3.685	6.95E-89	-2.983	1.24E-18



Appendix C. Key genes are differentially expressed upon loss of active Snf2l. (A) Fold change and qval of ISWI proteins, ISWI target En1 and GNP marker Atoh1 in differentiation (0h vs 72h) of WT and Ex6DEL GNPs, summarized from RNA-seq data. **(B)** Normalized ATAC seq reads (merged duplicates) for WT and Ex6DEL 0h and 72h GNP samples around Atoh1 locus. **(C-E)** Validation of RNA-seq DEGs by qPCR performed on RNA isolated from GNPs, normalized to housekeeping genes. Fold change relative to changes at 0h and 72h timepoints between WT and Ex6DEL GNPs for **(C)** Cdc25b, **(D)** Foxr2 and **(E)** Anks1b; *p<0.05.

Appendix D. TFBSs overrepresented for subset of down-regulated DEGS in Ex6DEL differentiation

TF	JASPAR ID	Class	Family	Z-score
Klf4	MA0039.2	Zinc-coordinating	BetaBetaAlpha-zinc finger	33.135
SP1	MA0079.2	Zinc-coordinating	BetaBetaAlpha-zinc finger	31.414
NFYA	MA0060.1	Other Alpha-Helix	NFY CCAAT-binding	29.158
MZF1_5-13	MA0057.1	Zinc-coordinating	BetaBetaAlpha-zinc finger	21.415
E2F1	MA0024.1	Winged Helix-Turn-Helix	E2F	21.069
HIF1A::ARNT	MA0259.1	Zipper-Type	Helix-Loop-Helix	19.537
Mycn	MA0104.2	Zipper-Type	Helix-Loop-Helix	18.19
Myc	MA0147.1	Zipper-Type	Helix-Loop-Helix	17.85
Egr1	MA0162.1	Zinc-coordinating	BetaBetaAlpha-zinc finger	16.731
MZF1_1-4	MA0056.1	Zinc-coordinating	BetaBetaAlpha-zinc finger	15.317
NF-kappaB	MA0061.1	Ig-fold	Rel	14.719
RELA	MA0107.1	Ig-fold	Rel	14.089
CTCF	MA0139.1	Zinc-coordinating	BetaBetaAlpha-zinc finger	13.445
INSM1	MA0155.1	Zinc-coordinating	BetaBetaAlpha-zinc finger	13.127
REL	MA0101.1	Ig-fold	Rel	13.111
Arnt	MA0004.1	Zipper-Type	Helix-Loop-Helix	12.283
PLAG1	MA0163.1	Zinc-coordinating	BetaBetaAlpha-zinc finger	12.072
ELK1	MA0028.1	Winged Helix-Turn-Helix	Ets	11.391
Zfx	MA0146.1	Zinc-coordinating	BetaBetaAlpha-zinc finger	11.211
SRF	MA0083.1	Other Alpha-Helix	MADS	11.032

Appendix E. TFBSs overrepresented for subset of up-regulated DEGS in Ex6DEL differentiation

TF	JASPAR ID	Class	Family	Z-score
MZF1_1-4	MA0056.1	Zinc-coordinating	BetaBetaAlpha-zinc finger	41.873
SP1	MA0079.2	Zinc-coordinating	BetaBetaAlpha-zinc finger	40.523
MZF1_5-13	MA0057.1	Zinc-coordinating	BetaBetaAlpha-zinc finger	38.935
Klf4	MA0039.2	Zinc-coordinating	BetaBetaAlpha-zinc finger	36.277
ZNF354C	MA0130.1	Zinc-coordinating	BetaBetaAlpha-zinc finger	34.42
REST	MA0138.2	Zinc-coordinating	BetaBetaAlpha-zinc finger	33.523
Tcfcp2l1	MA0145.1	Other	CP2	30.081
EBF1	MA0154.1	Zipper-Type	Helix-Loop-Helix	29.075
Zfp423	MA0116.1	Zinc-coordinating	BetaBetaAlpha-zinc finger	26.774
Myf	MA0055.1	Zipper-Type	Helix-Loop-Helix	25.345
Hand1::Tcfe2a	MA0092.1	Zipper-Type	Helix-Loop-Helix	22.97
ZEB1	MA0103.1	Zinc-coordinating	BetaBetaAlpha-zinc finger	21.452
Esrrb	MA0141.1	Zinc-coordinating	Hormone-nuclear Receptor	21.282
CTCF	MA0139.1	Zinc-coordinating	BetaBetaAlpha-zinc finger	21.166
INSM1	MA0155.1	Zinc-coordinating	BetaBetaAlpha-zinc finger	20.366
PPARG::RXRA	MA0065.2	Zinc-coordinating	Hormone-nuclear Receptor	18.576
NHLH1	MA0048.1	Zipper-Type	Helix-Loop-Helix	17.53
AP1	MA0099.2	Zipper-Type	Leucine Zipper	17.094
Arnt::Ahr	MA0006.1	Zipper-Type	Helix-Loop-Helix	16.721
Spz1	MA0111.1	Other	Other	16.29

Appendix F. TFBSs overrepresented for subset of down-regulated DEGS in WT differentiation

TF	JASPAR ID	Class	Family	Z-score
SP1	MA0079.2	Zinc-coordinating	BetaBetaAlpha-zinc finger	38.046
Klf4	MA0039.2	Zinc-coordinating	BetaBetaAlpha-zinc finger	35.371
NFYA	MA0060.1	Other Alpha-Helix	NFY CCAAT-binding	31.727
MZF1_5-13	MA0057.1	Zinc-coordinating	BetaBetaAlpha-zinc finger	27.189
MZF1_1-4	MA0056.1	Zinc-coordinating	BetaBetaAlpha-zinc finger	26.618
HIF1A::ARNT	MA0259.1	Zipper-Type	Helix-Loop-Helix	25.136
Mycn	MA0104.2	Zipper-Type	Helix-Loop-Helix	24.263
Myc	MA0147.1	Zipper-Type	Helix-Loop-Helix	23.425
E2F1	MA0024.1	Winged Helix-Turn-Helix	E2F	22.852
Arnt	MA0004.1	Zipper-Type	Helix-Loop-Helix	18.468
Zfx	MA0146.1	Zinc-coordinating	BetaBetaAlpha-zinc finger	17.941
Egr1	MA0162.1	Zinc-coordinating	BetaBetaAlpha-zinc finger	17.272
CTCF	MA0139.1	Zinc-coordinating	BetaBetaAlpha-zinc finger	17.256
ZNF354C	MA0130.1	Zinc-coordinating	BetaBetaAlpha-zinc finger	14.424
INSM1	MA0155.1	Zinc-coordinating	BetaBetaAlpha-zinc finger	14.06
HNF4A	MA0114.1	Zinc-coordinating	Hormone-nuclear Receptor	12.813
EBF1	MA0154.1	Zipper-Type	Helix-Loop-Helix	12.33
NF-kappaB	MA0061.1	Ig-fold	Rel	12.297
Tcfcp2l1	MA0145.1	Other	CP2	12.279
REL	MA0101.1	Ig-fold	Rel	11.829

Appendix G. TFBSs overrepresented for subset of up-regulated DEGS in WT differentiation

TF	JASPAR ID	Class	Family	Z-score
REST	MA0138.2	Zinc-coordinating	BetaBetaAlpha-zinc finger	34.022
MZF1_1-4	MA0056.1	Zinc-coordinating	BetaBetaAlpha-zinc finger	29.952
SP1	MA0079.2	Zinc-coordinating	BetaBetaAlpha-zinc finger	28.491
MZF1_5-13	MA0057.1	Zinc-coordinating	BetaBetaAlpha-zinc finger	26.31
ZNF354C	MA0130.1	Zinc-coordinating	BetaBetaAlpha-zinc finger	24.94
Klf4	MA0039.2	Zinc-coordinating	BetaBetaAlpha-zinc finger	23.217
Tcfcp2l1	MA0145.1	Other	CP2	21.758
Myf	MA0055.1	Zipper-Type	Helix-Loop-Helix	21.332
EBF1	MA0154.1	Zipper-Type	Helix-Loop-Helix	20.996
Zfp423	MA0116.1	Zinc-coordinating	BetaBetaAlpha-zinc finger	19.467
Hand1::Tcfe2a	MA0092.1	Zipper-Type	Helix-Loop-Helix	17.452
ZEB1	MA0103.1	Zinc-coordinating	BetaBetaAlpha-zinc finger	17.039
Arnt::Ahr	MA0006.1	Zipper-Type	Helix-Loop-Helix	16.786
INSM1	MA0155.1	Zinc-coordinating	BetaBetaAlpha-zinc finger	16.086
Egr1	MA0162.1	Zinc-coordinating	BetaBetaAlpha-zinc finger	15.933
AP1	MA0099.2	Zipper-Type	Leucine Zipper	15.153
YY1	MA0095.1	Zinc-coordinating	BetaBetaAlpha-zinc finger	14.84
NF-kappaB	MA0061.1	Ig-fold	Rel	14.386
NFKB1	MA0105.1	Ig-fold	Rel	13.497
Esrrb	MA0141.1	Zinc-coordinating	Hormone-nuclear Receptor	13.162

Appendix H. TFBSs overrepresented for subset of down-regulated DEGS in genotype comparison in 0h GNPs

TF	JASPAR ID	Class	Family	Z-score
REST	MA0138.2	Zinc-coordinating	BetaBetaAlpha-zinc finger	20.77
Tal1::Gata1	MA0140.1	Zipper-Type	Helix-Loop-Helix	11.635
Myf	MA0055.1	Zipper-Type	Helix-Loop-Helix	10.927
E2F1	MA0024.1	Winged Helix-Turn-Helix	E2F	10.777
NHLH1	MA0048.1	Zipper-Type	Helix-Loop-Helix	9.739
ZNF354C	MA0130.1	Zinc-coordinating	BetaBetaAlpha-zinc finger	8.971
PBX1	MA0070.1	Helix-Turn-Helix	Homeo	8.409
Spz1	MA0111.1	Other	Other	7.729
HIF1A::ARNT	MA0259.1	Zipper-Type	Helix-Loop-Helix	7.559
Arnt::Ahr	MA0006.1	Zipper-Type	Helix-Loop-Helix	7.155
RREB1	MA0073.1	Zinc-coordinating	BetaBetaAlpha-zinc finger	6.874
Gata1	MA0035.2	Zinc-coordinating	GATA	6.844
Mycn	MA0104.2	Zipper-Type	Helix-Loop-Helix	6.621
Egr1	MA0162.1	Zinc-coordinating	BetaBetaAlpha-zinc finger	5.811
Arnt	MA0004.1	Zipper-Type	Helix-Loop-Helix	5.179
MZF1_5-13	MA0057.1	Zinc-coordinating	BetaBetaAlpha-zinc finger	4.42
Myb	MA0100.1	Helix-Turn-Helix	Myb	4.261
ZEB1	MA0103.1	Zinc-coordinating	BetaBetaAlpha-zinc finger	4.245
CTCF	MA0139.1	Zinc-coordinating	BetaBetaAlpha-zinc finger	4.226
Pax6	MA0069.1	Helix-Turn-Helix	Homeo	4.076

Appendix I. TFBSs overrepresented for subset of up-regulated DEGS in genotype comparison in 0h GNPs

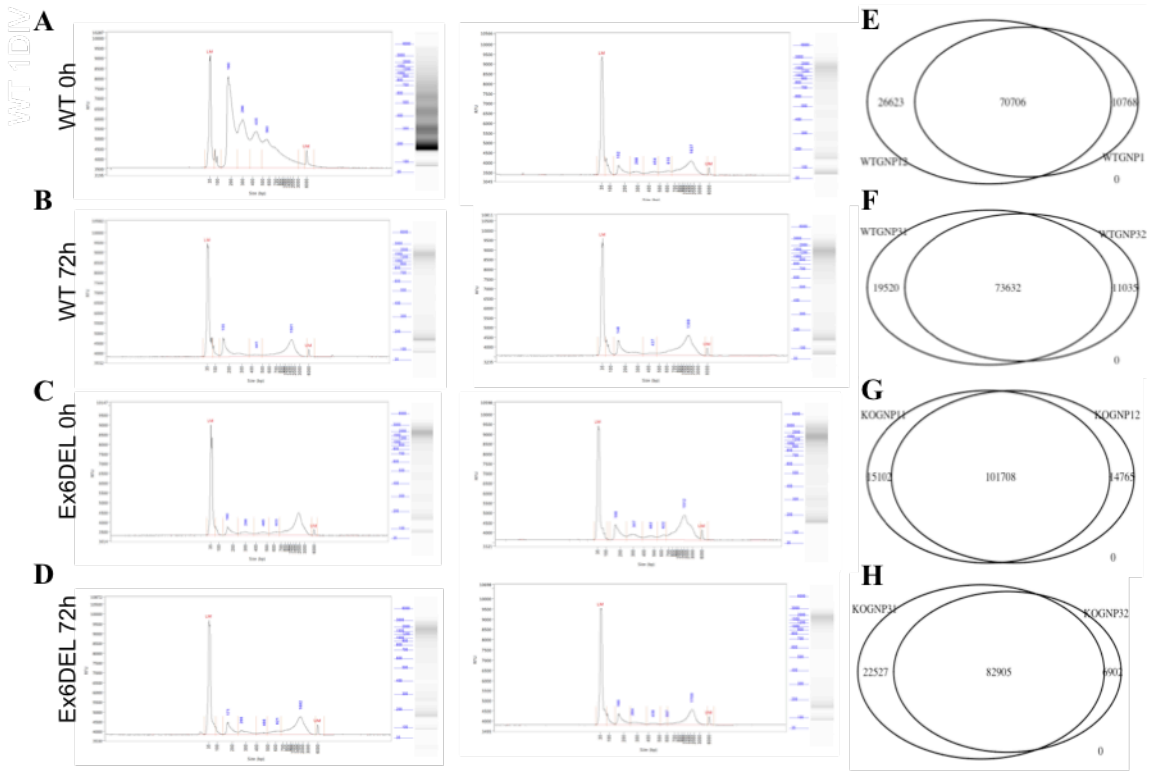
TF	JASPAR ID	Class	Family	Z-score
REL	MA0101.1	Ig-fold	Rel	20.87
NFKB1	MA0105.1	Ig-fold	Rel	18.047
RELA	MA0107.1	Ig-fold	Rel	16.303
ELF5	MA0136.1	Winged Helix-Turn-Helix	Ets	15.557
NF-kappaB	MA0061.1	Ig-fold	Rel	14.147
Klf4	MA0039.2	Zinc-coordinating	BetaBetaAlpha-zinc finger	12.658
FEV	MA0156.1	Winged Helix-Turn-Helix	Ets	12.032
SPIB	MA0081.1	Winged Helix-Turn-Helix	Ets	11.889
EBF1	MA0154.1	Zipper-Type	Helix-Loop-Helix	10.669
RREB1	MA0073.1	Zinc-coordinating	BetaBetaAlpha-zinc finger	10.594
MZF1_1-4	MA0056.1	Zinc-coordinating	BetaBetaAlpha-zinc finger	10.57
RUNX1	MA0002.2	Ig-fold	Runt	10.153
SP1	MA0079.2	Zinc-coordinating	BetaBetaAlpha-zinc finger	10.008
SPI1	MA0080.2	Winged Helix-Turn-Helix	Ets	9.363
FOXF2	MA0030.1	Winged Helix-Turn-Helix	Forkhead	8.939
HNF4A	MA0114.1	Zinc-coordinating	Hormone-nuclear Receptor	8.59
ELK1	MA0028.1	Winged Helix-Turn-Helix	Ets	8.228
SRF	MA0083.1	Other Alpha-Helix	MADS	7.825
Tal1::Gata1	MA0140.1	Zipper-Type	Helix-Loop-Helix	7.334
Foxa2	MA0047.2	Winged Helix-Turn-Helix	Forkhead	7.334

Appendix J. TFBSs overrepresented for subset of down-regulated DEGS in genotype comparison in 72h GNPs

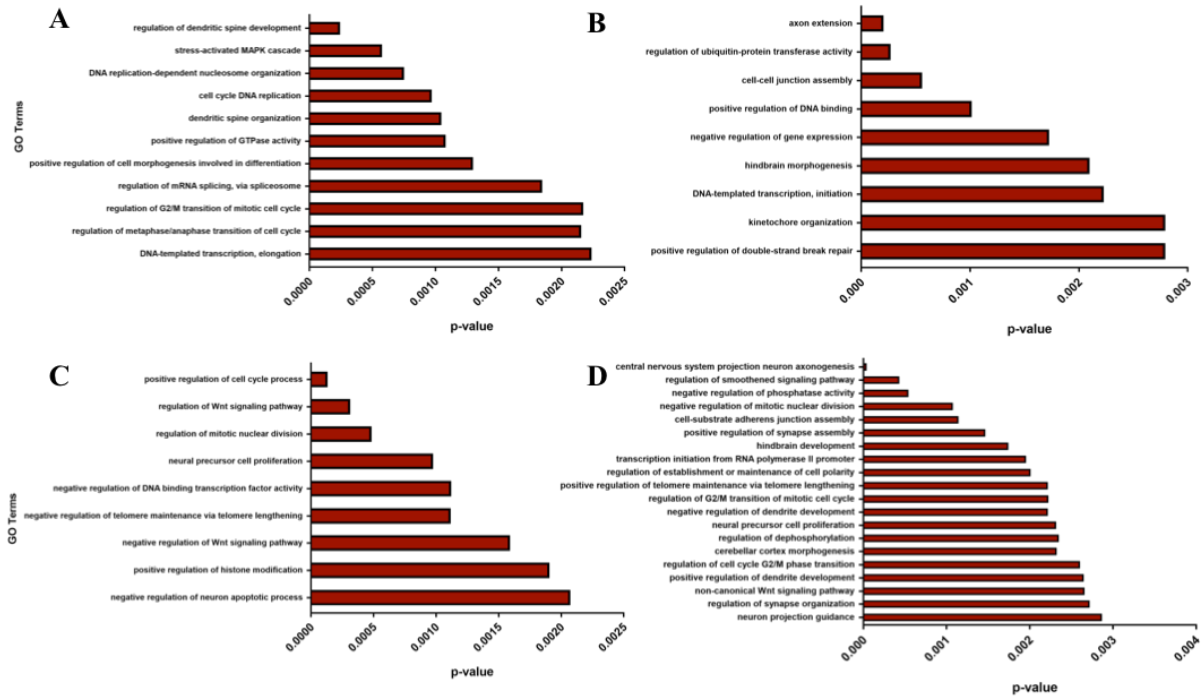
TF	JASPAR ID	Class	Family	Z-score
TAL1::TCF3	MA0091.1	Zipper-Type	Helix-Loop-Helix	6.309
HOXA5	MA0158.1	Helix-Turn-Helix	Homeo	6.135
FOXD1	MA0031.1	Winged Helix-Turn-Helix	Forkhead	5.953
IRF2	MA0051.1	Winged Helix-Turn-Helix	IRF	5.69
FOXA1	MA0148.1	Winged Helix-Turn-Helix	Forkhead	5.567
Sox2	MA0143.1	Other Alpha-Helix	High Mobility Group	5.26
Ddit3::Cebpa	MA0019.1	Zipper-Type	Leucine Zipper	4.605
Sox17	MA0078.1	Other Alpha-Helix	High Mobility Group	4.52
HNF4A	MA0114.1	Zinc-coordinating	Hormone-nuclear Receptor	4.43
Gata1	MA0035.2	Zinc-coordinating	GATA	4.355
HNF1A	MA0046.1	Helix-Turn-Helix	Homeo	4.298
TLX1::NFIC	MA0119.1	Helix-Turn-Helix::Other	Homeo::Nuclear Factor I-CCAAT-binding	4.283
YY1	MA0095.1	Zinc-coordinating	BetaBetaAlpha-zinc finger	4.018
Pdx1	MA0132.1	Helix-Turn-Helix	Homeo	4.01
Pou5f1	MA0142.1	Helix-Turn-Helix	Homeo	3.946
FEV	MA0156.1	Winged Helix-Turn-Helix	Ets	3.919
Foxa2	MA0047.2	Winged Helix-Turn-Helix	Forkhead	3.915
Gfi	MA0038.1	Zinc-coordinating	BetaBetaAlpha-zinc finger	3.834
HLF	MA0043.1	Zipper-Type	Leucine Zipper	3.735

Appendix K. TFBSs overrepresented for subset of up-regulated DEGS in genotype comparison in 72h GNPs

TF	JASPAR ID	Class	Family	Z-score
EBF1	MA0154.1	Zipper-Type	Helix-Loop-Helix	23.549
SP1	MA0079.2	Zinc-coordinating	BetaBetaAlpha-zinc finger	20.738
Klf4	MA0039.2	Zinc-coordinating	BetaBetaAlpha-zinc finger	20.188
TEAD1	MA0090.1	Helix-Turn-Helix	Homeo	19.216
MZF1_1-4	MA0056.1	Zinc-coordinating	BetaBetaAlpha-zinc finger	18.614
RUNX1	MA0002.2	Ig-fold	Runt	18.449
Hand1::Tcfe2a	MA0092.1	Zipper-Type	Helix-Loop-Helix	18.234
REL	MA0101.1	Ig-fold	Rel	17.689
Zfp423	MA0116.1	Zinc-coordinating	BetaBetaAlpha-zinc finger	17.032
NF-kappaB	MA0061.1	Ig-fold	Rel	16.912
MZF1_5-13	MA0057.1	Zinc-coordinating	BetaBetaAlpha-zinc finger	16.229
STAT1	MA0137.2	Ig-fold	Stat	15.881
Tcfcp2l1	MA0145.1	Other	CP2	15.834
ZNF354C	MA0130.1	Zinc-coordinating	BetaBetaAlpha-zinc finger	15.568
Stat3	MA0144.1	Ig-fold	Stat	15.387
SRF	MA0083.1	Other Alpha-Helix	MADS	14.474
NFATC2	MA0152.1	Ig-fold	Rel	13.144
RELA	MA0107.1	Ig-fold	Rel	12.402
TLX1::NFIC	MA0119.1	Helix-Turn-Helix::Other	Homeo::Nuclear Factor I-CCAAT-binding	12.272
PPARG::RXRA	MA0065.2	Zinc-coordinating	Hormone-nuclear Receptor	12.218



Appendix L. ATAC-seq of WT and Ex6DEL GNP differentiation. Fragment analyzer runs of amplified tagmented DNA for biological duplicates of WT **(A,B)** and Ex6DEL **(C,D)** progenitors and differentiated cells, respectively. Number of consensus accessibility peaks following sequencing between both biological replicates of WT **(E)** and Ex6DEL **(G)** progenitors and differentiated cells **(F, H).**



Appendix M. Select Gene Ontology (GO) terms associated with significant DARs. Unique GO terms enriched in DARs in **(A)** WT progenitors, **(B)** WT differentiated neurons, **(C)** Ex6DEL progenitors and **(D)** Ex6DEL differentiated neurons.

Curriculum Vitae

LAURA R. GOODWIN

Education

M.Sc. in Biochemistry (Specialization in Human and Molecular Genetics)
Thesis supervisor: Dr. David Picketts
University of Ottawa (May 2016 – Anticipated August 2018)

B.Sc. Honours in Biomedical Sciences, CO-OP (Specialization in Cellular and Molecular Medicine)
Honours Thesis supervisor: Dr. Marc-André Langlois
University of Ottawa, Magna Cum Laude (2011-2016)

Relevant Work Experience

- **M.Sc. Candidate, OHRI/University of Ottawa** (2016-2018)
  - Performed high-throughput Next Generation Sequencing (NGS) data manipulation and analysis (RNA-seq, ATAC-seq) employing R and UNIX platforms for statistical computation and data processing
  - Developed Master's research project and independently conducted a wide range of experiments (*in vitro* culture of primary neurons, NGS, coIP, immunoblotting, immunofluorescence, qRT-PCR)
  - Trained and mentored a Third-Year Summer Student

- **Teaching Assistant, University of Ottawa** (2015-2018)

- **Research Assistant, HECSB, Health Canada** (Sept 2015-Apr 2016)
  - Drafted an article manuscript for a project assessing the transcriptomic changes and inflammatory effects of silica nanoparticles on FE1 cells
  - Generated and analyzed data for three ongoing projects relating to the assessment of toxicity of various nanoparticles on lung tissue

- **Research Assistant, Faculty of Medicine, University of Ottawa** (2014-2015)
  - Worked independently, under the supervision of a PhD candidate, on a number of projects investigating the APOBEC3 proteins

- **Evaluation Officer, PMRA, Health Canada** (Jan-Apr 2014)
  - Gathered extensive pesticide exposure, toxicology and occupational risk data and compiled it into a conservative risk assessment of risk of an active ingredient
  - Drafted a comprehensive monograph detailing the risk assessment process and safety recommendations

- **Laboratory Data Assistant, Statistics Canada** (June-Dec 2013)
  - Tested the household, clinic and laboratory computer applications for the Canadian Health Measures Survey (CHMS)
  - Gathered and compiled extensive environmental and air quality data to compliment and validate CHMS findings
  - Collected over 20 new articles to be added to the current CHMS bibliography

Publications

Nikota J, Banville A, Goodwin LR, Wu D, Williams A, Yauk CL, Wallin H, Vogel U, Halappanavar S. Stat-6 signaling pathway and not Interleukin-1 mediates multi-walled carbon nanotube-induced lung fibrosis in mice: insights from an adverse outcome pathway framework. Part Fibre Toxicol. 2017 Sep 13;14(1):37. doi: 10.1186/s12989-017-0218-0.

Goodwin LR, Picketts DJ. The role of ISWI chromatin remodeling complexes in brain development and neurodevelopmental disorders. Mol Cell Neurosci. 2017 Dec 14. pii: S1044-7431(17)30233-6. doi: 10.1016/j.mcn.2017.10.008.

Renner TM, Bélanger K, Goodwin LR, Campbell M, Langlois M-A. Molecular attributes influencing LINE-1 restriction by all seven human APOBEC3 proteins. Virology. *In press*.

Recognitions and Awards

- Queen Elizabeth II Graduate Scholarship, University of Ottawa (2017-2018)
- Masters Poster Award, Brain Health Research Day, University of Ottawa (2017)
- Registration Award, Epigenomics Data Analysis workshop, McGill (2017)
- Admission Scholarship: Masters, University of Ottawa (2016-2018)
- Dean's Honours List (2012-2016)
- Presented at the Project Pulse Conference 2016, IgNITE Science Case Competition
- Second Place Award for Undergraduate Presentation, Faculty of Medicine Summer Student Program (2015)
- Undergraduate Admission Scholarship and French Studies Bursary, University of Ottawa

Volunteer Experience

- **Outreach Volunteer**, Let's Talk Science, University of Ottawa (2016-2017)
- **Translator**, UOCatalyst, University of Ottawa (2014 – 2016)
- **Leader and Side Walker**, TROtt Therapeutic Riding Association (2012-2013)
- **Judge**, **Faculty of Science**, in the 2013 Good Ideas Contest, University of Ottawa
- **Data Analyst**, Heart and Stroke Foundation (2012)